NAVAL POSTGRADUATE SCHOOL

MONTEREY, CALIFORNIA

THESIS

ANALYSIS AND FORECASTS OF 300 hPa DIVERGENCE ASSOCIATED WITH SEVERE CONVECTION USING ETA-212 AND MM5 MODEL DATA

by

Scott C. Lisko

March 2005

Thesis Advisor:	Wendell A. Nuss
Second Reader:	Carlyle H. Wash

Approved for public release; distribution is unlimited.

THIS PAGE INTENTIONALLY LEFT BLANK

REPORT DOCUMENTATION PAGE			Form Approved OMB No. 0704-0188
Public reporting burden for this collection of information is estimated to average 1 hour per response, including the time for reviewing instruction, searching existing data sources, gathering and maintaining the data needed, and completing and reviewing the collection of information. Send comments regarding this burden estimate or any other aspect of this collection of information, including suggestions for reducing this burden, to Washington headquarters Services, Directorate for Information Operations and Reports, 1215 Jefferson Davis Highway, Suite 1204, Arlington, VA 22202-4302, and to the Office of Management and Budget, Paperwork Reduction Project (0704-0188) Washington DC 20503.			
1. AGENCY USE ONLY ***(Leave blank)***	**2. REPORT DATE** March 2005	**3. REPORT TYPE AND DATES COVERED** Master's Thesis	
4. TITLE AND SUBTITLE: Title (Mix case letters) Analysis and Forecasts of 300 hPa Divergence Associated With Severe Convection Using ETA-212 and MM5 Model Data			**5. FUNDING NUMBERS**
6. AUTHOR(S) Scott C. Lisko			
7. PERFORMING ORGANIZATION NAME(S) AND ADDRESS(ES) Naval Postgraduate School Monterey, CA 93943-5000			**8. PERFORMING ORGANIZATION REPORT NUMBER**
9. SPONSORING /MONITORING AGENCY NAME(S) AND ADDRESS(ES) N/A			**10. SPONSORING/MONITORING AGENCY REPORT NUMBER**
11. SUPPLEMENTARY NOTES The views expressed in this thesis are those of the author and do not reflect the official policy or position of the Department of Defense or the U.S. Government.			
12a. DISTRIBUTION / AVAILABILITY STATEMENT Approved for public release; distribution is unlimited.			**12b. DISTRIBUTION CODE**

13. ABSTRACT (maximum 200 words)

This study investigates severe weather events occurring in the Midwest, Central, and Northeastern United States from May through September 2004. Severe weather events are pinpointed using tornado and hail reports and correlating them with NEXRAD radar data to determine maximum intensity of the event. Severe storms that occur within 30 minutes of a model forecast hour are catalogued for further investigation. Once these events are diagnosed, ETA-212 and MM5 model data is regridded, centered on the storm. Divergence values at 300 hPa are extracted from the model data for each storm event. These storms are then grouped in three ways: all storms, tornadic storms, and hail producing storms. The averaged maximum divergence values from the ETA-212 for each group are examined from the 0 hour analysis through the 21 hour forecast. From these averaged divergence values, a matrix of recommended divergence threshold values is derived. For the MM5 data, a subset of storms is examined. The MM5 and ETA-212 are run on an identical set of storms, and the divergence forecasts are compared.

14. SUBJECT TERMS Analysis, Forecasts, 300 hPa, Divergence, Severe Convection, ETA-212, MM5			**15. NUMBER OF PAGES** 135
			16. PRICE CODE
17. SECURITY CLASSIFICATION OF REPORT Unclassified	**18. SECURITY CLASSIFICATION OF THIS PAGE** Unclassified	**19. SECURITY CLASSIFICATION OF ABSTRACT** Unclassified	**20. LIMITATION OF ABSTRACT** UL

NSN 7540-01-280-5500 Standard Form 298 (Rev. 2-89)
Prescribed by ANSI Std. 239-18

THIS PAGE INTENTIONALLY LEFT BLANK

Approved for public release; distribution is unlimited

ANALYSIS AND FORECASTS OF 300 hPa DIVERGENCE ASSOCIATED WITH SEVERE CONVECTION USING ETA-212 AND MM5 MODEL DATA

Scott C. Lisko
Captain, United States Air Force
B.S., University of Wisconsin - Madison, 1997

Submitted in partial fulfillment of the
requirements for the degree of

MASTER OF SCIENCE IN METEOROLOGY

from the

NAVAL POSTGRADUATE SCHOOL
MARCH 2005

Author:

Scott C. Lisko

Approved by:

Wendell A. Nuss
Thesis Advisor

Carlyle H. Wash
Second Reader

Philip A. Durkee
Chairman
Department of Meteorology

THIS PAGE INTENTIONALLY LEFT BLANK

ABSTRACT

This study investigates severe weather events occurring in the Midwest, Central, and Northeastern United States from May through September 2004. Severe weather events are pinpointed using tornado and hail reports and correlating them with NEXRAD radar data to determine maximum intensity of the event. Severe storms that occur within 30 minutes of a model forecast hour are catalogued for further investigation. Once these events are diagnosed, ETA-212 and MM5 model data is regridded, centered on the storm. Divergence values at 300 hPa are extracted from the model data for each storm event. These storms are then grouped in three ways: all storms, tornadic storms, and hail producing storms. The averaged maximum divergence values from the ETA-212 for each group are examined from the 0 hour analysis through the 21 hour forecast. From these averaged divergence values, a matrix of recommended divergence threshold values is derived. For the MM5 data, a subset of storms is examined. The MM5 and ETA-212 are run on an identical set of storms, and the divergence forecasts are compared.

THIS PAGE INTENTIONALLY LEFT BLANK

TABLE OF CONTENTS

LIST OF FIGURES

LIST OF TABLES

THIS PAGE INTENTIONALLY LEFT BLANK

ACKNOWLEDGMENTS

I would like to thank my advisor, Professor Wendell A. Nuss of the Department of Meteorology, Naval Postgraduate School, for his guidance and support during the development of this thesis. His meteorological expertise and programming skill was instrumental in the analysis and processing of the vast amount of data required for this study. Additionally, I thank Dr. Carlyle H. Wash, Department of Meteorology, Naval Postgraduate School, who served as my second reader. His insight and recommendations during the writing and revision process were invaluable to the completion of my thesis.

I also owe a debt of gratitude to Mr. Robert Creasey, staff meteorologist, Naval Postgraduate School. He provided countless hours of computer, UNIX and LINUX support, as well as finding any radar or model data that I asked for. His help made the data gathering portion of my research proceed smoothly.

Finally, I would like to thank Mr. Gregory Harris of the 15th Operational Weather Squadron, Scott Air Force Base, Illinois, for providing a point of contact from the agency who initiated this thesis topic, and the meteorologists of the Storm Prediction Center for their first-rate online archive of severe thunderstorm events.

THIS PAGE INTENTIONALLY LEFT BLANK

I. INTRODUCTION

Upper level divergence is one of the most important parameters related to convective activity. It contributes directly to the strength of vertical motions in weather systems, which in turn contributes to the intensity of thunderstorm updrafts. Strong divergence values at upper levels in the atmosphere serve as a trigger for convective activity and are indicative of thunderstorm activity.

Which divergence values, however, are related to severe weather versus non-severe weather? More specifically, how can a forecaster look at a divergence value and tell if it relates to a "garden variety" thunderstorm or a storm that will produce hail or tornadoes? For the U.S. Air Force, this is a vital question. Air Force forecasters use the 300 hPa divergence model charts as a tool to diagnose and predict thunderstorm activity. If a forecaster could take a 300 hPa divergence value and compare it with a known matrix of divergence values versus severe weather events, the accuracy of the forecast and lead time for severe weather watches and warnings would be greatly enhanced.

The 15th Operational Weather Squadron (OWS) at Scott Air Force Base, Illinois proposed a research topic to address this issue of a divergence threshold value for severe weather. The 15th OWS, one of four Air Force OWS facilities in the continental United States, is tasked with providing weather support for an area ranging from the Midwest through the Great Lakes into New England (Figure 1.1, purple region). This region experiences extensive convective activity during the spring and summer seasons.

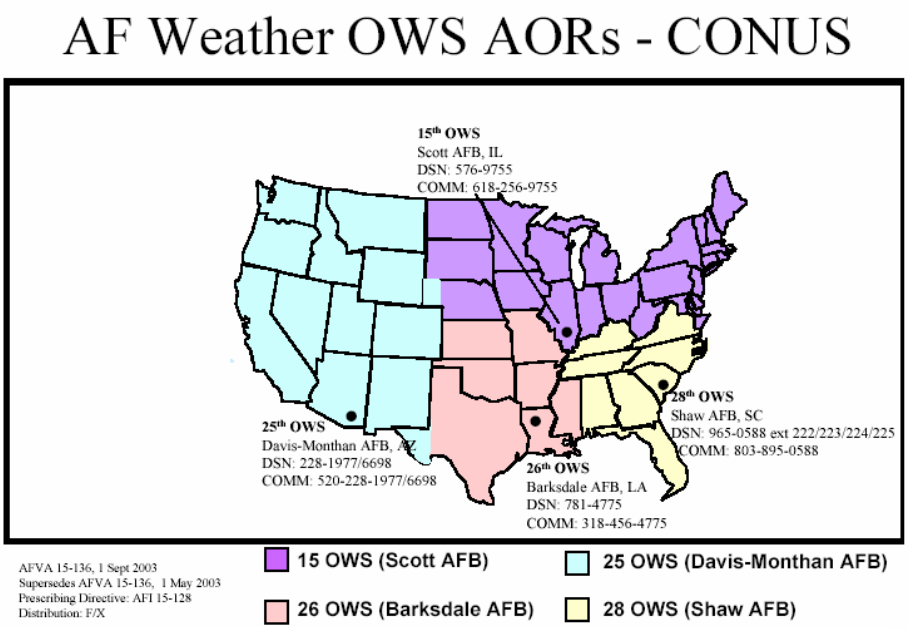

Figure 1.1. Areas of responsibility (AOR) for the four continental United States Operational Weather Squadrons (OWS). The 15th OWS has responsibility for the AOR highlighted in purple, ranging from the Dakotas through the Great Lakes region into New England. (From Ref. Air Force Visual Aid 15-136, 1 Sep 2003)

Within this area, the 15tn OWS is responsible for providing severe weather warnings for 217 active duty military, Air National Guard, Air Force Reserve, and Department of Defense installations (Figure 1.2). With forecast locations spread over such a wide geographical area, timely and accurate weather warnings are crucial for safety and resource protection.

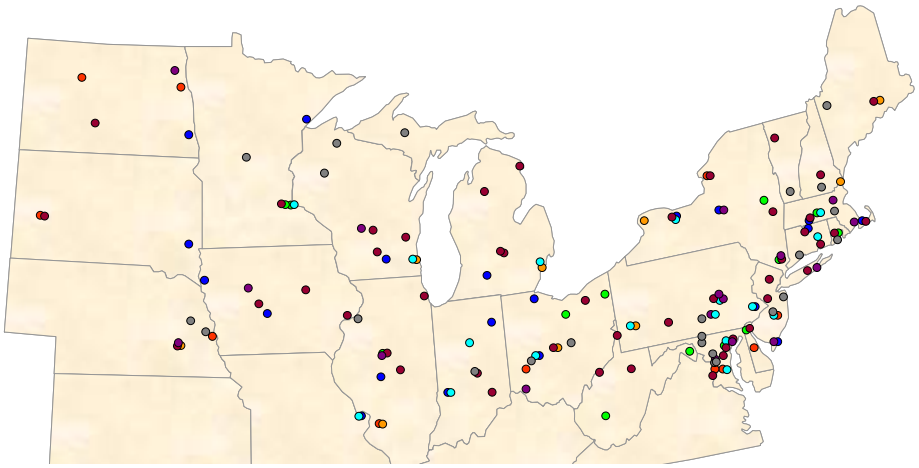

Figure 1.2. Military installations within the 15th OWS AOR. The 15th is responsible for weather warnings for 217 active duty, guard, reserve, and DoD installations. (From Ref. 15th OWS Orientation Briefing, 8 Jan 2004)

The primary goal of this thesis is to focus on one aspect of thunderstorm development, upper level divergence, and determine a reasonable threshold or range of intensities associated with severe weather events. For purposes of this study, "upper level" is assumed to be 300 hPa. While this will not always be the level of maximum divergence, it is a standard atmospheric and model data level. While the level of strongest divergence may vary, the 300 hPa level should produce a consistent signature of divergence that will correlate with severe thunderstorm development. Additionally, Air Force forecasters use divergence values from 300 hPa when forecasting severe weather. The divergence values resulting from this study will be derived directly from the same data used operationally by Air Force forecasters.

In addition to the primary goal of identifying divergence threshold values from ETA-212 model data, two secondary goals are listed below.

1. Compare the ETA-212 and MM5 model output and highlight similarities or differences in the divergence values.
2. Consider tornado-producing storms and hail-producing storms separately, and examine divergence data for each to assess possible differences in intensity.

THIS PAGE INTENTIONALLY LEFT BLANK

II. CHARACTERISTICS OF CONVECTIVE STORMS

Before investigating the divergence characteristics of severe weather, the general pattern of convective development must be understood. Convective storms exist under a wide variety of conditions and evolve in an equally wide variety of ways. Storm behavior is inherently dependent on the environment in which the storm grows, including thermodynamic stability, vertical wind profiles, and mesoscale forcing influences. Because of the complexity of convective development, however, the knowledge of storm dynamics is most applicable to relatively isolated convective events such as an individual thunderstorm cell or a simple squall line. Since larger scale systems are made up of individual convective cells, knowledge of the properties of isolated convection is still useful. However, as interactions among cells, along with mesoscale and synoptic-scale influences become important, any conclusions regarding storm behavior become less certain.

This chapter (derived from Weisman and Klemp, 1986) discusses the properties of isolated individual convective cells, which will serve as a basis for understanding how divergence relates to thunderstorm development and intensity. After providing a broad overview of thunderstorm structure, we will focus specifically on divergence as an indicator of severe weather.

A. OBSERVED TYPES OF CONVECTIVE STORMS

The concept of the convective cell is fundamental to a discussion of convective storms. Generally speaking, a convective cell is a region of strong updraft (at least 10 m/s) with a horizontal cross section of 10-100 km^2 that extends in the vertical through most of the troposphere. Each cell is associated with a region of precipitation that can easily be identified on radar. Convective cells observed on radar usually evolve in identifiable, repeatable patterns. On the basis of these radar characteristics, conceptual models have been proposed for the most commonly observed storm types. These include the single-cell, multicell, and supercell storms.

1. The Single Cell Storm

The single cell storm is the most basic convective storm. It consists of a single updraft which rises rapidly through the troposphere and produces large amounts of liquid water and ice. When rain drops or ice particles become too heavy for the updraft to support, they begin to fall, creating a downdraft that quickly replaces the updraft. The downdraft is initially nearly saturated, but as it falls into the lower troposphere and mixes with drier air, strong evaporational cooling may occur. This cooling accelerates the downdraft, which spreads out horizontally as a cold surge (or gust front) on reaching the surface. The life cycle of a single cell storm is typically 30-50 minutes. Single cell storms occasionally produce small hail, but tornadoes are rare.

2. The Multicell Storm

The multicell storm is basically a cluster of short-lived single cells. The cold surges from each individual cell combine to form a larger gust front, which triggers new updraft development as it spreads out from the decaying parent storm. New cells evolve from these triggered updrafts as described in part 1, and the process perpetuates itself. Because of their ability to renew themselves constantly through new cell growth, multicell storms may last several hours and affect a broad area. Exceptionally strong updrafts may produce hail, and short-lived tornadoes are possible along the gust front in the vicinity of strong updraft centers.

3. The Supercell Storm

The supercell storm is the most dangerous of the convective storm types, producing high winds, large hail and long-lived tornadoes over a wide area. It consists of a quasi-steady, rotating updraft which may have a lifetime of several hours. The structure of the supercell allows it to maintain its strength as it moves, so widespread, long-lasting severe weather can occur.

B. CONDITIONS AFFECTING STORM GROWTH AND EVOLUTION

Convective storm type and severity are strongly dependent on the environmental conditions in which the storm grows. The two most important factors are the thermodynamic structure of the atmosphere and vertical wind shear. The ambient thermodynamic profile exerts a fundamental control on convective storm strength, since it affects the ability of air parcels to accelerate vertically. Vertical wind shear is important because it influences the structure of the convection, determining whether a storm evolves as a single cell, multicell, or supercell.

1. Thermodynamic Structure

The first factor in assessing severe weather potential is the thermodynamic structure of the ambient environment. The degree of atmospheric instability is usually measured by any one of several indices such as the Lifted Index, Showalter Index, or Total Totals. A more accurate measure, however, is obtained by explicitly calculating the amount of buoyant energy available to an air parcel rising vertically through an undisturbed environment. This is done by calculating the convective available potential energy, or CAPE. CAPE is determined by the following equation, taken from the American Meteorological Society glossary (http://amsglossary.allenpress.com/glossary/, January 2005):

$$\text{CAPE} = \int_{p_n}^{p_f} \left(\alpha_p - \alpha_e\right) dp \qquad (2.1)$$

In the above equation, α_e is the environmental specific volume profile, α_p is the specific volume of an air parcel moving upward moist adiabatically from the level of free convection, p_f is the atmospheric pressure at the level of free convection, and p_n is the atmospheric pressure at the level of neutral buoyancy. This calculation is equivalent to evaluating the positive area represented on a skew-T diagram (Figure 2.1). If pressure perturbation effects, water loading, and mixing are ignored, CAPE can be directly related to the maximum vertical velocity obtained by a parcel rising vertically through the troposphere:

$$W_{max} = \left(2 \times CAPE\right)^{1/2} \qquad (2.2)$$

Magnitudes of CAPE may be as large as 4500 J/kg, but generally range from 1000 to 2500 J/kg for moderately unstable convective days. A CAPE of 2500 J/kg would translate to a maximum possible updraft strength of 70 m/s. However, water loading, perturbed vertical pressure gradients, and mixing effects reduce these estimates by as much as 50%.

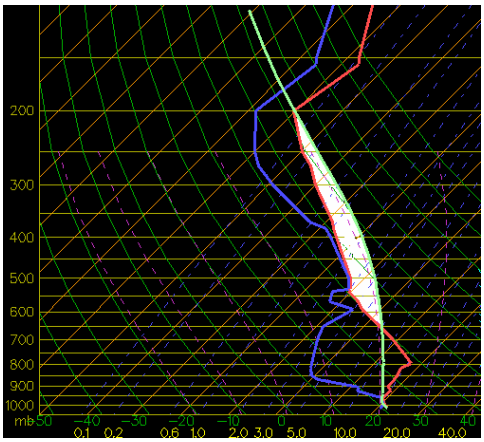

Figure 2.1. Thermodynamic diagram (skew-T), with area of CAPE highlighted in white. (From Ref. The Ohio State University Weather Server, http://twister.sbs.ohio-state.edu/helpdocs/cape.html, February 2005)

A second important aspect of thermodynamic structure is the moisture stratification. Large amounts of moisture are needed in the boundary layer to support updraft growth, but the absence of moisture above the boundary layer often enhances storm severity. If a dry layer exists above the moist boundary layer, the storm's downdraft and outflow strength is increased as the rainy downdraft falls through and entrains the dry mid-level air. The enhanced outflow strength that accompanies these cases may also indirectly enhance storm severity by strengthening the gust front, increasing the likelihood of updraft redevelopment as the outflow boundary propagates away from the parent storm.

2. Vertical Wind Shear

While the thermodynamic structure of the atmosphere strongly influences the vertical accelerations in a convective storm, vertical wind shear has a strong influence on the form that the convection will take. There are two physical mechanisms that explain the organizational capacity of vertical wind shear. The first is the ability of a gust front to trigger new convective cells, and the second is the ability of a storm updraft to interact with the environmental wind shear to produce an enhanced, quasi-steady storm structure.

First, consider the case of a convective cell evolving in an environment with no wind (and thereby, no vertical wind shear). The convective downdraft produces a pool of cold air which spreads horizontally at the surface equally in all directions. As the gust front spreads out, it triggers new convection if there is sufficient lifting to raise air parcels to the level of free convection. Since there is no environmental wind above the surface outflow, the new updraft cells will be motionless while the gust front continues to spread out at the surface. The new cells now find themselves in the cold, stable environment behind the gust front, and the updrafts won't develop any further. This situation is reminiscent of the single cell storm described in section A.1.

A different situation arises when environmental winds increase from zero at the surface to a moderate value at higher levels. A cell developing in this idealized, linear wind shear environment will still produce outflow due to the pool of cold air at the surface. Cells generated from the updrafts created by the outflow boundary, however, will now tend to move downwind at approximately the mean wind over the lowest 5-7 km above ground level. This enhances cell growth along the downwind portion of the gust front by increasing both the relative inflow into the developing cell and the time that the cells feed on the warm air out ahead of the gust front. In the ideal situation, the cell motion and gust front motion are the same, leading to a continual redevelopment of updrafts. This situation, where increasing winds aloft keep the developing updrafts in the warm, unstable air ahead of the gust front, lead to the sustenance of the multicell storms described in section A.2.

As vertical wind shear becomes stronger, the interaction of the updraft with the sheared flow becomes an important factor in the organization and sustenance of the convection. As vertical shear increases, a rotation on the flank of the updraft develops

due to tilting of horizontal vorticity inherent in the vertically sheared flow. If the vertical shear extends through the middle levels of the storm, the rotation dynamically induces low pressure at mid-levels, creating a vertical pressure gradient that accelerates surface air upward. This forcing helps to sustain the updraft as well as create storm propagation that deviates from the mean wind. In the idealized case for this storm structure, winds still increase from zero at the surface to a moderate value at higher levels, but the wind shear vector turns clockwise with height throughout the depth of the profile. These conditions result in long-lived, supercell storms described in section A.3.

C. DIVERGENCE AND CONVECTION

An understanding of basic divergence theory is an essential part of meteorology. Simply stated, divergence is a value that measures a vector field's tendency to originate from or converge upon a given point. In the atmosphere, divergence plays an important part in both mass continuity and vertical motion, which will be discussed later in this section.

1. Definition of Divergence

In a standard Cartesian coordinate system, the divergence of a continuously differentiable vector field

$$\mathrm{F} = Fx\mathbf{i} + Fy\mathbf{j} + Fz\mathbf{k} \qquad (2.3)$$

is defined to be the scalar-valued function

$$\mathrm{div}\ \mathrm{F} = \nabla \bullet \mathrm{F} = \frac{\partial Fx}{\partial x} + \frac{\partial Fy}{\partial y} + \frac{\partial Fz}{\partial \mathrm{z}} \qquad (2.4)$$

where either notation, the del operator dotted with the vector F or the individual partial differentials, are commonly used.

2. Dines Compensation

The net mass convergence into a column of air (from the surface to the tropopause) is generally much smaller than the convergence at any particular level, since convergence at one level tends to be offset by divergence at another. This phenomenon is known as *Dines compensation.* Mathematically, this is explained by examining the mass continuity equation

$$\frac{\partial u}{\partial x} + \frac{\partial v}{\partial y} = -\frac{\partial \omega}{\partial p} \qquad (2.5)$$

which shows that the two-dimensional horizontal divergence is related to the vertical motion. Simply stated, if we have a positive left hand side of this equation (horizontal divergence), we must have a positive right hand side (vertical convergence) to balance the equation. In physical terms, this means if we have horizontal divergence at a certain level in the atmosphere (say 300 hPa), we need vertical convergence to balance it out. This means downward or zero vertical motion from above the 300 hPa level, but more importantly, upward vertical motion from below the 300 hPa level. Conversely, if we have a negative left hand side (horizontal convergence), the right hand side must also be negative (vertical divergence) to balance the equation, resulting in downward vertical motion below the level and upward vertical motion above.

If we integrate 2.5 with height, subject to zero vertical motion at the top and bottom as boundary conditions, we get

$$\int \left(\frac{\partial u}{\partial x} + \frac{\partial v}{\partial y} \right) dz = 0 \qquad (2.6)$$

which shows that summation of the divergence values at all levels of the atmosphere gives zero. Therefore, mass divergence at one level of the atmosphere must be offset by mass convergence at another level.

Physically, Dines compensation occurs because convergence in the lower troposphere implies that air in the atmospheric column must ascend. However, very little air escapes through the tropopause into the stratosphere, and the height of the tropopause does not change much. Since the uplifted air can not break through into the stratosphere, it must spread out somewhere below the tropopause. Therefore, low-level convergence implies divergence somewhere aloft in the troposphere, thus Dines compensation.

3. Divergence and Severe Weather

Dines compensation provides insight into severe weather development when we consider mesoscale processes involved in thunderstorm dynamics. In the simple thunderstorm model, low-level convergence induces vertical motion. Following the Dines compensation process, this surface convergence is coupled to divergence at upper levels to maintain mass continuity (Figure 2.2). The stronger the upward motion, the stronger the divergence.

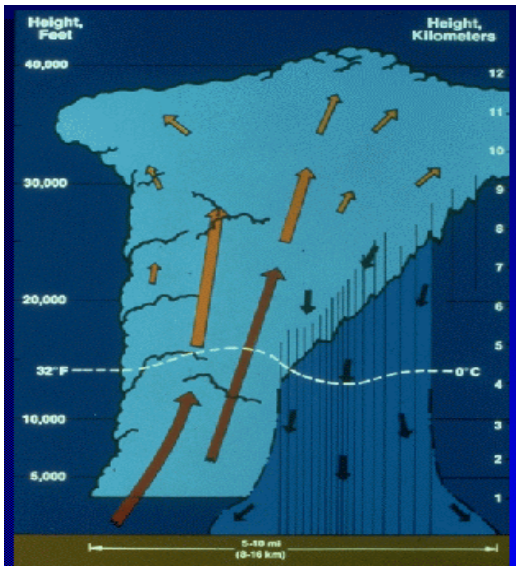

Figure 2.2. Simple thunderstorm model, illustrating Dines compensation. The updraft induced by low-level convergence results in upper level divergence, as mass "spreads out" as it reaches the tropopause. (From. Ref. University of Wisconsin-Stevens Point Department of Geology and Geography, http://www.uwsp.edu/geo/faculty/ritter/geog101/textbook/weather_systems/thunderstorms_p_2.htm, December 2004)

This theory can be applied to the previous descriptions of convection types to relate divergence to severe weather development. For single cell storms, the convection is brief and the updraft is relatively weak. Therefore, single cell storm cases will have relatively small divergence values aloft, since they exhibit weak, short-lived updrafts. The multicell storms are longer-lived, and have stronger, more sustained upward vertical motion. Therefore, multicell storms will exhibit stronger upper-level divergence values to counteract the stronger updrafts. Finally, supercell storms should show the strongest upper-level divergence values, as their intense, long-lived updrafts require large values of upper tropospheric divergence to maintain mass continuity.

Since most hail and tornado producing storms are of the multicell or supercell variety, it logically follows that any storm that produces severe weather will exhibit a strong upper level divergence signature due to the strong, long-lived updraft at the core of the storm. While much is known about the correlation between strong upper-level divergence and severe weather occurrences, virtually all previous studies have focused on synoptic-scale motions, specifically divergence related to upper level troughs and jet streaks. Beebe and Bates (1955) were among the first to hypothesize that upper tropospheric divergence located above low-level moisture, instability and convergence led to severe weather. House (1958) expanded on this idea, showing how jet stream divergence, combined with airmass modification, can lead to severe weather development. McNulty (1978) and Maddox and Doswell (1982) both demonstrated a relationship between severe weather in the central United States and upper-tropospheric divergence associated with jet streaks at 300 hPa. Rose, Hobbs, Locatelli and Stoelinga (2004) expanded on this idea, correlating tornado occurrence to entrance and exit regions of jet streaks.

One of the first severe weather studies to shift focus from synoptic scale divergence down to the mesoscale was David (1978). While not focusing on divergence, he tabulated a variety of other parameters such as temperature, dew point, wind speed and wind direction at various levels in the atmosphere at the time of tornado occurrences.

More recent studies have taken this idea further. Stensrud, Cortinas and Brooks (1997) attempted to discriminate between tornadic and nontornadic thunderstorms using

mesoscale model output. They did not look at divergence, but instead focused on helicity and Richardson number shear to indicate whether tornado development was likely. Mills and Colquhoun (1998) tried to objectively predict severe thunderstorm environments by linking a decision tree with a regional model in Australia. This study was the only one that actually used a mesoscale divergence "threshold" value. They did not focus on upper level divergence, however; they looked at low-level convergence as a lifting mechanism for thunderstorm development. They chose a threshold value at 900 hPa of -5.0×10^{-3} s^{-1} as a cutoff for severe thunderstorm development; any low-level convergence values less than this were deemed unsuitable for severe weather. Finally, Fowle and Roebber (2003) studied short-range prediction of convective occurrence, mode and location. While not determining divergence intensities or severe storms, they focused on forecast skill for convective events. They found that credible forecast information concerning convective occurrence can be obtained from forecast models to at least a 2-day forecast range.

The goal of this thesis is to focus specifically on the mesoscale divergence related to severe weather development. By quantifying the divergence data gathered from numerous model forecasts of individual storm systems, a reasonable "threshold" value or range of values indicative of hail or tornado producing severe storms will be obtained.

III. METHODS AND PROCEDURES

During the course of the research for this thesis, several hundred hail and tornado producing storms that occurred in the 15th OWS's area of responsibility during the spring and summer of 2004 were catalogued and investigated. The methods and procedures used to gather data on these severe storms is outlined below.

A. STORM IDENTIFICATION

Severe thunderstorm events were identified using the Storm Prediction Center's (SPC) database (http://www.spc.ncep.noaa.gov/exper/archive/events/searchindex.html). This website is a daily archive of all severe storm reports received by the SPC. The daily reports include a map of storm occurrences and a list of the day's severe storm events, from 12Z on the current day until 12Z the following day. A sample map is shown in Figure 3.1, and a sample storm listing, with appropriate storms highlighted in yellow, can be found in Appendix A. From these reports, all tornado or hail producing storms that occurred within 30 minutes of a model forecast hour were identified (plus or minus 30 minutes from 00Z, 03Z, 06Z, 09Z, 12Z, 15Z, 18Z, and 21Z). All storms that met these criteria were catalogued for further investigation.

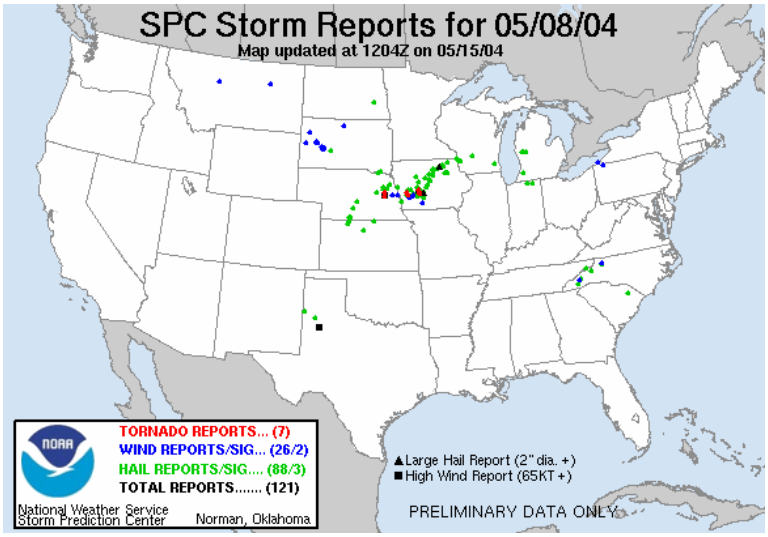

Figure 3.1. Sample SPC storm report map from 08 May 2004, covering 08 May / 12Z to 09 May / 12Z. (From Ref. Storm Prediction Center Severe Weather Events Archive, http://www.spc.ncep.noaa.gov/exper/archive/events/searchindex.html, January 2005)

B. RADAR DATA

Once the appropriate tornado or hail producing storms were identified from the SPC reports, NEXRAD radar data was used to further pinpoint storm location and time of occurrence. Since the SPC reports often contain multiple hail or tornado sightings from the same storm as it moves through an area, radar data is extremely useful to identify the single storm causing multiple severe weather reports. For example, the SPC report may contain hail reports at 2338Z, 2348Z, 2359Z and 0017Z, with similar latitudes and longitudes for each report. By looking at the radar loop and correlating each radar image with each hail report, it becomes clear that all four reports involve the same storm. In these instances, the time closest to the model forecast time is selected as the representative time and location for the storm (2359Z in the previous example). A sample radar image is shown in Figure 3.2.

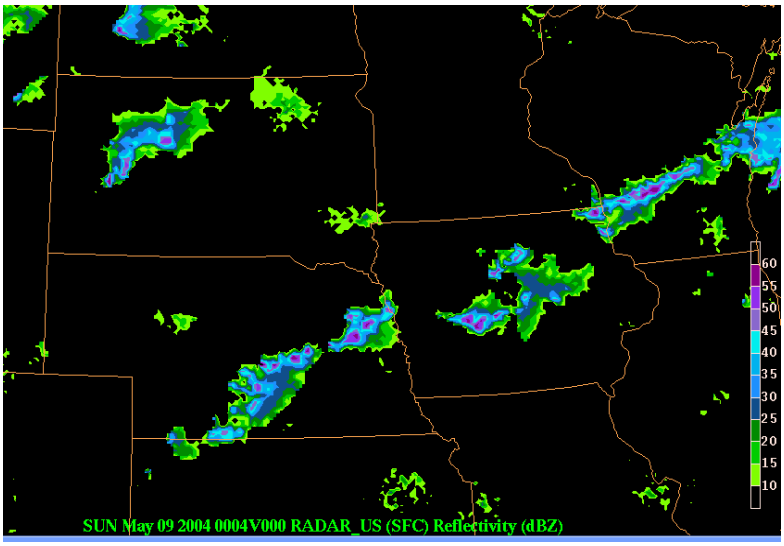

Figure 3.2. Example of a NEXRAD radar image from 09 May 2004 / 0004Z.

C. MODEL DATA

After the time and location of the individual storms have been identified using SPC reports and NEXRAD imagery, forecast data is utilized from both the ETA-212 and MM5 models out to a maximum of 21 hours. Using a program called REGRID (described below), the model grid is re-centered over the latitude and longitude of each

individual storm, and the model output is then interpolated to this new grid. Results of the REGRID process are viewed using a graphics program called VISUAL (described below, see Figure 3.3 for a VISUAL image of regridded ETA-212 divergence). At the conclusion of this step, each individual storm has a complete set of model data centered on the location of the storm at the time closest to the event occurrence. Details of both forecast models, as well as the REGRID and VISUAL programs, are provided below.

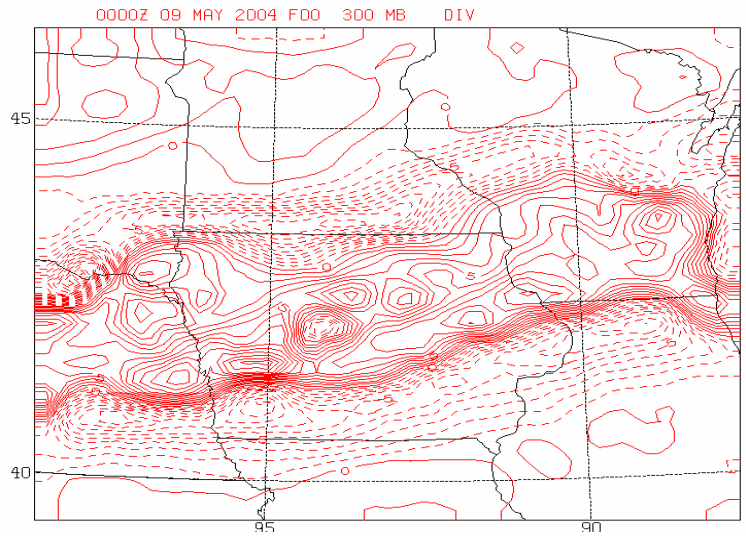

Figure 3.3. Example of regridded divergence data from the ETA-212 model for 09 May 2004 / 00Z, centered on a storm in central Iowa.

1. ETA-212 Information

The ETA-212 is a grid-point model using the Eta vertical coordinate system. The data utilized in this study uses a 12 kilometer horizontal resolution interpolated to a 40 km model grid, with 30 layers of vertical resolution (COMET Operational Models Matrix, http://meted.ucar.edu/nwp/pcu2/index.htm, February 2005). The model is initialized every six hours at 00Z, 06Z, 12Z and 18Z, with three hourly output intervals. Because of this, each severe weather case in this study has four separate ETA-212 model runs associated with it. For example, a storm occurring at 21Z will have the 21 hour forecast from the 00Z run, the 15 hour forecast from the 06Z run, the 9 hour forecast from the 12Z run, and the 3 hour forecast from the 18Z run. The ETA-212 provided the primary source of model data for this study; each storm from May through September was examined using this model. These results are described in chapters V and VI.

2. MM5 Information

The MM5 is a non-hydrostatic grid-point model that uses a sigma vertical coordinate system. The MM5 data used in this study came from the Air Force Weather Agency (AFWA). The AFWA MM5 model consists of a 15 km horizontal resolution and 23 levels of vertical resolution (COMET Operational Models Matrix, http://meted.ucar.edu/nwp/pcu2/index.htm, February 2005). The model is initialized every twelve hours at 06Z and 18Z, with three hourly output intervals. Additionally, there is no 0 hour analysis or 3 hour forecast for MM5 data; the model utilizes a 6 hour data assimilation period where short-term model forecasts are blended with updated observations to create a more accurate short-term product. As a result, the first data available from the 06Z and 18Z analyses are the blended 6 hour forecasts. Therefore, the storm cases in this study that utilize MM5 model data have either one or two individual model runs associated with them, depending on time of occurrence. For example, a storm occurring at 00Z will be encompassed by the 18 hour forecast from the 06Z run and the 6 hour forecast from the 18Z run. A storm occurring at 21Z, however, will only have one MM5 forecast associated with it: the 15 hour forecast from the 06Z run. Since there is no 3 hour forecast, the 18Z analysis will not cover a storm occurring at 21Z.

The MM5 provided a secondary source of model data for this study; 15 km horizontal resolution data was used to examine storms from the end of June through September. The MM5 results are compared to the same ETA-212 results in chapter VII.

3. The REGRID Program

The REGRID program is a FORTRAN program developed by Professor Wendell Nuss that takes gridded model fields on any grid and interpolates them to a user specified grid. The method uses multiquadric interpolation (Nuss and Titley 1994) where the interpolation to a specified point on the new grid is based on fitting the surrounding 36 grid points on the original grid. The approach is applied horizontally level by level to produce a three dimensional data set on the desired grid. The method allows for model data on all types of map projections (Lambert Conformal, Latitude/Longitude, Mercator,

etc) to be re-mapped to any other grid on a different map projection. This allows different models to be directly compared on the common grid.

4. The VISUAL Program

The VISUAL program is a FORTRAN program developed by Prof. Wendell Nuss to display a wide variety of meteorological datasets. The program is based on NCAR Graphics and XGKS graphical software for plotting. The program allows a variety of computations to be performed on gridded dataset in addition to plotting the grids. Horizontal, cross section, and sounding displays of basic and computed parameters can be done and overlaid on each other for comparison.

D. COMPOSITING CASES

The process described in parts A through C was repeated for each identified storm from May through September of 2004. After all of the individual storm cases were completed, the storms were composited together using a program called AVERAGE. AVERAGE is a FORTRAN program written by Prof. Wendell Nuss that takes a list of gridded datasets and computes the mean and standard deviation of the specified field at individual grid points. The result is a composite grid of the field over the domain which can then be displayed. The storms were categorized into type A and type B storms to group storms from the same model forecast hour together: Type A storms are the "on hour" storms that occurred at the hours of 00Z, 06Z, 12Z, and 18Z, which have model output times of f00, f06, f12 and f18. Type B storms are the "off hour" storms, occurring at 03Z, 09Z, 15Z and 21Z. These storms have model output times of f03, f09, f15 and f21. The individual storm cases were combined by forecast hour (f00, f03, f06, f09, f12, f15, f18, or f21) and by intensity (tornadic and hail storms combined together, as well as tornadic storms and hail producing storms grouped separately). The results from the various composite categories are presented in the remaining chapters of the thesis.

THIS PAGE INTENTIONALLY LEFT BLANK

IV. OVERVIEW OF 2004 SEVERE WEATHER REPORTS

A. STORM REPORTS BY STATE

A total of 755 storms were catalogued for the 2004 storm season – 110 tornadic storms and 645 hail producing storms. The vast majority of severe weather reports came from the Great Plains and Midwest, with scattered occurrences through the Appalachians region into New England. Tables 4.1 and 4.2 show the distribution of tornado and hail reports by state for the entire five-month period.

MAY - SEPT TORNADO REPORTS BY STATE	
State	**Number of Reports**
Nebraska	22
Iowa	20
Illinois	13
Minnesota	11
North Dakota	9
Indiana	7
South Dakota	6
Wisconsin	6
Michigan	5
Maryland	4
Pennsylvania	3
New York	2
New Jersey	2
Ohio	1

Table 4.1. May - Sept tornado reports by state.

MAY-SEPT HAIL REPORTS BY STATE	
State	**Number of Reports**
Nebraska	110
Iowa	81
South Dakota	81
Illinois	55
Minnesota	49
Michigan	43
Ohio	40
Indiana	38
North Dakota	38
Wisconsin	32
New York	23
Pennsylvania	22
West Virginia	14
Massachusetts	9
Connecticut	8
Maryland	6
Vermont	4
New Jersey	2
Maine	1
New Hampshire	1
Rhode Island	1

Table 4.2. May - Sept hail reports by state.

Tables 4.3 and 4.4 list the tornado and hail reports, by state, on a month by month basis. The monthly totals for each are listed in the header.

TORNADO REPORTS BY STATE							
May (59 Storms)		**June (18 Storms)**		**July (20 Storms)**		**Aug / Sept (13 Storms)**	
State	**# of Reports**	**State**	**# of Reports**	**State**	**# of Reports**	**State**	**# of Reports**
Nebraska	16	North Dakota	4	Illinois	3	Minnesota	4
Iowa	13	Iowa	3	North Dakota	3	Iowa	2
Illinois	9	Nebraska	2	Nebraska	3	Maryland	2
Indiana	5	Pennsylvania	2	Iowa	2	Indiana	1
Michigan	4	Illinois	1	Minnesota	2	North Dakota	1
Minnesota	4	Maryland	1	South Dakota	2	Nebraska	1
South Dakota	3	Michigan	1	Wisconsin	2	South Dakota	1
Wisconsin	2	Minnesota	1	Indiana	1	Wisconsin	1
Maryland	1	New Jersey	1	New Jersey	1		
North Dakota	1	New York	1	Ohio	1		
New York	1	Wisconsin	1				
Pennsylvania	1						

Table 4.3. Monthly tornado reports by state.

HAIL REPORTS BY STATE							
May (270 Storms)		**June (115 Storms)**		**July (137 Storms)**		**Aug / Sept (123 Storms)**	
State	**# of Reports**	**State**	**# of Reports**	**State**	**# of Reports**	**State**	**# of Reports**
Iowa	48	Nebraska	27	Nebraska	28	Minnesota	18
Nebraska	37	South Dakota	16	South Dakota	24	Nebraska	18
Illinois	32	North Dakota	12	Illinois	15	South Dakota	18
Ohio	28	Minnesota	10	North Dakota	12	Iowa	17
Indiana	24	Iowa	9	Minnesota	9	North Dakota	12
South Dakota	23	Michigan	9	Indiana	8	Pennsylvania	10
Michigan	18	Ohio	7	Iowa	7	Michigan	9
West Virginia	14	Wisconsin	7	Michigan	7	Wisconsin	7
Minnesota	12	Illinois	5	Wisconsin	7	New York	4
Wisconsin	11	Indiana	5	New York	6	Illinois	3
New York	10	New York	3	Maryland	4	Massachusetts	3
Pennsylvania	10	Connecticut	1	Massachusetts	3	Ohio	3
Connecticut	3	Massachusetts	1	Connecticut	2	Connecticut	2
Massachusetts	2	Maine	1	Ohio	2	Indiana	1
Maryland	2	New Jersey	1	Vermont	2		
North Dakota	2	Pennsylvania	1	Pennsylvania	1		
New Hampshire	1	Vermont	1	Rhode Island	1		
New Jersey	1						
Vermont	1						

Table 4.4. Monthly hail reports by state.

B. STORM REPORTS BY TIME

While an analysis of severe weather report location shows a majority occurring in the Midwest, an analysis of time of severe weather occurrence illustrates a strong correlation to late afternoon / early evening. Tables 4.5 and 4.6 show the distribution of tornado and hail reports by hour group.

MAY - SEPT TORNADO REPORTS BY HOUR GROUP	
Time	**Number of Reports**
00Z	50
03Z	15
06Z	2
09Z	1
12Z	2
15Z	3
18Z	6
21Z	31

Table 4.5. May - Sept tornado reports by hour group.

MAY - SEPT HAIL REPORTS BY HOUR GROUP	
Time	**Number of Reports**
00Z	211
03Z	112
06Z	39
09Z	15
12Z	15
15Z	21
18Z	60
21Z	172

Table 4.6. May - Sept hail reports by hour group.

Note that the majority of reported severe events occurred at either 21Z, 00Z or 03Z. Tables 4.7 and 4.8 show the month by month breakdown of severe storm report times. The monthly totals for each are listed in the header.

TORNADO REPORTS BY HOUR GROUP							
May (59 Storms)		**June (18 Storms)**		**July (20 Storms)**		**Aug / Sept (13 Storms)**	
Time	**# of Reports**	**Time**	**# of Reports**	**Time**	**# of Reports**	**Time**	**# of Reports**
00Z	32	00Z	6	00Z	6	00Z	6
03Z	8	03Z	3	03Z	3	03Z	1
06Z	0	06Z	1	06Z	1	06Z	0
09Z	0	09Z	0	09Z	0	09Z	1
12Z	1	12Z	0	12Z	0	12Z	1
15Z	1	15Z	0	15Z	1	15Z	1
18Z	1	18Z	2	18Z	2	18Z	1
21Z	16	21Z	6	21Z	7	21Z	2

Table 4.7. Monthly tornado reports by hour group.

HAIL REPORTS BY HOUR GROUP							
May (270 Storms)		**June (115 Storms)**		**July (137 Storms)**		**Aug / Sept (123 Storms)**	
Time	**# of Reports**	**Time**	**# of Reports**	**Time**	**# of Reports**	**Time**	**# of Reports**
00Z	90	00Z	42	00Z	31	00Z	48
03Z	47	03Z	21	03Z	28	03Z	16
06Z	17	06Z	4	06Z	15	06Z	3
09Z	8	09Z	1	09Z	3	09Z	3
12Z	9	12Z	2	12Z	2	12Z	2
15Z	10	15Z	4	15Z	3	15Z	4
18Z	19	18Z	14	18Z	14	18Z	13
21Z	70	21Z	27	21Z	41	21Z	34

Table 4.8. Monthly hail reports by hour group.

Complete listings of each storm event utilized in this study can be found in Appendices B through F. Storms are listed by month, date, time, location, latitude and longitude, storm type (A or B), and whether ETA-212 and/or MM5 data was analyzed.

V. DIVERGENCE ANALYSIS – ETA-212, F00 AND F03

This chapter examines the composite divergence charts from the 0 and 3 hour ETA-212 model forecasts to establish baseline divergence threshold values. The following section examines composites from the entire 2004 storm season. Each image in this chapter shows a 375 km X 375 km area, while the maximum value scatter plots are taken over a 105 km X 105 km region.

A. DIVERGENCE COMPOSITES - 2004 STORM SEASON

The composite divergence images and scatter plots in this section are comprised of storms from the entire 2004 storm season (May through September).

1. Type A Tornadic and Hail Producing Storms – 0 Hour Analysis

There were a total of 385 type A storms (tornado producing and hail producing combined) reported in 2004. The 0 hour composite from these storms is shown in Figure 5.1. From these 385 events, the composite chart shows an average divergence value of 2.6×10^{-5} s^{-1} at the center of the region.

Figure 5.1. 0 hour divergence composite from all reported type A tornado and hail events during the 2004 storm season. The image consists of a 375 km X 375 km area with a 0.2 contour interval.

A scatter plot of the maximum divergence value from each of the 385 storms is shown in Figure 5.2. The average of these maximum values is 8.5 x 10^{-5} s^{-1}, with a standard deviation of 5.5 x 10^{-5} s^{-1}.

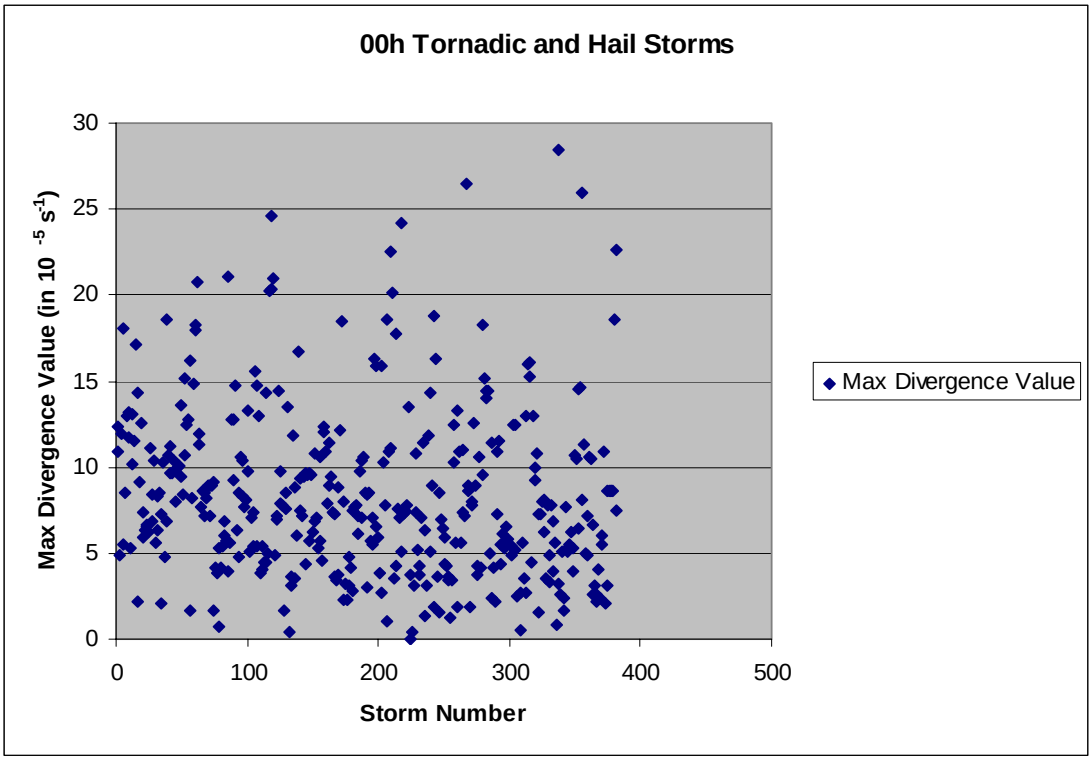

Figure 5.2. Maximum divergence values from the 0 hour analysis of all reported type A tornado and hail events during the 2004 storm season. The maxima were taken from a 52.5 km radius around the center point of the model grid.

2. Type A Tornadic Storms – 0 Hour Analysis

There were 60 type A tornado producing storms in 2004. The 0 hour composite chart from these storms is shown in Figure 5.3. These storms produced a composite divergence value of 3.0×10^{-5} s^{-1} at the center of the image.

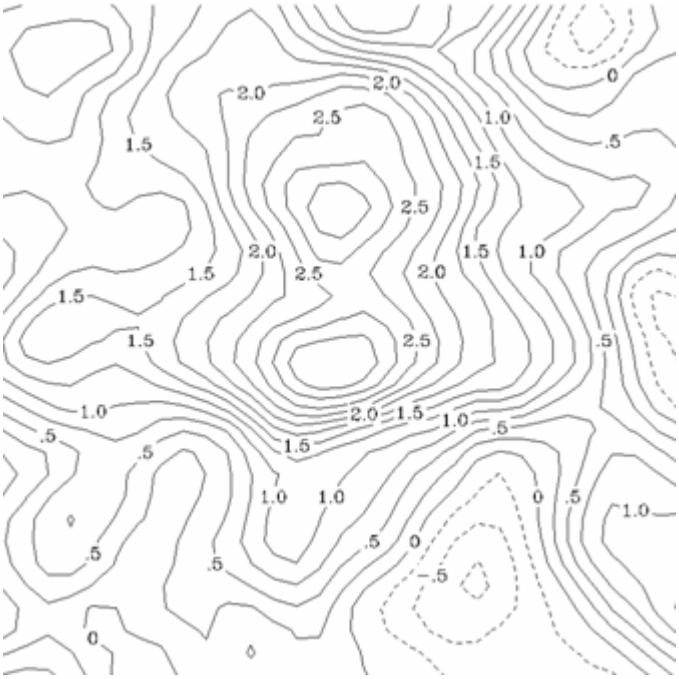

Figure 5.3. 0 hour divergence composite from all reported type A tornado events during the 2004 storm season. The image consists of a 375 km X 375 km area with a 0.25 contour interval.

Figure 5.4 displays the scatter plot of maximum divergence values from these 60 tornadic storms. The average of the tornadic maximum values is 8.3 x 10^{-5} s^{-1}, with a standard deviation of 4.5 x 10^{-5} s^{-1}.

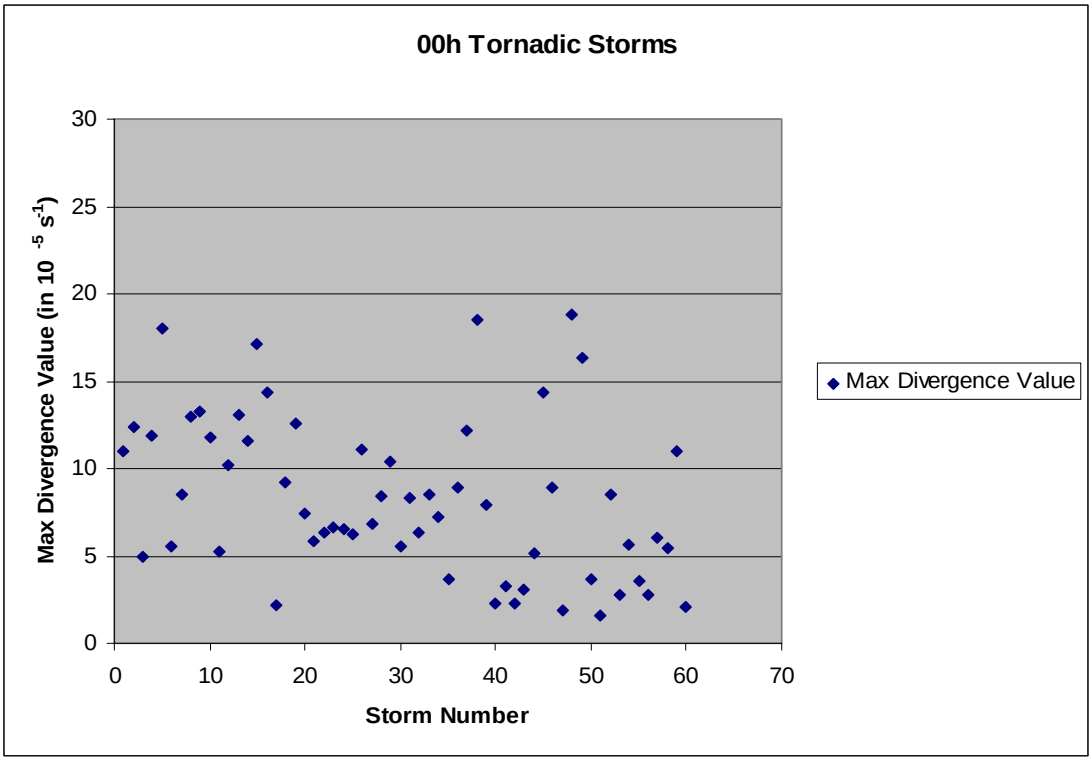

Figure 5.4. Maximum divergence values from the 0 hour analysis of all reported type A tornado events during the 2004 storm season. The maxima were taken from a 52.5 km radius around the center point of the model grid.

3. Type A Hail Producing Storms – 0 Hour Analysis

There were 325 hail producing type A storms during the 2004 storm season. The 0 hour composite chart from these storms is shown in Figure 5.5. The composite of the 325 hail storms shows an average divergence value of 2.5 x 10^{-5} s^{-1} at the center of the domain.

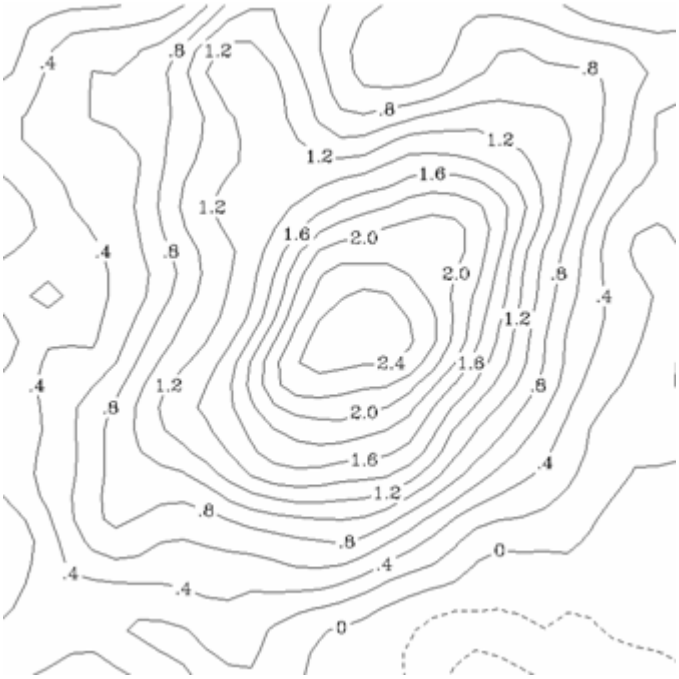

Figure 5.5. 0 hour divergence composite from all reported type A hail events during the 2004 storm season. The image consists of a 375 km X 375 km area with a 0.2 contour interval.

The scatter plot of maximum divergence values from the 325 hail producing storms is shown in Figure 5.6 below. The average of the maximum values from the hail storms is 8.6 x 10^{-5} s^{-1}, with a standard deviation of 5.7 x 10^{-5} s^{-1}.

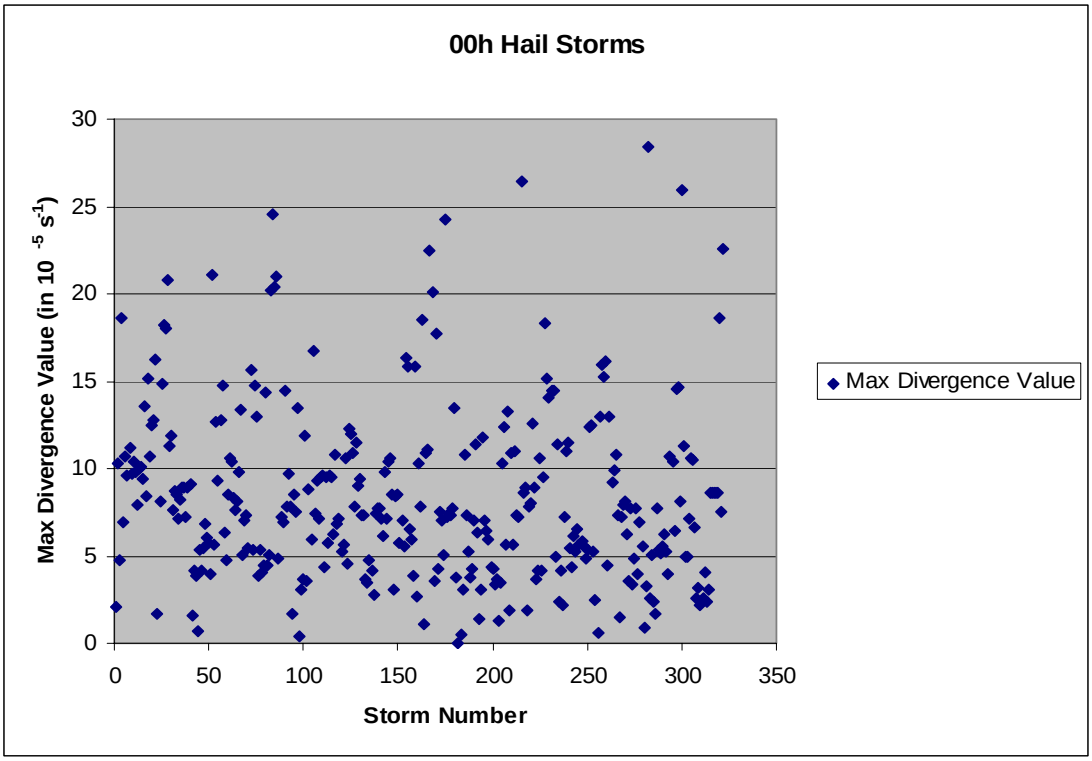

Figure 5.6. Maximum divergence values from the 0 hour analysis of all reported type A hail events during the 2004 storm season. The maxima were taken from a 52.5 km radius around the center point of the model grid.

4. Type B Tornadic and Hail Producing Storms – 3 Hour Forecast

There were a total of 370 type B storms (tornado producing and hail producing combined) reported in 2004. The 3 hour composite from these storms is shown in Figure 5.7. From these 370 events, the composite chart shows an average divergence value of 1.6×10^{-5} s^{-1} at the center of the region.

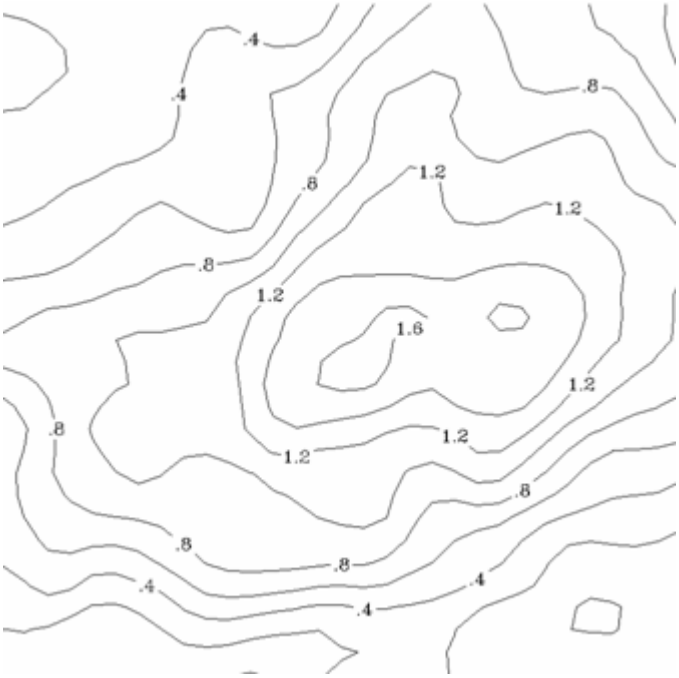

Figure 5.7. 3 hour divergence composite from all reported type B tornado and hail events during the 2004 storm season. The image consists of a 375 km X 375 km area with a 0.2 contour interval.

Figure 5.8 displays the scatter plot of maximum divergence values from each of the 370 storms. The average of these maximum values is 7.8 x 10^{-5} s^{-1}, with a standard deviation of 4.4 x 10^{-5} s^{-1}.

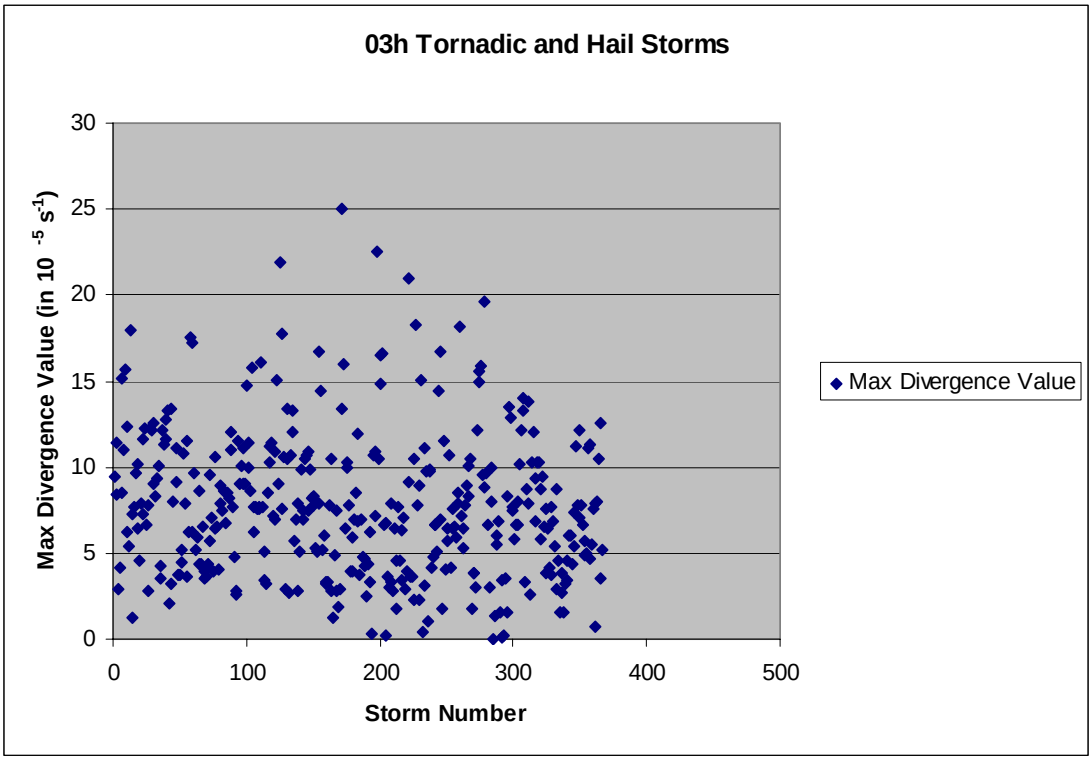

Figure 5.8. Maximum divergence values from the 3 hour forecast of all reported type B tornado and hail events during the 2004 storm season. The maxima were taken from a 52.5 km radius around the center point of the model grid.

5. Type B Tornadic Storms – 3 Hour Forecast

There were 50 type B tornado producing storms in 2004. The 3 hour composite chart from these storms is shown in Figure 5.9. These storms produced a composite divergence value of 2.1 x 10^{-5} s^{-1} at the upper left center of the domain.

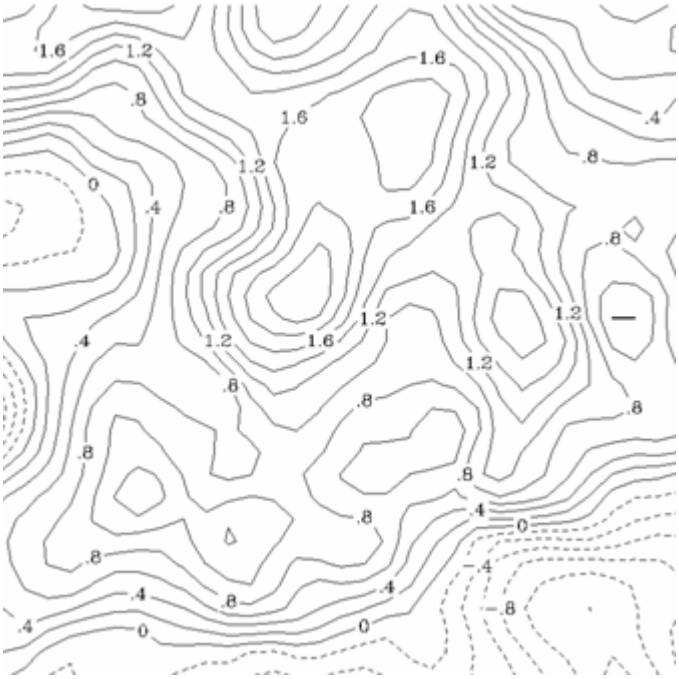

Figure 5.9. 3 hour divergence composite from all reported type B tornado events during the 2004 storm season. The image consists of a 375 km X 375 km area with a 0.2 contour interval.

Figure 5.10 displays the scatter plot of maximum divergence values from these 50 tornadic storms. The average of the maximum values is 7.7 x 10^{-5} s^{-1}, with a standard deviation of 4.5 x 10^{-5} s^{-1}.

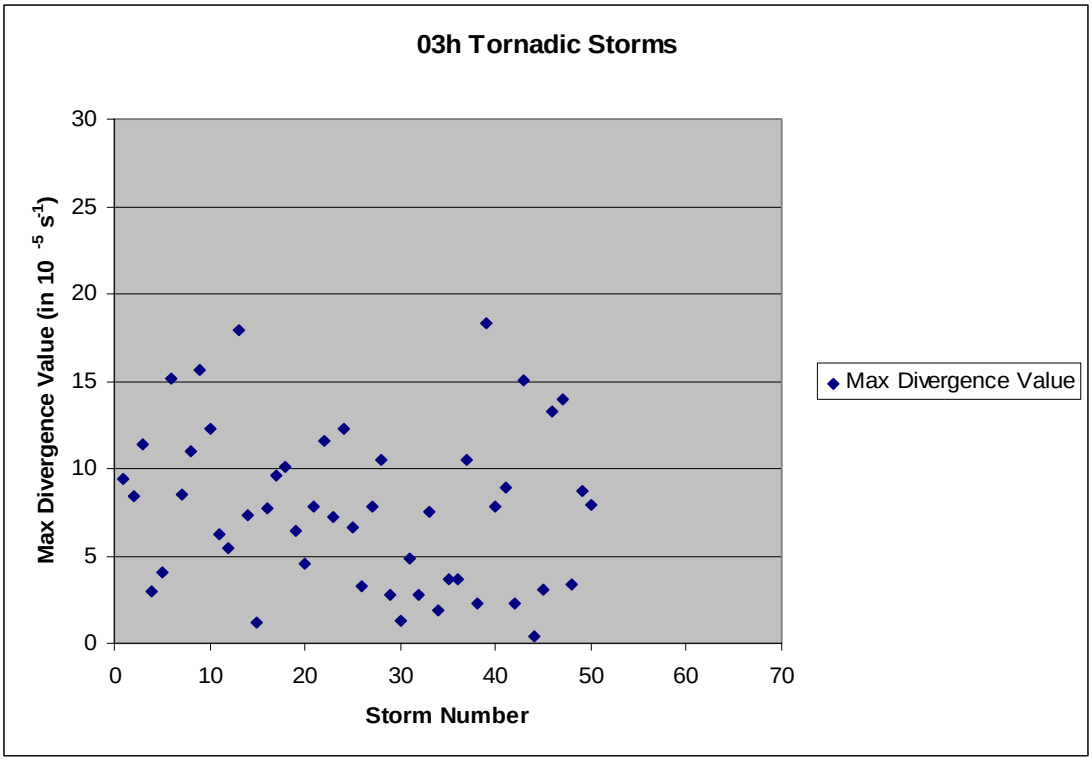

Figure 5.10. Maximum divergence values from the 3 hour forecast of all reported type B tornado events during the 2004 storm season. The maxima were taken from a 52.5 km radius around the center point of the model grid.

6. Type B Hail Producing Storms – 3 Hour Forecast

There were 320 hail producing type B storms during the 2004 storm season. The 3 hour composite chart from these storms is shown in Figure 5.11. The composite of the 320 hail storms shows an average divergence value of 1.7×10^{-5} s^{-1} at the center of the region.

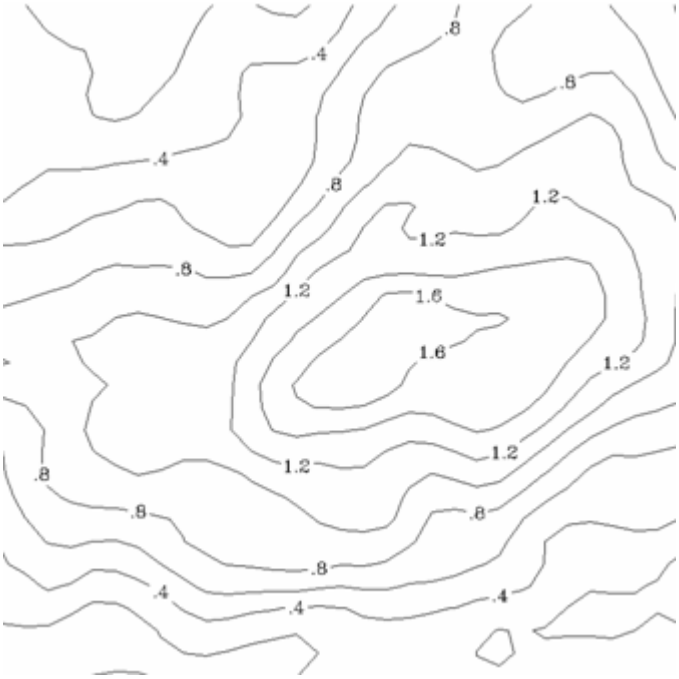

Figure 5.11. 3 hour divergence composite from all reported type B hail events during the 2004 storm season. The image consists of a 375 km X 375 km area with a 0.2 contour interval.

The scatter plot of maximum divergence values from the 320 hail producing storms is shown in Figure 5.12 below. The average of the maximum values from the hail storms is 7.8 x 10^{-5} s^{-1}, with a standard deviation of 4.4 x 10^{-5} s^{-1}.

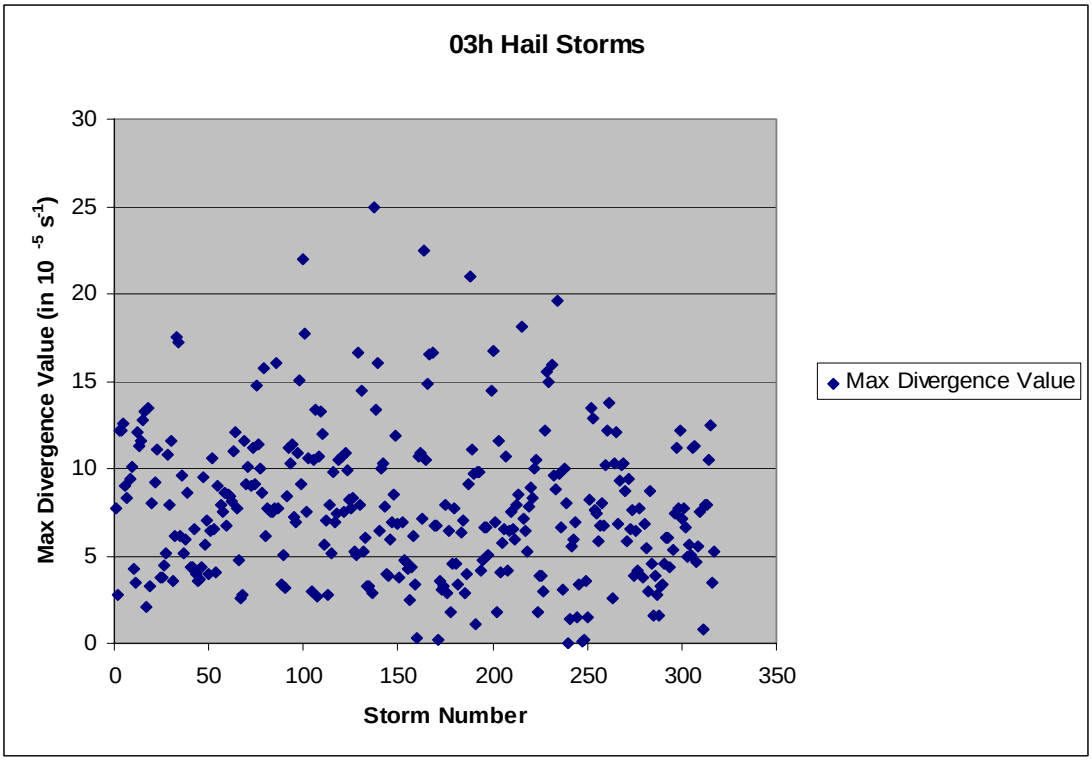

Figure 5.12. Maximum divergence values from the 3 hour forecast of all reported type B hail events during the 2004 storm season. The maxima were taken from a 52.5 km radius around the center point of the model grid.

7. Discussion of 0 Hour and 3 Hour Seasonal Composites

The divergence values gathered from the 0 and 3 hour model time steps will be considered the "baseline" values indicative of severe events. While the values derived from Figures 5.1 – 5.12 are significant, it is important to consider them in their proper context. The contour plots are derived from an averaging of both the locations and magnitudes of divergence values across the entire domain. The contours give a good indication of how well the model is resolving the divergence forecast; a local maximum centered on the domain of the composite provides a good general indication of the types of divergence values that represent severe storms. The scatter plots look at the data in a different way: they are independent of location, focusing only on the magnitude of the maximum divergence value anywhere within a 52.5 km radius of the center of the

sampled storms. This approach derives a more accurate depiction of the divergence intensity at the expense of the location of the maxima, but the 52.5 km radius was chosen as a reasonable "error area" for the divergence maxima to vary across.

Table 5.1 summarizes the results of sections 1 through 6. Results of each case are shown, with time, storm type and sample size displayed along with the average divergence values from both the contour plots and scatter plots. The standard deviation from the scatter plots is shown as well.

Time	Storm Type	Sample Size	Contoured Max. Divergence	Scatter Plot Max. Divergence	Scatter Plot Standard Deviation
00h	All	385 Storms	$2.6 \times 10^{-5}\ s^{-1}$	$8.5 \times 10^{-5}\ s^{-1}$	$5.5 \times 10^{-5}\ s^{-1}$
00h	Tornado	60 Storms	$3.0 \times 10^{-5}\ s^{-1}$	$8.3 \times 10^{-5}\ s^{-1}$	$4.5 \times 10^{-5}\ s^{-1}$
00h	Hail	325 Storms	$2.5 \times 10^{-5}\ s^{-1}$	$8.6 \times 10^{-5}\ s^{-1}$	$5.7 \times 10^{-5}\ s^{-1}$
03h	All	370 Storms	$1.6 \times 10^{-5}\ s^{-1}$	$7.8 \times 10^{-5}\ s^{-1}$	$4.4 \times 10^{-5}\ s^{-1}$
03h	Tornado	50 Storms	$2.1 \times 10^{-5}\ s^{-1}$	$7.7 \times 10^{-5}\ s^{-1}$	$4.5 \times 10^{-5}\ s^{-1}$
03h	Hail	320 Storms	$1.7 \times 10^{-5}\ s^{-1}$	$7.8 \times 10^{-5}\ s^{-1}$	$4.4 \times 10^{-5}\ s^{-1}$

Table 5.1. Average maximum divergence values and standard deviation for the six cases presented in section A.

In all three cases (all storms, tornadic storms, and hail producing storms), the average divergence values drop significantly from the 0h to the 3h time period, and the standard deviation values in the "all" and "hail" cases fall as well. The maximum divergence values should be expected to decrease with increasing time due to increasing forecast error, but the slight drop in the standard deviation values is somewhat surprising. This result is most likely due to the effect of the model resolving differences in initialization data; the 0 hour standard deviations are probably higher due to a wide range of observations put in during the model analysis. Most of the initial imbalances are gone by the 3 hour point, resulting in a drop in the standard deviation values.

THIS PAGE INTENTIONALLY LEFT BLANK

VI. DIVERGENCE FORECASTS – ETA-212, F06 THROUGH F21

This chapter investigates the divergence composites for the 6 hour through 21 hour ETA-212 model forecasts from the entire 2004 storm season. As in the previous chapter, each divergence chart in chapter VI consists of a 375 km X 375 km domain and the scatter plots are derived from a 105 km X 105 km region.

A. DIVERGENCE COMPOSITES – ENTIRE 2004 STORM SEASON

The composite divergence images and scatter plots in this section are made up of storms from the entire 2004 storm season (May through September).

1. Type A Tornadic and Hail Producing Storms – 6, 12 and 18 Hour Forecasts

The 6, 12, and 18 hour composite divergence charts from the 385 type A storms (tornado and hail producing combined) reported in 2004 are displayed in Figure 6.1. All three composite divergence charts show a distinct maximum in the upper portion of the domain. 6.1.a), the 6 hour forecast composite, shows a maximum divergence value of 1.8 x 10^{-5} s^{-1} in the upper center of the image. The 12 hour composite, shown in 6.1.b), has a max of 1.4 x 10^{-5} s^{-1} in the same approximate location. 6.1.c), the 18 hour composite, shows the same maximum value as the 12 hour chart, 1.4 x 10^{-5} s^{-1} in the same location.

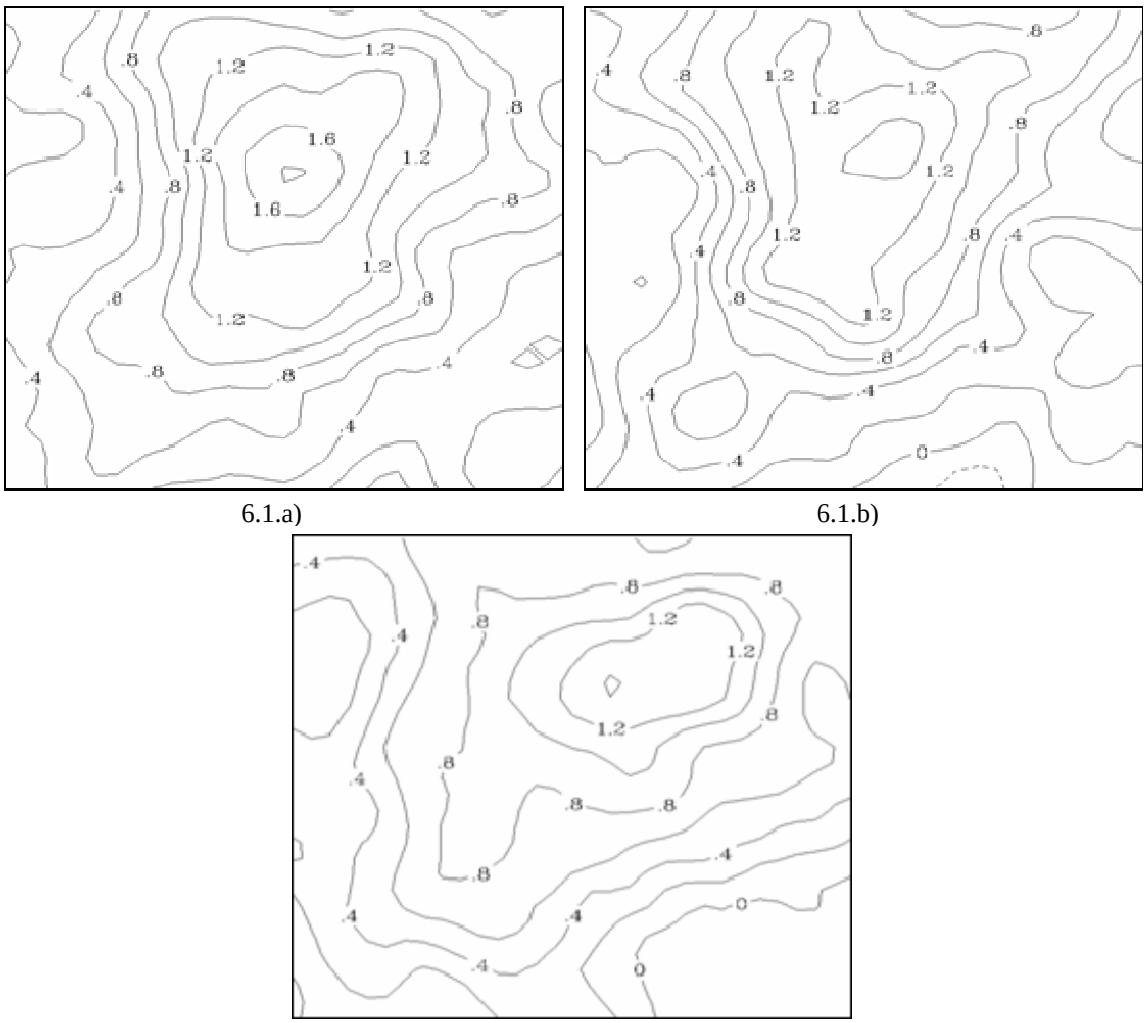

6.1.a) 6.1.b)

6.1.c)

Figure 6.1. 6, 12, and 18 hour divergence composites from all reported type A tornado and hail events during the 2004 storm season. 6.1.a) is the 6 hour image, 6.1.b) is the 12 hour, and 6.1.c) is the 18 hour. Each image consists of a 375 km X 375 km area with a 0.2 contour interval.

Scatter plots of the maximum divergence values from the 6, 12, and 18 hour forecasts of the 385 type A storms are shown in Figure 6.2. The 6 hour plot, 6.2.a), has an average of 7.2 x 10^{-5} s^{-1} with a standard deviation of 5.0 x 10^{-5} s^{-1}. The 12 hour plot, shown in 6.2.b), results in an average of 7.5 x 10^{-5} s^{-1} and a standard deviation of 5.4 x 10^{-5} s^{-1}. 6.2.c), the 18 hour plot, shows an average of 6.9 x 10^{-5} s^{-1} with a standard deviation of 5.7 x 10^{-5} s^{-1}.

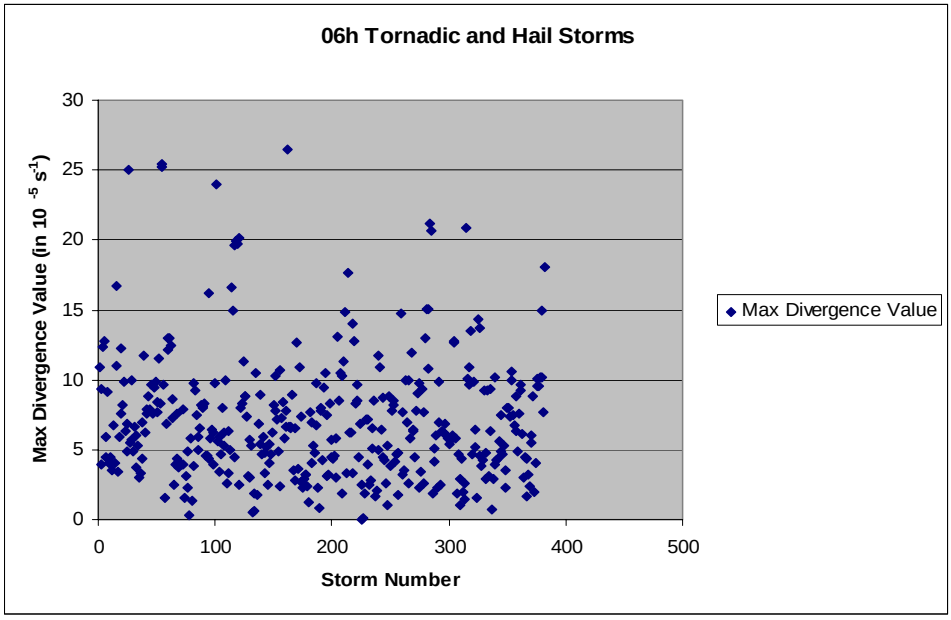

6.2.a)

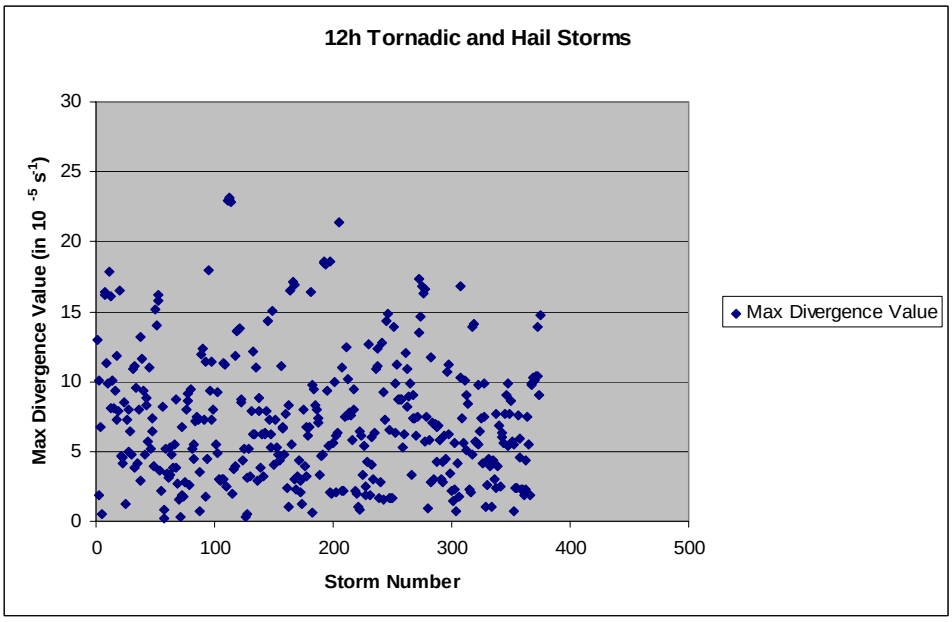

6.2.b)

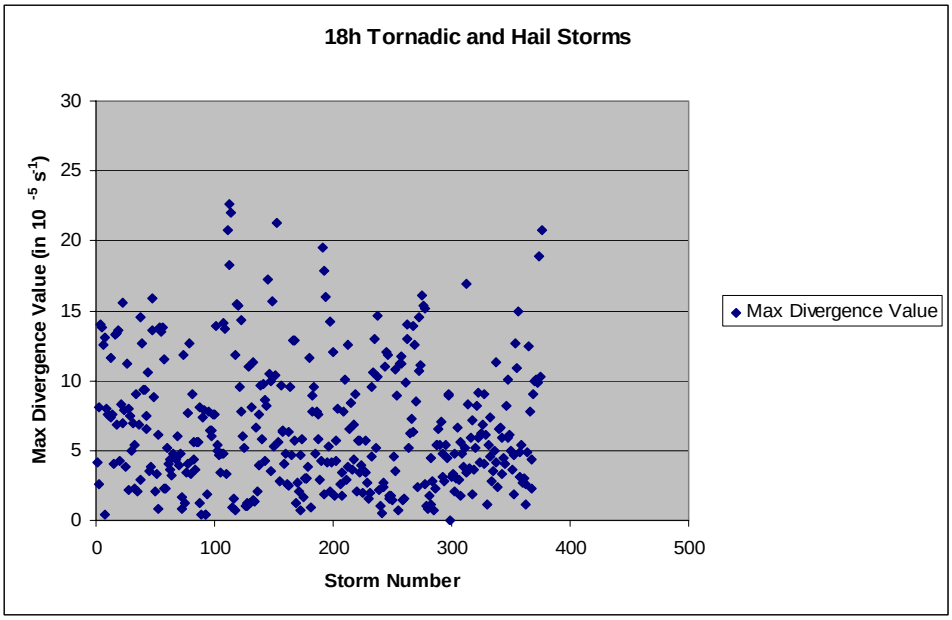

6.2.c)

Figure 6.2. Maximum divergence values from the 6, 12 and 18 hour forecasts of all reported type A tornado and hail events during the 2004 storm season. The maxima were taken from a 52.5 km radius around the center point of the model grid. 6.2.a) is the 6 hour plot, 6.2.b) the 12 hour, and 6.2.c) the 18 hour.

2. Type A Tornadic Storms – 6, 12, and 18 Hour Forecasts

The 6, 12, and 18 hour composite divergence charts from the 60 type A tornado producing storms reported in 2004 are displayed in Figure 6.3. 6.3.a), the 6 hour forecast composite, shows two divergence maxima: 1.9×10^{-5} s $^{-1}$ near the middle of the image, and 2.2×10^{-5} s $^{-1}$ at the upper left. The 12 hour composite, shown in 6.3.b), shows a divergence maximum of 2.2×10^{-5} s $^{-1}$ in the upper left corner of the chart. The 18 hour composite, displayed in 6.3.c), has a maximum of 2.1×10^{-5} s $^{-1}$ in the upper center of the diagram.

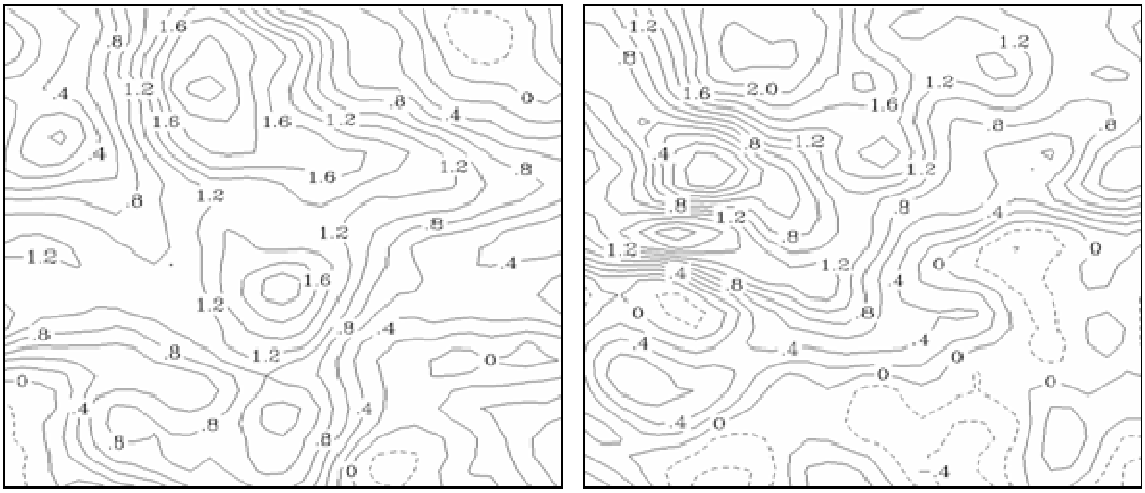

6.3.a) 6.3.b)

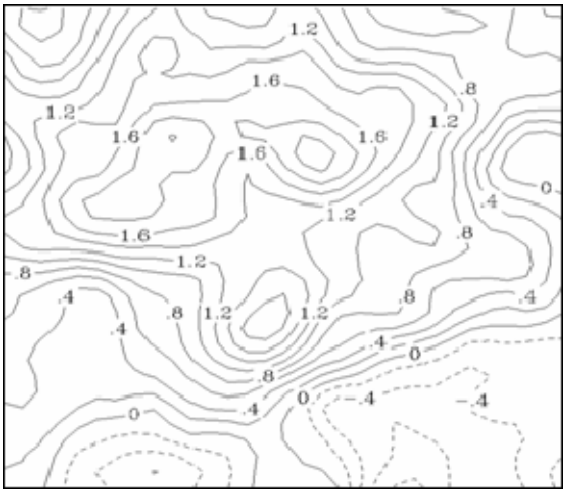

6.3.c)

Figure 6.3. 6, 12, and 18 hour divergence composites from all reported type A tornado events during the 2004 storm season. 6.3.a) is the 6 hour image, 6.3.b) is the 12 hour, and 6.3.c) is the 18 hour. Each image consists of a 375 km X 375 km area with a 0.2 contour interval.

Scatter plots of the maximum divergence values from the 6, 12, and 18 hour forecasts of the 60 type A tornadic storms are shown in Figure 6.4. The 6 hour plot, 6.4.a), has an average of 6.6 x 10^{-5} s^{-1} with a standard deviation of 4.1 x 10^{-5} s^{-1}. The 12 hour plot, shown in 6.4.b), results in an average of 8.4 x 10^{-5} s^{-1} and a standard deviation of 5.9 x 10^{-5} s^{-1}. 6.4.c), the 18 hour plot, shows an average of 7.3 x 10^{-5} s^{-1} with a standard deviation of 4.2 x 10^{-5} s^{-1}.

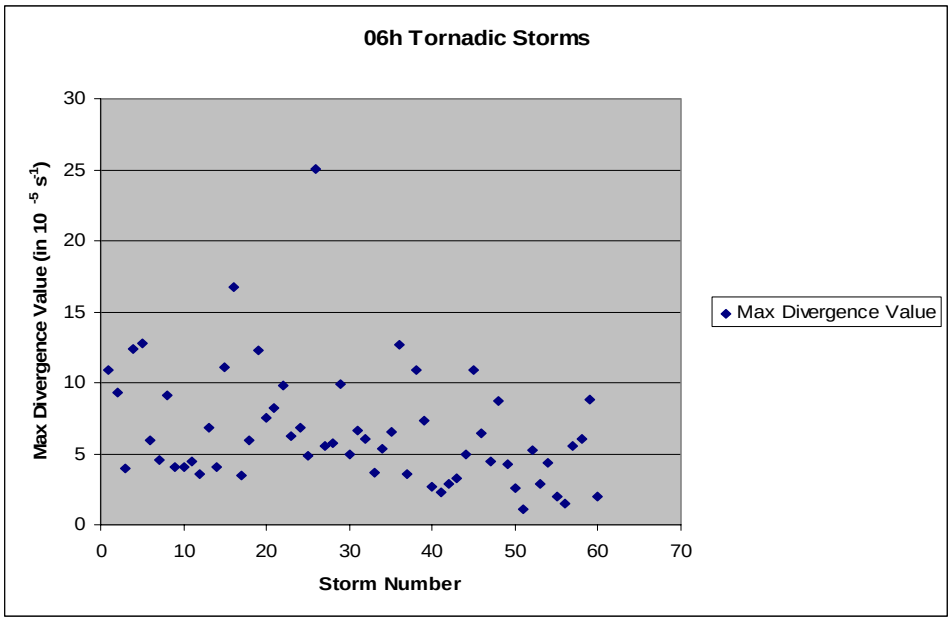

6.4.a)

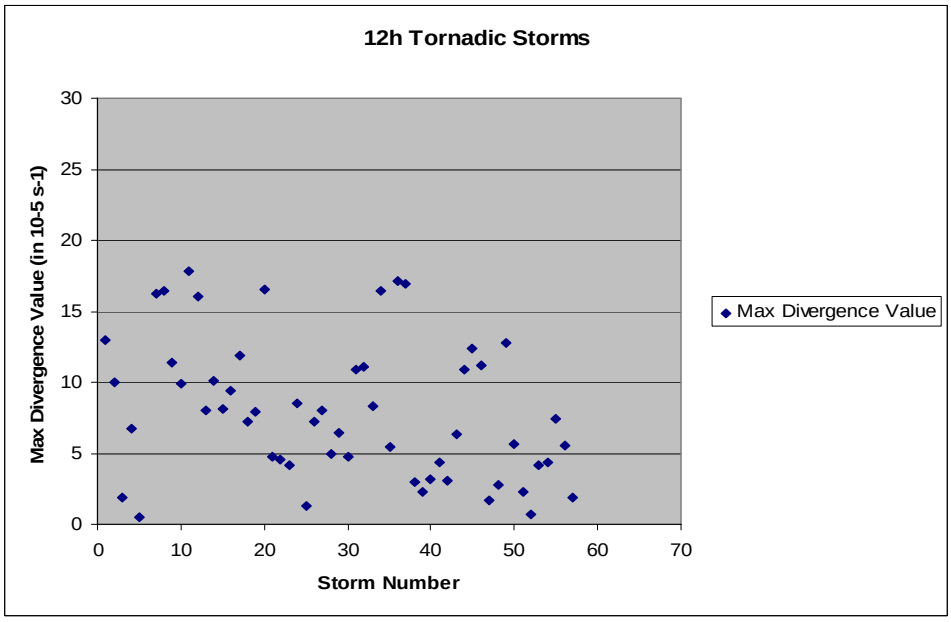

6.4.b)

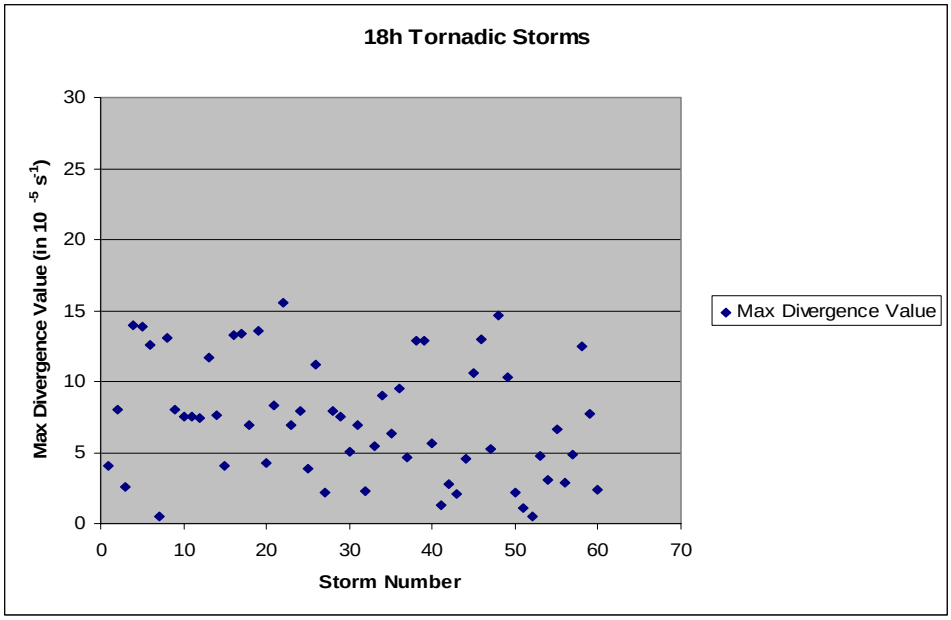

6.4.c)

Figure 6.4. Maximum divergence values from the 6, 12 and 18 hour forecasts of all reported type A tornado events during the 2004 storm season. The maxima were taken from a 52.5 km radius around the center point of the model grid. 6.4.a) is the 6 hour plot, 6.4.b) the 12 hour, and 6.4.c) the 18 hour.

3. Type A Hail Producing Storms – 6, 12, and 18 Hour Forecasts

The 6, 12, and 18 hour composite divergence charts from the 325 type A hail producing storms reported in 2004 are displayed in Figure 6.5. 6.5.a), the 6 hour forecast composite, shows a divergence maximum of 1.8×10^{-5} s $^{-1}$ at the upper center of the image. The 12 hour composite, shown in 6.5.b), also has its area of maximum divergence at the upper center of the image, with a magnitude of 1.4×10^{-5} s $^{-1}$. The 18 hour composite, displayed in 6.5.c), has a maximum of 1.3×10^{-5} s $^{-1}$ located in the upper right of the domain.

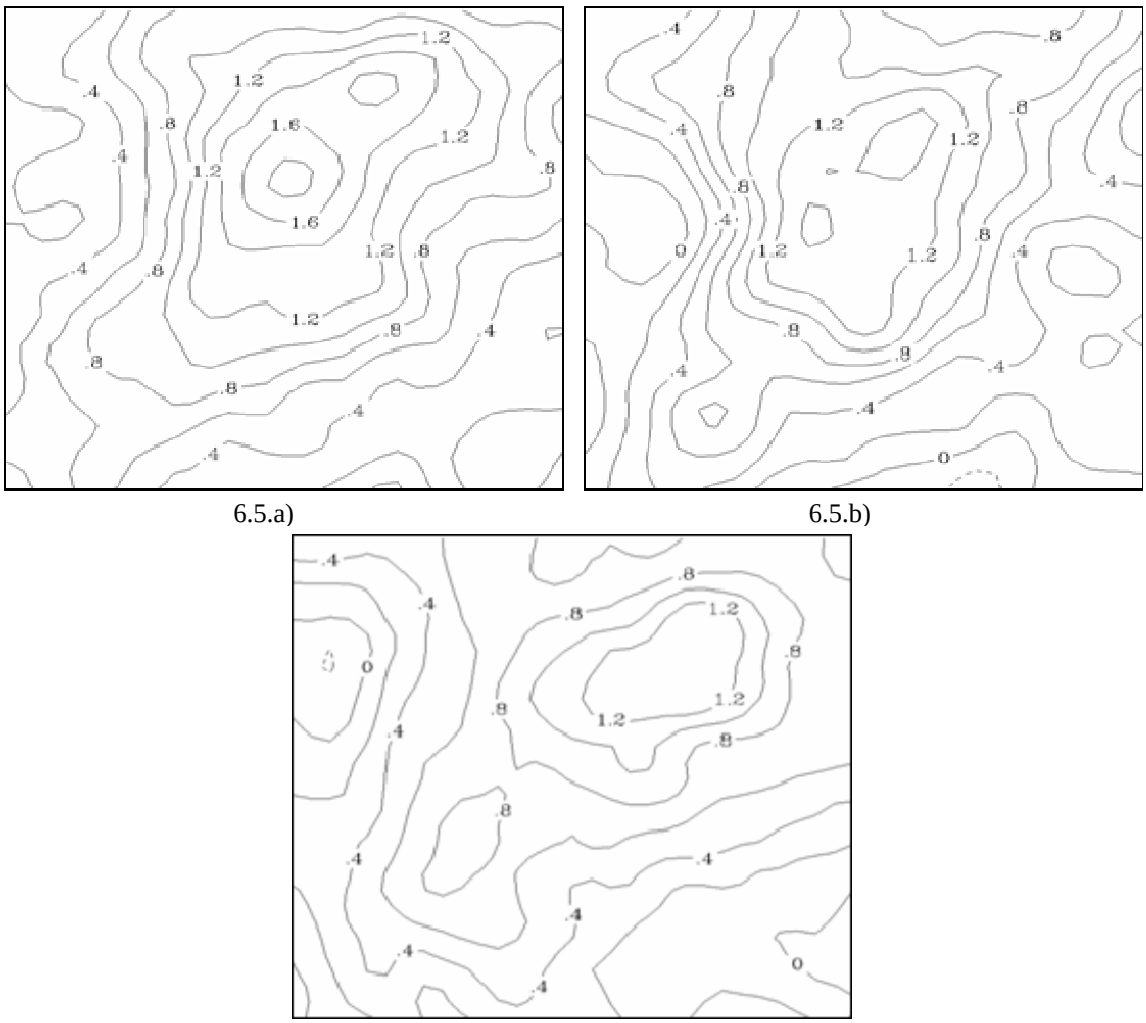

6.5.a) 6.5.b)

6.5.c)

Figure 6.5. 6, 12, and 18 hour divergence composites from all reported type A hail events during the 2004 storm season. 6.5.a) is the 6 hour image, 6.5.b) is the 12 hour, and 6.5.c) is the 18 hour. Each image consists of a 375 km X 375 km area with a 0.2 contour interval.

Figure 6.6 displays the scatter plots of maximum divergence values from the 6, 12, and 18 hour forecasts of the 325 type A hail storms. The 6 hour plot, 6.6.a), has an average of 7.3 x 10^{-5} s^{-1} with a standard deviation of 5.2 x 10^{-5} s^{-1}. The 12 hour plot, shown in 6.6.b), results in an average of 7.3 x 10^{-5} s^{-1} and a standard deviation of 5.3 x 10^{-5} s^{-1}. 6.6.c), the 18 hour plot, shows an average of 6.8 x 10^{-5} s^{-1} with a standard deviation of 5.9 x 10^{-5} s^{-1}.

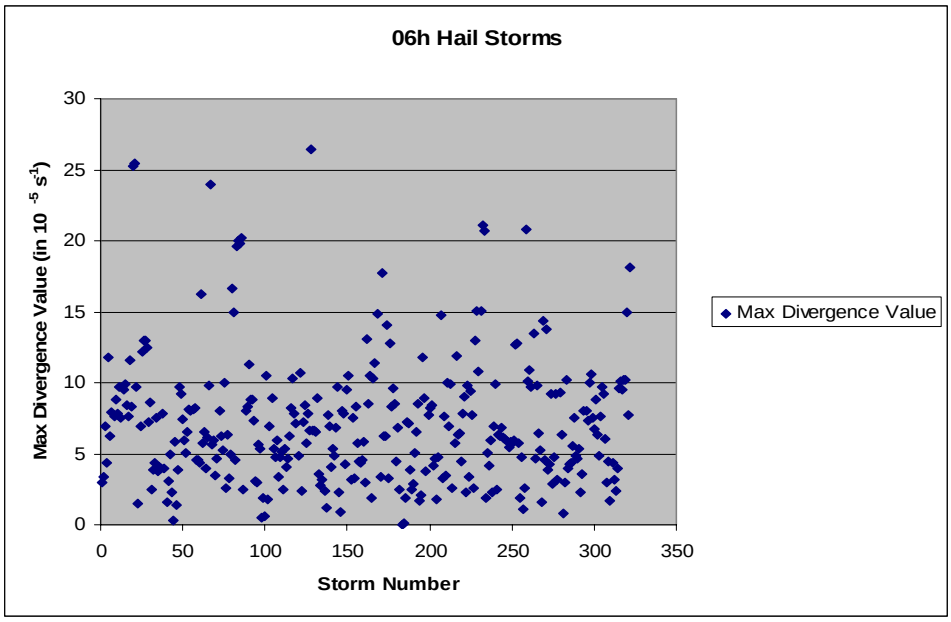

6.6.a)

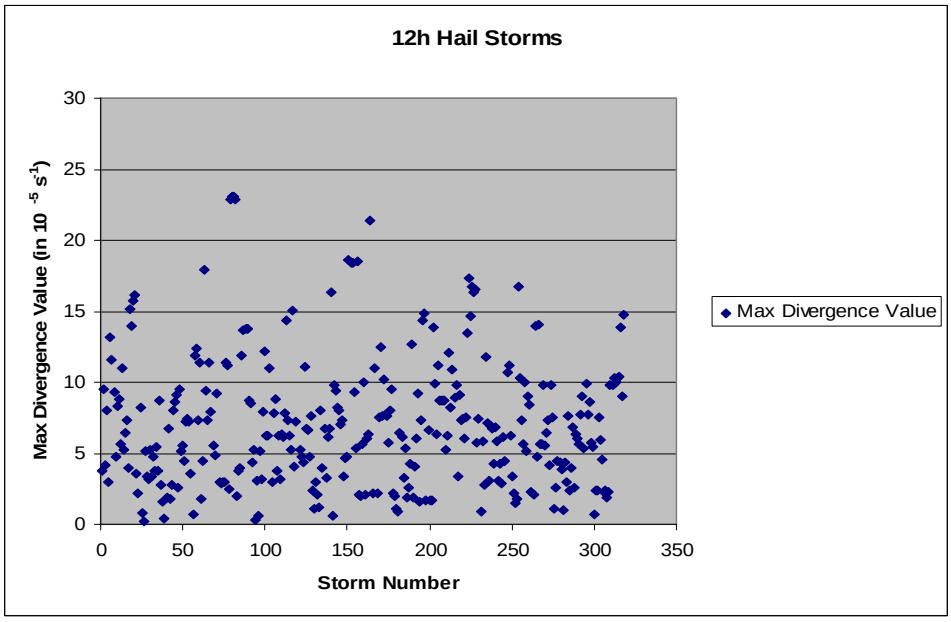

6.6.b)

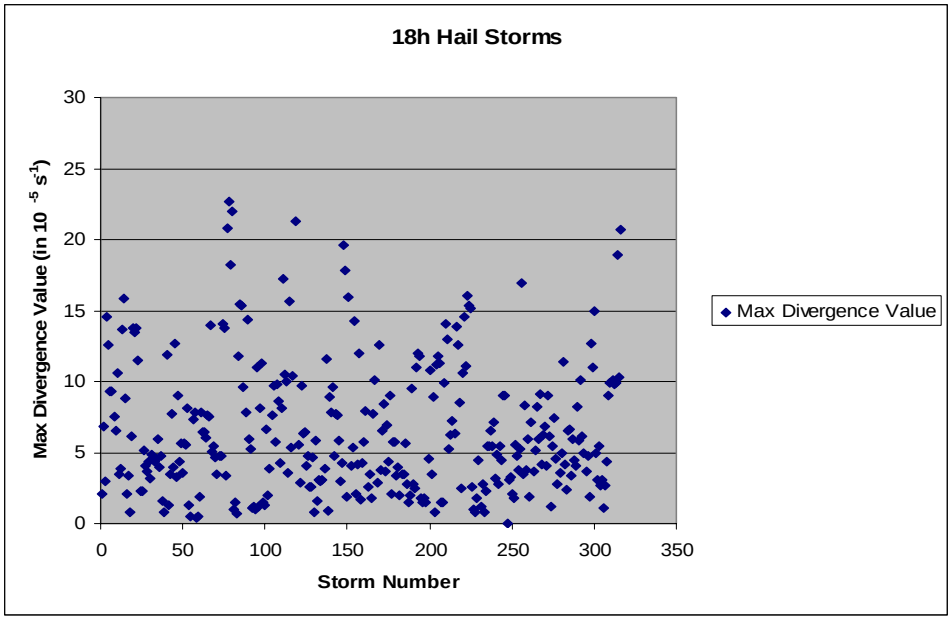

6.6.c)

Figure 6.6. Maximum divergence values from the 6, 12 and 18 hour forecasts of all reported type A hail events during the 2004 storm season. The maxima were taken from a 52.5 km radius around the center point of the model grid. 6.6.a) is the 6 hour plot, 6.6.b) the 12 hour, and 6.6.c) the 18 hour.

4. Type B Tornadic and Hail Producing Storms – 9, 15, and 21 Hour Forecasts

The 9, 15, and 21 hour composite divergence charts from the 370 type B storms (tornado and hail producing combined) reported in 2004 are displayed in Figure 6.7. 6.7.a), the 9 hour forecast composite, shows a maximum divergence value of 1.4 x 10^{-5} s^{-1} in the center of the image. The 15 hour composite, shown in 6.7.b), has a max of 1.0 x 10^{-5} s^{-1} at the upper right edge of the domain. 6.7.c), the 21 hour composite, shows a maximum value of 1.2 x 10^{-5} s^{-1} at the center of the chart.

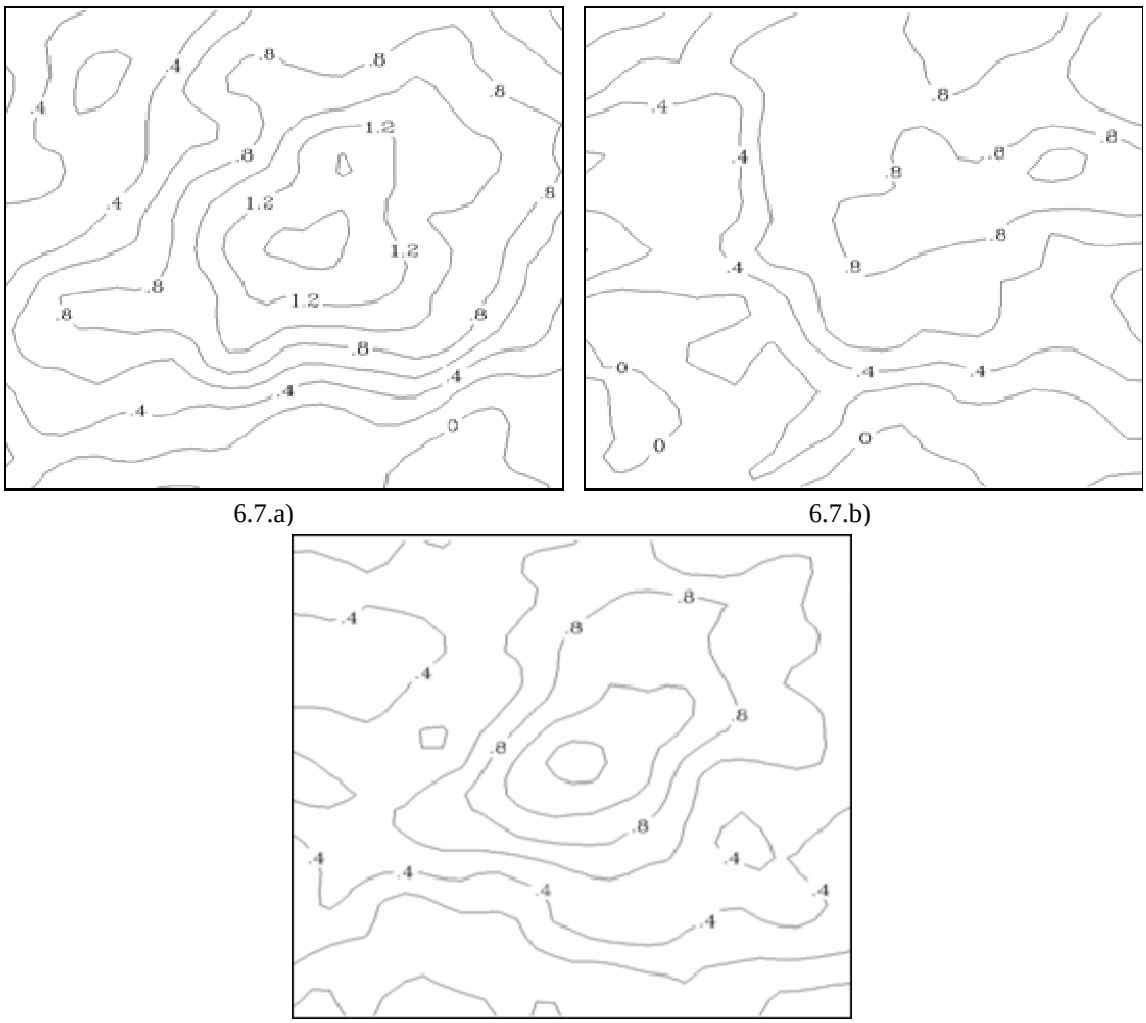

6.7.a) 6.7.b)

6.7.c)

Figure 6.7. 9, 15, and 21 hour divergence composites from all reported type B tornado and hail events during the 2004 storm season. 6.7.a) is the 9 hour image, 6.7.b) is the 15 hour, and 6.7.c) is the 21 hour. Each image consists of a 375 km X 375 km area with a 0.2 contour interval.

Scatter plots of the maximum divergence values from the 9, 15, and 21 hour forecasts of the 370 type B storms are shown in Figure 6.8. The 9 hour plot, 6.8.a), has an average of 7.5 x 10^{-5} s^{-1} with a standard deviation of 5.0 x 10^{-5} s^{-1}. The 15 hour plot, shown in 6.8.b), results in an average of 6.9 x 10^{-5} s^{-1} and a standard deviation of 4.8 x 10^{-5} s^{-1}. 6.8.c), the 21 hour plot, shows an average of 6.9 x 10^{-5} s^{-1} with a standard deviation of 4.9 x 10^{-5} s^{-1}.

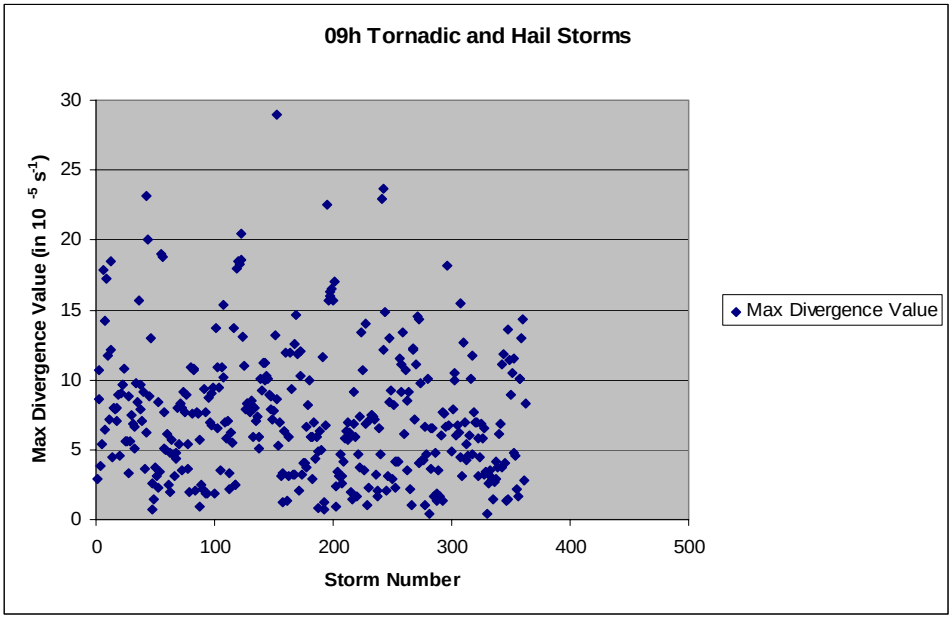

6.8.a)

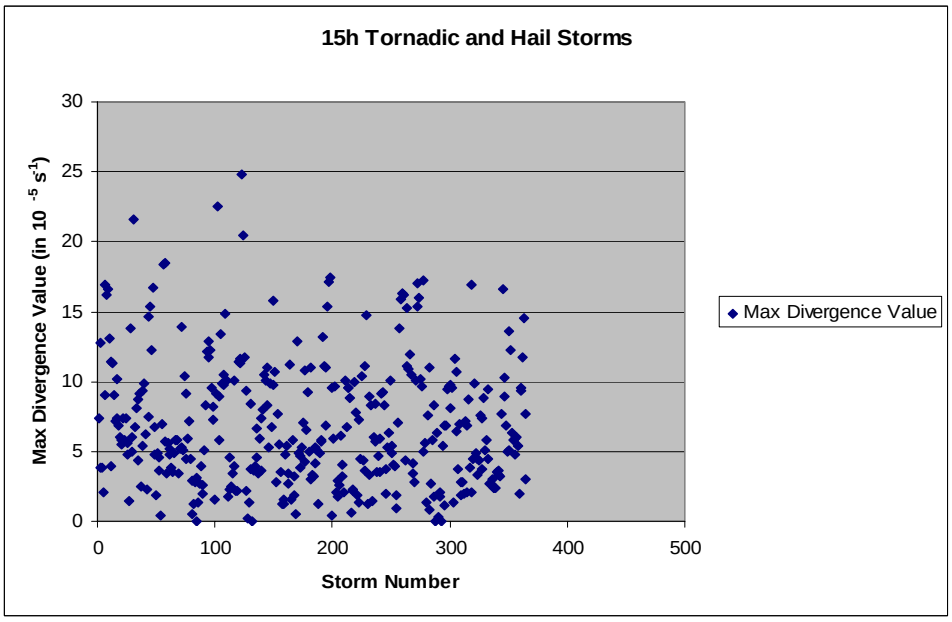

6.8.b)

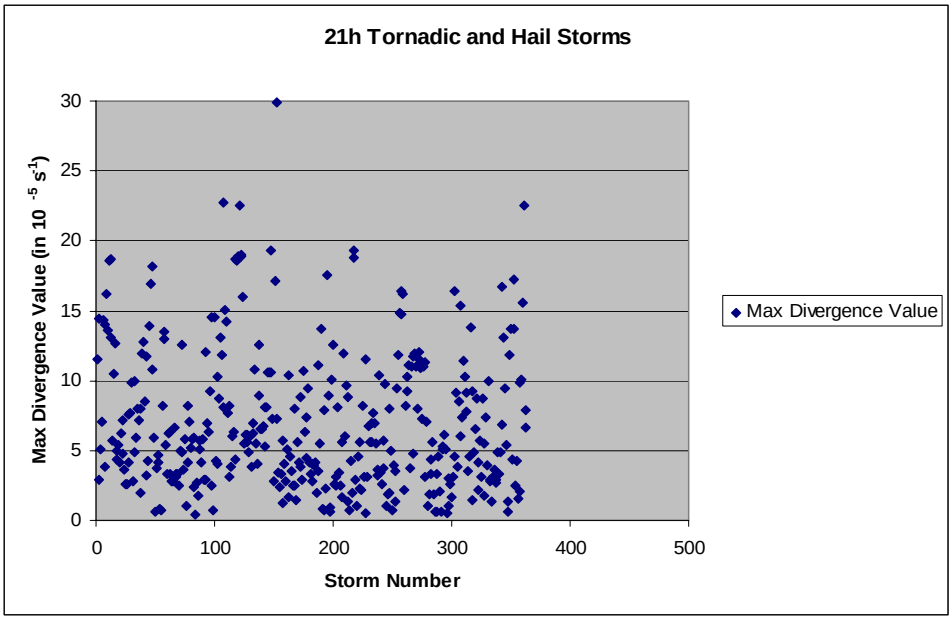

6.8.c)

Figure 6.8. Maximum divergence values from the 9, 15 and 21 hour forecasts of all reported type B tornado and hail events during the 2004 storm season. The maxima were taken from a 52.5 km radius around the center point of the model grid. 6.8.a) is the 9 hour plot, 6.8.b) the 15 hour, and 6.8.c) the 21 hour.

5. Type B Tornadic Storms – 9, 15, and 21 Hour Forecasts

The 9, 15, and 21 hour composite divergence charts from the 50 type B tornado producing storms reported in 2004 are displayed in Figure 6.9. 6.9.a), the 9 hour forecast composite, shows a maximum divergence value of 1.6×10^{-5} s^{-1} in the center of the image. The 15 hour composite, shown in 6.9.b), has a max of 1.6×10^{-5} s^{-1} near the bottom of the chart. 6.9.c), the 21 hour composite, shows a maximum value of 1.6×10^{-5} s^{-1} at the upper center of the domain.

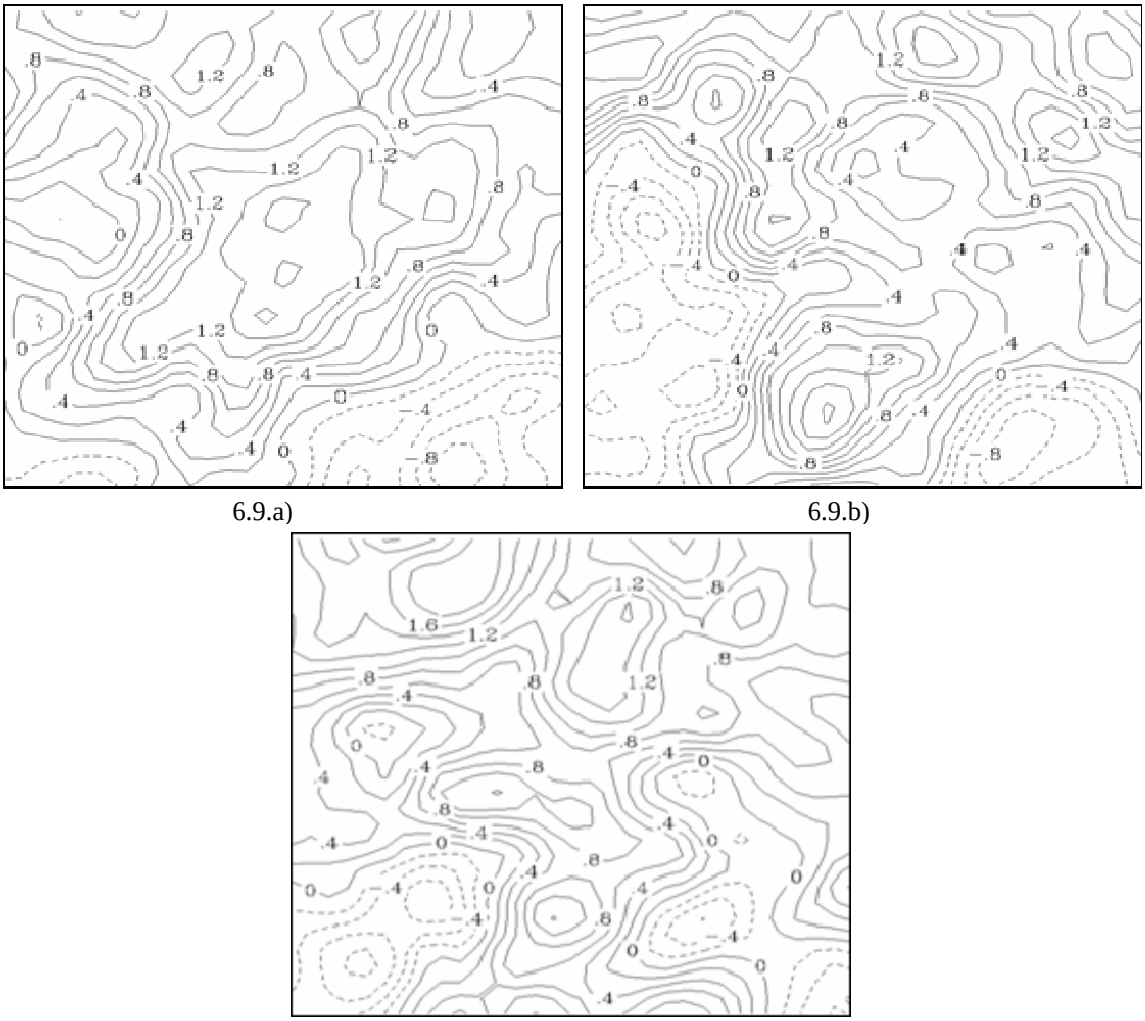

6.9.a) 6.9.b)

6.9.c)

Figure 6.9. 9, 15, and 21 hour divergence composites from all reported type B tornado events during the 2004 storm season. 6.9.a) is the 9 hour image, 6.9.b) is the 15 hour, and 6.9.c) is the 21 hour. Each image consists of a 375 km X 375 km area with a 0.2 contour interval.

Figure 6.10 displays the scatter plots of maximum divergence values from the 9, 15, and 21 hour forecasts of the 50 type B tornadic storms. The 9 hour plot, 6.10.a), has an average of 7.9 x 10^{-5} s^{-1} with a standard deviation of 4.3 x 10^{-5} s^{-1}. The 15 hour plot, shown in 6.10.b), results in an average of 6.9 x 10^{-5} s^{-1} and a standard deviation of 4.2 x 10^{-5} s^{-1}. 6.10.c), the 21 hour plot, shows an average of 7.2 x 10^{-5} s^{-1} with a standard deviation of 4.9 x 10^{-5} s^{-1}.

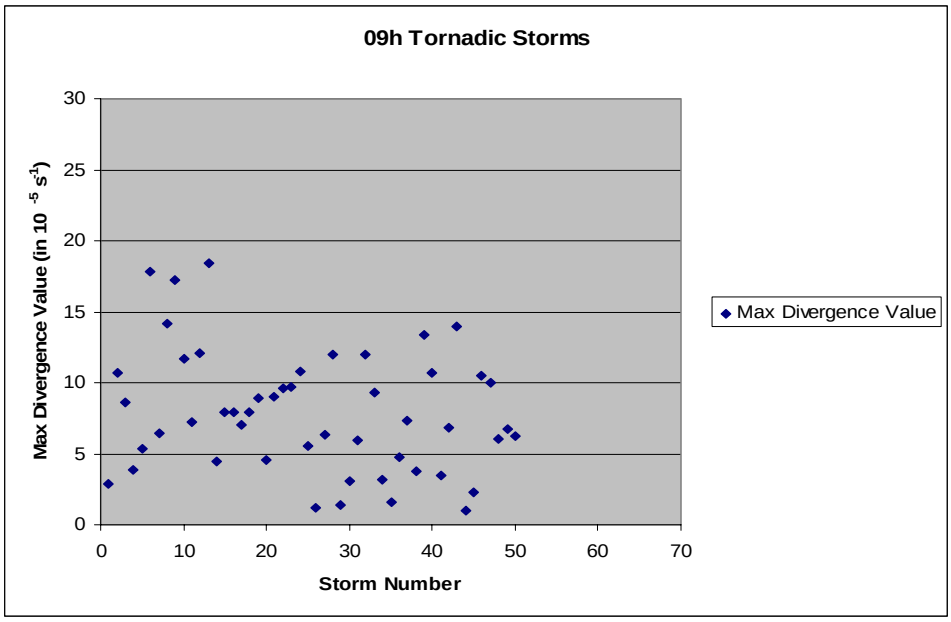

6.10.a)

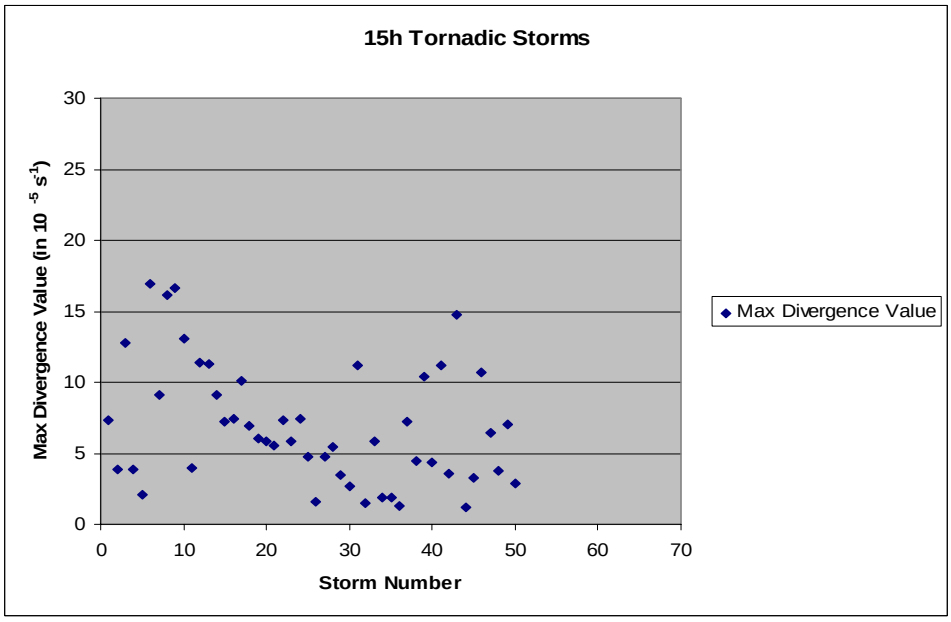

6.10.b)

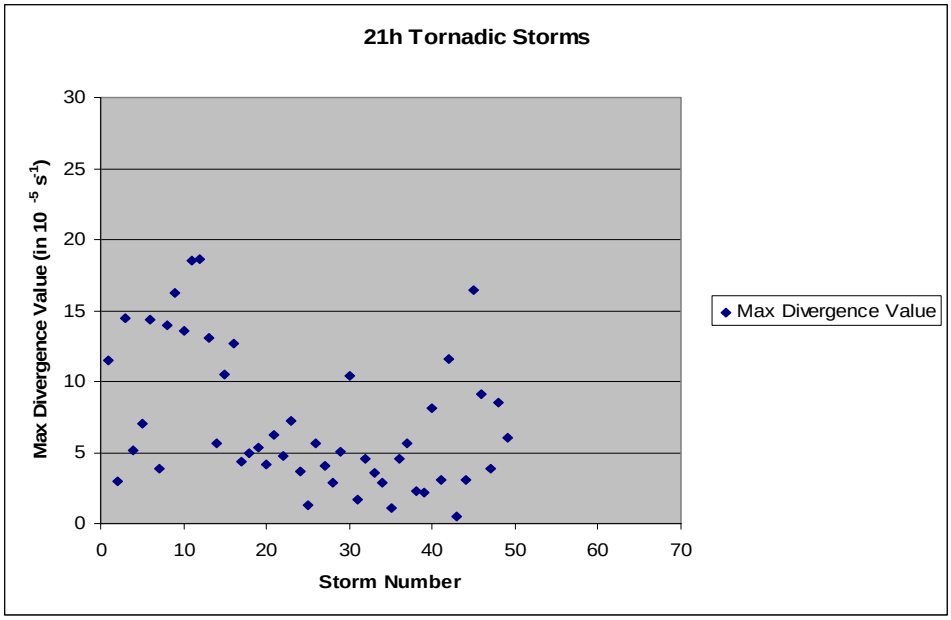

6.10.c)

Figure 6.10. Maximum divergence values from the 9, 15 and 21 hour forecasts of all reported type B tornado events during the 2004 storm season. The maxima were taken from a 52.5 km radius around the center point of the model grid. 6.10.a) is the 9 hour plot, 6.10.b) the 15 hour, and 6.10.c) the 21 hour.

6. Type B Hail Producing Storms – 9, 15, and 21 Hour Forecasts

The 9, 15, and 21 hour composite divergence charts from the 320 type B hail producing storms reported in 2004 are displayed in Figure 6.11. 6.11.a), the 9 hour forecast composite, shows a maximum divergence value of 1.4×10^{-5} s $^{-1}$ in the center of the image. The 15 hour composite, shown in 6.11.b), has a max of 1.0×10^{-5} s $^{-1}$ running from the center through the right center of the chart. 6.11.c), the 21 hour composite, shows a maximum value of 1.3×10^{-5} s $^{-1}$ at the upper center of the domain.

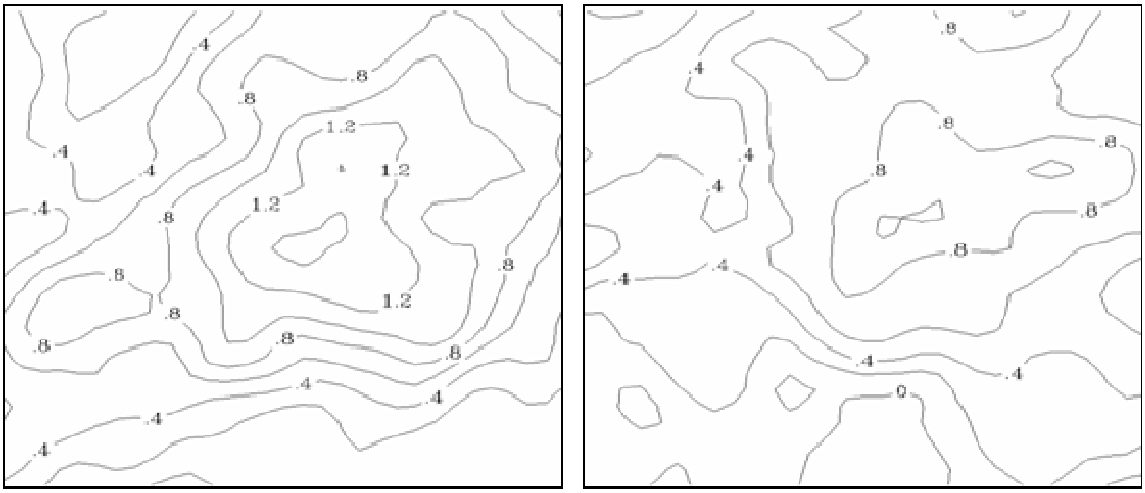

6.11.a) 6.11.b)

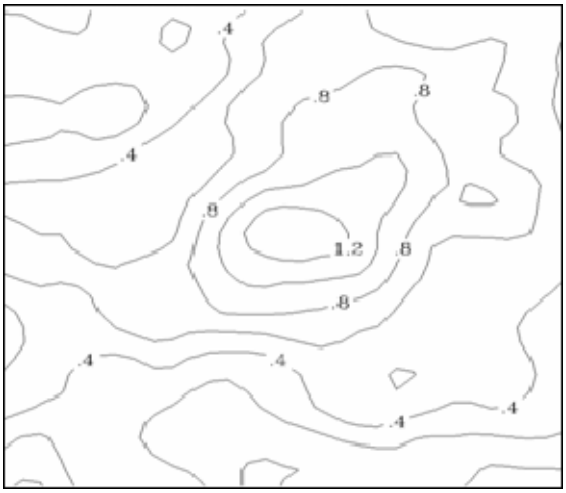

6.11.c)

Figure 6.11. 9, 15, and 21 hour divergence composites from all reported type B hail events during the 2004 storm season. 6.11.a) is the 9 hour image, 6.11.b) is the 15 hour, and 6.11.c) is the 21 hour. Each image consists of a 375 km X 375 km area with a 0.2 contour interval.

Figure 6.12 displays the scatter plots of maximum divergence values from the 9, 15, and 21 hour forecasts of the 320 type B hail storms. The 9 hour plot, 6.12.a), has an average of 7.5 x 10^{-5} s^{-1} with a standard deviation of 5.1 x 10^{-5} s^{-1}. The 15 hour plot, shown in 6.12.b), results in an average of 6.9 x 10^{-5} s^{-1} and a standard deviation of 4.9 x 10^{-5} s^{-1}. 6.12.c), the 21 hour plot, shows identical values to the 15 hour data, with an average of 6.9 x 10^{-5} s^{-1} and a standard deviation of 4.9 x 10^{-5} s^{-1}.

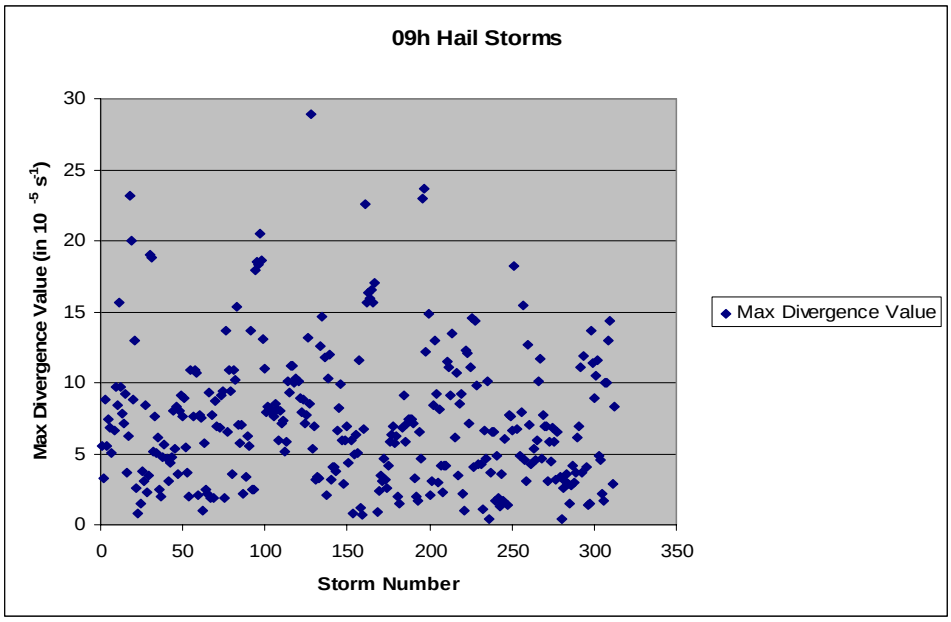

6.12.a)

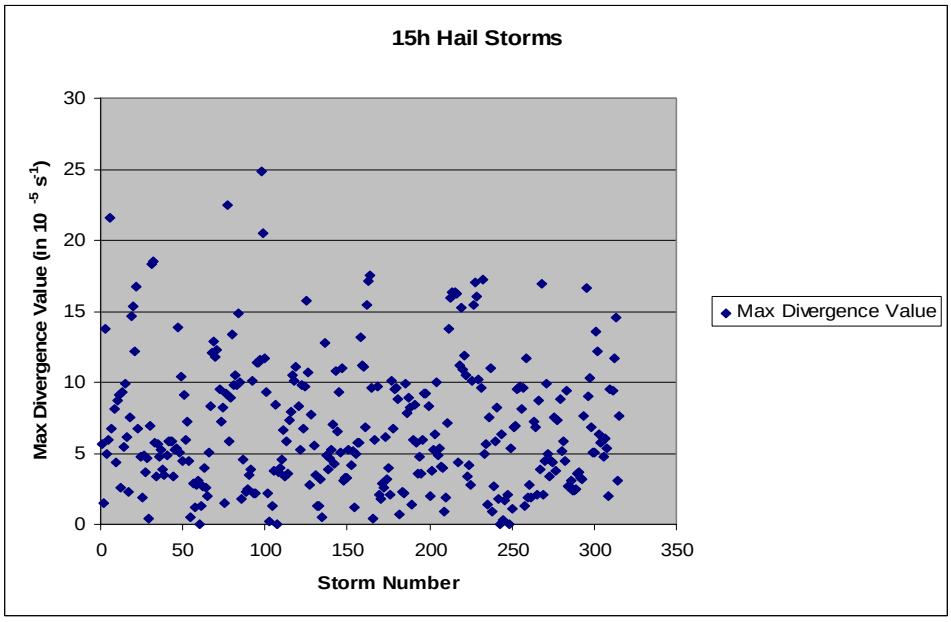

6.12.b)

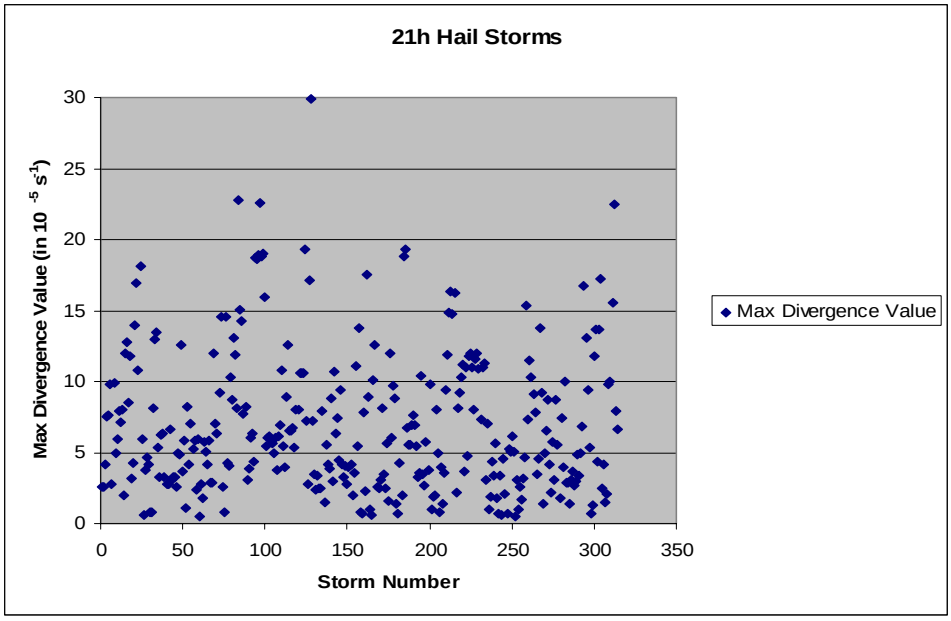

6.12.c)

Figure 6.12. Maximum divergence values from the 9, 15 and 21 hour forecasts of all reported type B hail events during the 2004 storm season. The maxima were taken from a 52.5 km radius around the center point of the model grid. 6.12.a) is the 9 hour plot, 6.12.b) the 15 hour, and 6.12.c) the 21 hour.

7. Discussion of 6 Hour Through 21 Hour Forecasts

When considering the longer range divergence forecasts presented in sections 1 through 6, it is expected that a gradual decline in average maximum divergence values will be seen with increasing time steps, due to increasing forecast error. Table 6.1 provides a summary of the averaged divergence values and standard deviations from each forecast hour, grouped by storm type. As in the previous chapter, the contoured maximum divergence values give a good description of how the model is predicting the spatial divergence forecasts, while the scatter plot maxima provide information on the magnitude of the divergence forecasts within the acceptable 52.5 km error radius.

Time	Storm Type	Sample Size	Contoured Max Divergence	Scatter Plot Max. Divergence	Scatter Plot Standard Deviation
06h	All	385 Storms	$1.8 \times 10^{-5}\ s^{-1}$	$7.2 \times 10^{-5}\ s^{-1}$	$5.0 \times 10^{-5}\ s^{-1}$
09h	All	370 Storms	$1.4 \times 10^{-5}\ s^{-1}$	$7.5 \times 10^{-5}\ s^{-1}$	$5.0 \times 10^{-5}\ s^{-1}$
12h	All	385 Storms	$1.4 \times 10^{-5}\ s^{-1}$	$7.5 \times 10^{-5}\ s^{-1}$	$5.4 \times 10^{-5}\ s^{-1}$
15h	All	370 Storms	$1.0 \times 10^{-5}\ s^{-1}$	$6.9 \times 10^{-5}\ s^{-1}$	$4.8 \times 10^{-5}\ s^{-1}$
18h	All	385 Storms	$1.4 \times 10^{-5}\ s^{-1}$	$6.9 \times 10^{-5}\ s^{-1}$	$5.7 \times 10^{-5}\ s^{-1}$
21h	All	370 Storms	$1.2 \times 10^{-5}\ s^{-1}$	$6.9 \times 10^{-5}\ s^{-1}$	$4.9 \times 10^{-5}\ s^{-1}$

6.1.a)

06h	Tornado	60 Storms	$2.1 \times 10^{-5}\ s^{-1}$	$6.6 \times 10^{-5}\ s^{-1}$	$4.1 \times 10^{-5}\ s^{-1}$
09h	Tornado	50 Storms	$1.6 \times 10^{-5}\ s^{-1}$	$7.9 \times 10^{-5}\ s^{-1}$	$4.3 \times 10^{-5}\ s^{-1}$
12h	Tornado	60 Storms	$2.2 \times 10^{-5}\ s^{-1}$	$8.4 \times 10^{-5}\ s^{-1}$	$5.9 \times 10^{-5}\ s^{-1}$
15h	Tornado	50 Storms	$1.6 \times 10^{-5}\ s^{-1}$	$6.9 \times 10^{-5}\ s^{-1}$	$4.2 \times 10^{-5}\ s^{-1}$
18h	Tornado	60 Storms	$2.1 \times 10^{-5}\ s^{-1}$	$7.3 \times 10^{-5}\ s^{-1}$	$4.2 \times 10^{-5}\ s^{-1}$
21h	Tornado	50 Storms	$1.6 \times 10^{-5}\ s^{-1}$	$7.2 \times 10^{-5}\ s^{-1}$	$4.9 \times 10^{-5}\ s^{-1}$

6.1.b)

06h	Hail	325 Storms	$1.8 \times 10^{-5}\ s^{-1}$	$7.3 \times 10^{-5}\ s^{-1}$	$5.2 \times 10^{-5}\ s^{-1}$
09h	Hail	320 Storms	$1.4 \times 10^{-5}\ s^{-1}$	$7.5 \times 10^{-5}\ s^{-1}$	$5.1 \times 10^{-5}\ s^{-1}$
12h	Hail	325 Storms	$1.4 \times 10^{-5}\ s^{-1}$	$7.3 \times 10^{-5}\ s^{-1}$	$5.3 \times 10^{-5}\ s^{-1}$
15h	Hail	320 Storms	$1.0 \times 10^{-5}\ s^{-1}$	$6.9 \times 10^{-5}\ s^{-1}$	$4.9 \times 10^{-5}\ s^{-1}$
18h	Hail	325 Storms	$1.3 \times 10^{-5}\ s^{-1}$	$6.8 \times 10^{-5}\ s^{-1}$	$5.9 \times 10^{-5}\ s^{-1}$
21h	Hail	320 Storms	$1.3 \times 10^{-5}\ s^{-1}$	$6.9 \times 10^{-5}\ s^{-1}$	$4.9 \times 10^{-5}\ s^{-1}$

6.1.c)

Table 6.1. Average maximum divergence values and standard deviations for the 6 hour through 21 hour forecasts of 2004 storms.

For the contoured maximum divergence values, this general declining trend is observed mainly in the hail producing cases listed in 6.1.c). The tornadic storms shown in 6.1.b) do not follow the expected declining trend; their behavior is more erratic due to the smaller sample size and larger forecast error in the location and magnitude of divergence maxima. As a result, the contoured divergence values for the combined storms (6.1.a)) show a more fluctuating trend with time. Based on the contoured max divergence values, it appears that the data from the tornadic storms may be contributing to less accurate measurements of minimum divergence values for severe storms.

The scatter plot data from table 6.1 provides additional information regarding divergence values for severe storms. As with the contoured values, a general decline in averaged maximum scatter plot values is expected as model time steps get larger due to increasing forecast error. The standard deviation values are expected to remain the same or increase with time, again due to forecast error. This trend is most evident in the hail producing storm data in 6.1.c), where both a decrease in the scatter plot maximum values and an increase in standard deviation values are seen. Keeping in mind that the 6, 12 and 18 hour forecasts are a different set of storms than the 9, 15 and 21 hour forecasts, each data set displays the expected trend. The standard deviation values from the hail storms remain fairly steady; with the exception of a high value at the 18 hour point, the standard deviations remain within a few tenths of a point of each other. The tornadic storms in 6.1.b) show less steady behavior from the scatter plot data; the maximum divergence values fluctuate greatly from time step to time step. The standard deviation values are generally smaller than seen in the hail case, but there is a far smaller sample size for the tornadic cases. As a result, the combined cases in 6.1.a) are affected by the tornadic storms, and display a slightly less accurate representation of low-end divergence values for severe storms.

By combining the longer range average divergence forecasts discussed in this chapter with the "baseline" values derived in chapter 5, a full picture of divergence versus time can be obtained. Table 6.2 shows a plot of maximum divergence values versus model output hour from the contour plot averages for the three types of storms. The plot of tornadic storms shows a decline in maximum divergence values until the 9 hour point. The plots of all storms and hail storms show a general decreasing trend out to the 21 hour time step, with the hail plot representing a slightly steadier decline versus time. The lone exception in each of these is the 15 hour time point, but in general each of these plots shows a identifiable pattern of divergence maxima decreasing with time.

Table 6.3. is a similar plot to 6.2, but shows the data from the scatter plots. Each group of storms behaves in a similar fashion to 6.2, but the effects are more pronounced in the scatter plot case. The tornadic storms show a declining trend through the 6 hour time step, but become noisy after that point. The all storms and hail storms plots display a identifiable decreasing trend out to the 21 hour point, with the all storms again being

somewhat skewed due to the inclusion of the tornadic storms. As was the case with the contour plots, the scatter plot data from hail producing storms should provide the best estimate of low-end divergence values for severe storm events.

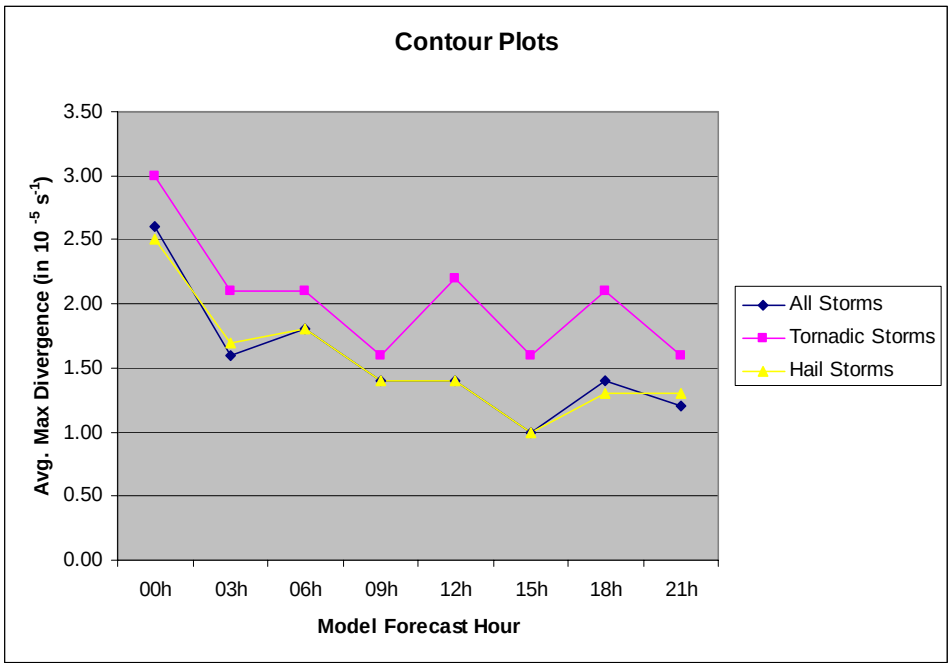

Table 6.2. Average contour plot maximum divergence vs. ETA-212 forecast hour for severe events from the 2004 storm season.

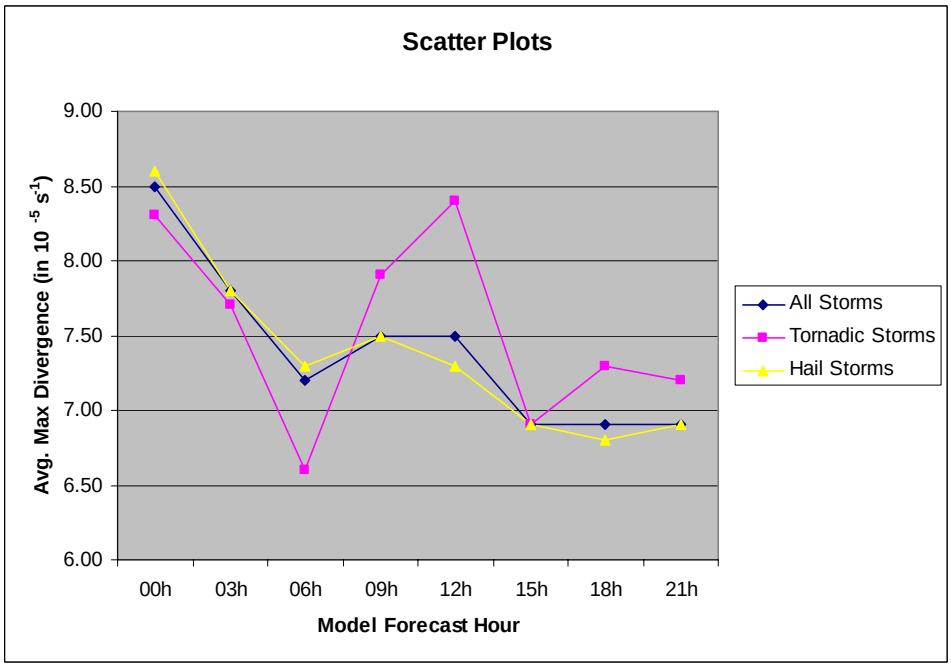

Table 6.3. Average scatter plot maximum divergence vs. ETA-212 forecast hour for severe events from the 2004 storm season.

VII. ETA-212 AND MM5 DATA COMPARISON

This chapter compares data from the ETA-212 and MM5 models over a subset of severe events from the 2004 storm season. Each contoured image in this chapter represents a 375 km X 375 km area, and each scatter plot has its maximum values taken over a 105 km X 105 km region.

A. OVERVIEW OF MODEL COMPARISON DATA

Due to data collection and assimilation problems, this study was not able to obtain MM5 model data from the entire 2004 severe weather season. MM5 data became available for storms after June 17th, and the majority of storms after this date were encompassed by MM5 model forecasts (with a few days' worth of data not available due to technical problems). For a detailed listing of dates encompassed by the MM5 data, refer to Appendices C through F.

The model composites for the MM5 differed from the previous chapters' examples of the ETA-212 data due to the less frequent model initialization times. As previously discussed, the ETA-212 is initialized every six hours, so each storm event is encompassed by four ETA-212 model runs. The MM5 model is initialized every twelve hours, but there are no 0 or 3 hour forecasts, so each storm has only one or two MM5 model forecasts associated with it depending on time of occurrence (refer to the "MM5 Information" section on page 18 for a more detailed explanation).

Due to the smaller storm sample size investigated in this chapter, there are no separate considerations of tornado and hail producing storms; the divergence composites in this section are composed of data from all storms. The hail storm divergence composites were virtually identical to the composites from the "all storms" data; the low number of tornadic storms had no appreciable effect on the averaged divergence charts. Table 7.1 shows the total number of storms for each forecast hour, along with number of tornadic and hail producing events. The MM5 divergence charts in the following sections are compared to ETA-212 charts run from identical events; the side-by-side comparisons are two different model forecasts of the exact same storms.

Forecast hour	Tornadic storms	Hail storms	Total storms
f06	12	77	89
f09	5	43	48
f12	4	39	43
f15	9	69	78
f18	13	76	89
f21	5	48	53

Table 7.1. Sample sizes for the forecast hours examined in Chapter VII.

B. DATA COMPARISON – ALL STORMS, 6 HOUR FORECAST

The divergence composites from the 6 hour ETA-212 and MM5 forecasts are shown in Figure 7.1, based on a sample size of 89 storms. The two divergence composites look quite similar; both display an elongated pattern of divergence from the lower left through the upper right of the diagram, with a maximum in the upper center of the image. 7.1.a), the MM5 composite, has a maximum divergence value of 1.6 x 10^{-5} s^{-1}, while the ETA-212 chart in 7.1.b) is slightly higher, at 2.0 x 10^{-5} s^{-1}. Each image also shows a secondary divergence maximum in the lower left center: 1.0 x 10^{-5} s^{-1} for the MM5 in a) and 1.4 x 10^{-5} s^{-1} for the ETA-212 in b).

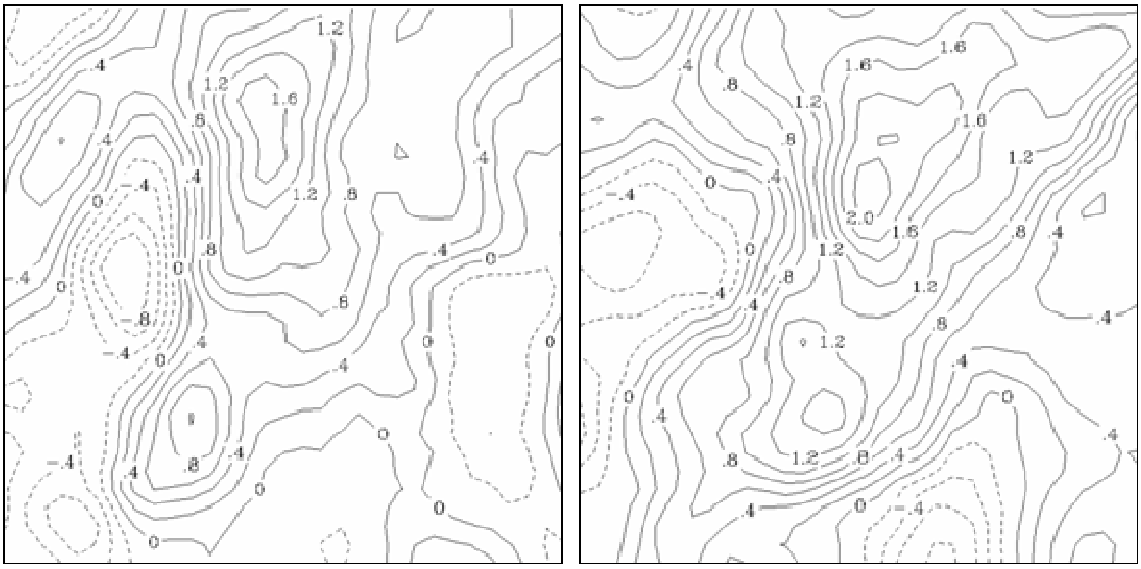

7.1.a) 7.1.b)

Figure 7.1. 6 hour divergence composites from MM5 and ETA-212 data, June-September 2004. 7.1.a) is the MM5 composite, and 7.1.b) is the ETA-212. Each image consists of a 375 km X 375 km area with a 0.2 contour interval.

Figure 7.2 shows the scatter plot of maximum divergence values for the 89 storms. The MM5 plot, 7.2.a), has an average of 7.6 x 10^{-5} s^{-1} with a standard deviation of 8.6 x 10^{-5} s^{-1}. 7.2.b), the ETA plot, shows an average of 7.3 x 10^{-5} s^{-1} and a standard deviation of 5.4 x 10^{-5} s^{-1}.

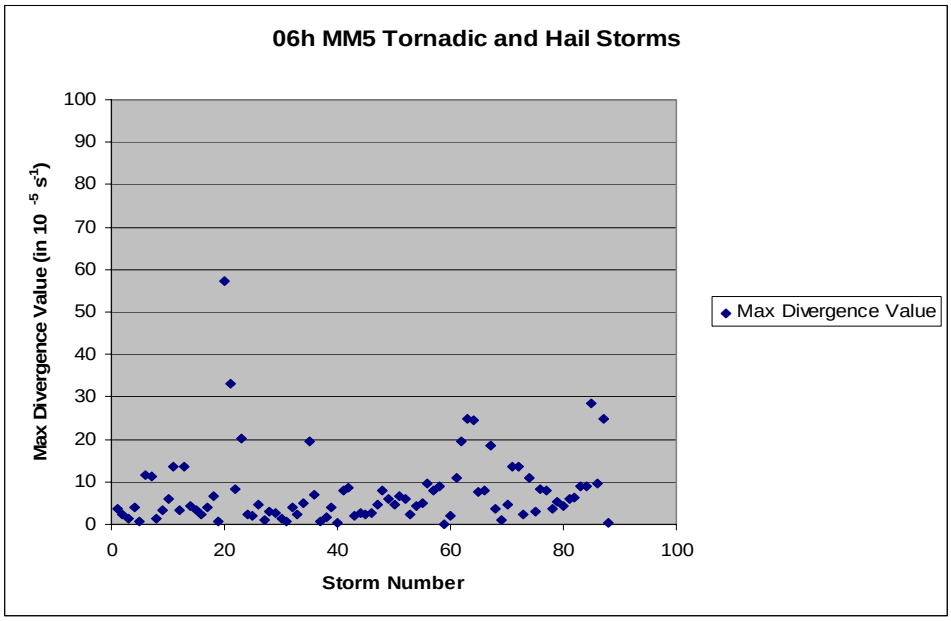

7.2.a)

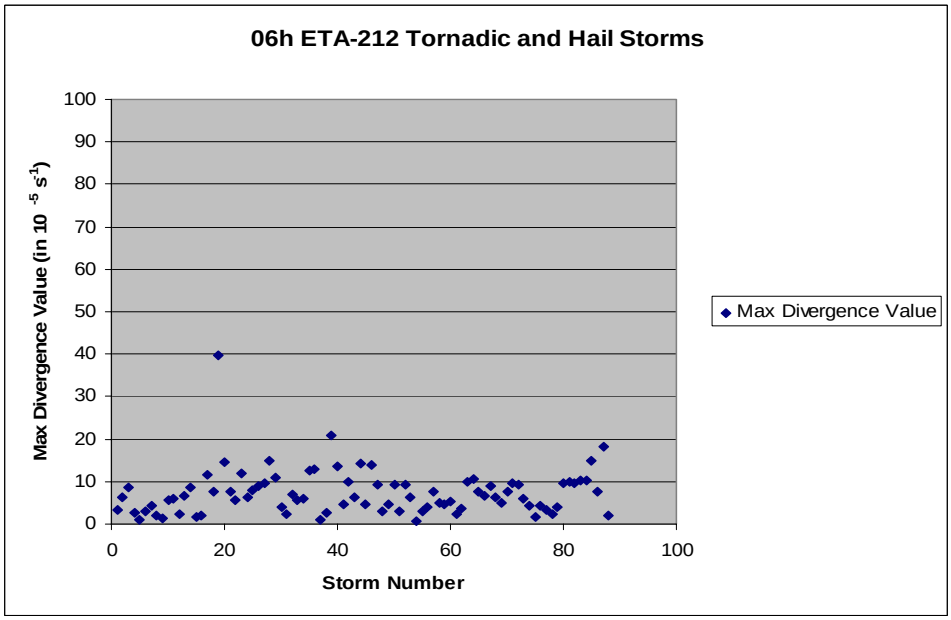

7.2.b)

Figure 7.2. Maximum divergence values from the 6 hour forecasts of MM5 and ETA-212 data, June-September 2004. The maxima were taken from a 52.5 km radius around the center point of the model grid. 7.2.a) is the MM5 plot, and 7.2.b) is the ETA-212 plot.

C. DATA COMPARISON – ALL STORMS, 9 HOUR FORECAST

The composites from the 9 hour forecasts (with a sample size of 48 storms) are shown below, in Figure 7.3. These two divergence composite images show a general pattern of maximum divergence values from the lower left center through the upper center of the images. Both the MM5 and ETA-212 images show a divergence max in the upper center of the domain. The MM5 composite has a maximum of 5.0 x 10^{-5} s^{-1} in 7.2.a), while the ETA-212 shows a much weaker max of 2.2 x 10^{-5} s^{-1} in 7.2.b).

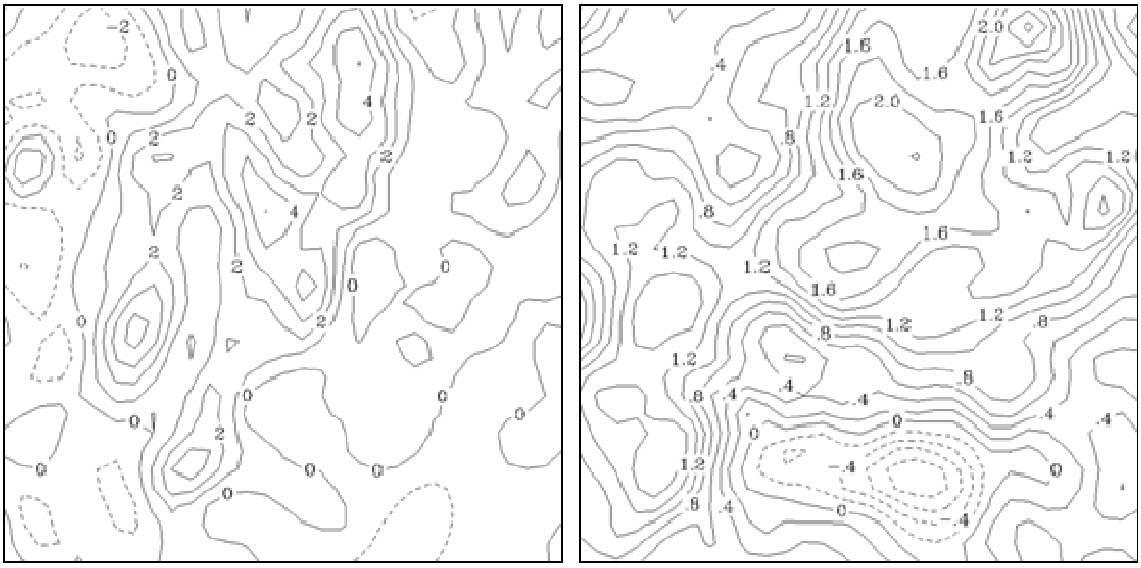

7.3.a) 7.3.b)

Figure 7.3. 9 hour divergence composites from MM5 and ETA-212 data, June-September 2004. 7.3.a) is the MM5 composite (1.0 contour interval), and 7.3.b) is the ETA-212 (0.2 contour interval). Each image consists of a 375 km X 375 km area.

The scatter plots of maximum divergence values from these 48 storms are shown in Figure 7.4. The MM5 plot, 7.4.a), has an average of 22.5 x 10^{-5} s^{-1} with a standard deviation of 28.0 x 10^{-5} s^{-1}. 7.4.b), the ETA plot, shows an average of 8.5 x 10^{-5} s^{-1} and a standard deviation of 5.1 x 10^{-5} s^{-1}.

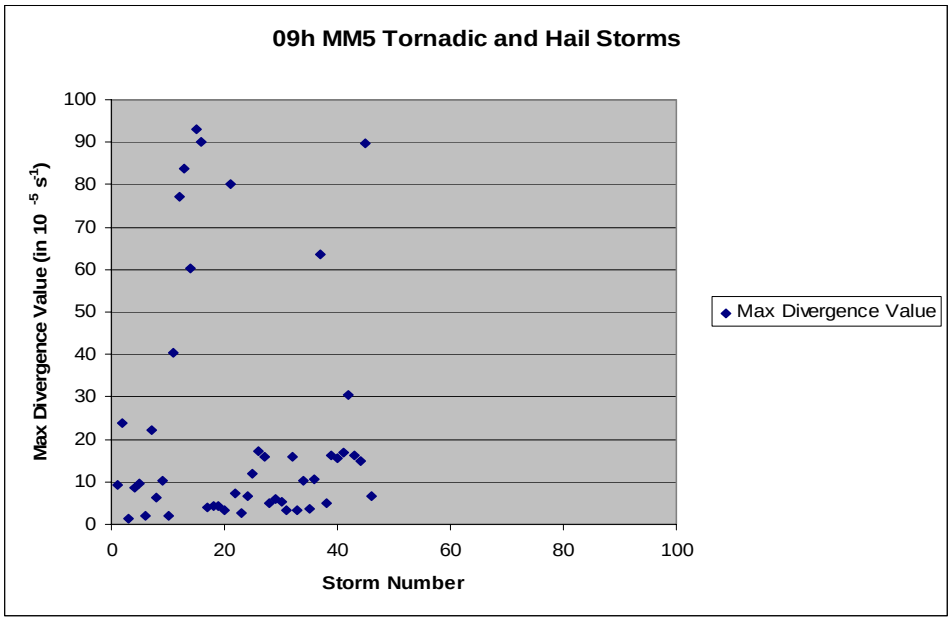

7.4.a)

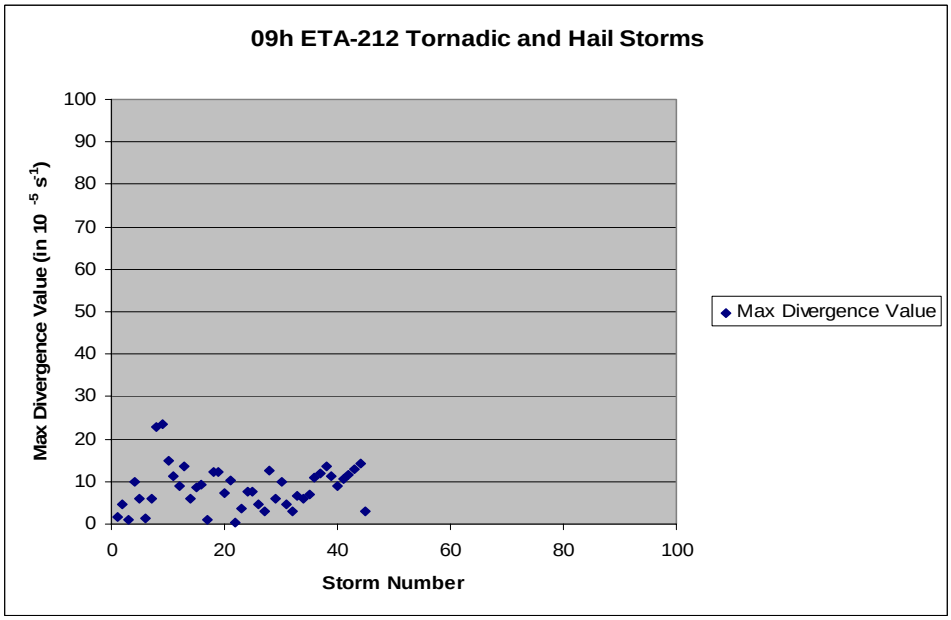

7.4.b)

Figure 7.4. Maximum divergence values from the 9 hour forecasts of MM5 and ETA-212 data, June-September 2004. The maxima were taken from a 52.5 km radius around the center point of the model grid. 7.4.a) is the MM5 plot, and 7.4.b) is the ETA-212 plot.

D. DATA COMPARISON – ALL STORMS, 12 HOUR FORECAST

The 12 hour forecast composites are displayed in Figure 7.5. Each image consists of a sample size of 43 storms. These two images both have a general region of stronger divergence at the upper center of their domains, and share an identical maximum divergence value of 2.0 x 10^{-5} s^{-1}. The MM5 image (7.5.a)) has this maximum near the upper center of the domain, while the ETA-212 chart (7.5.b)) has its max at the upper center of the image.

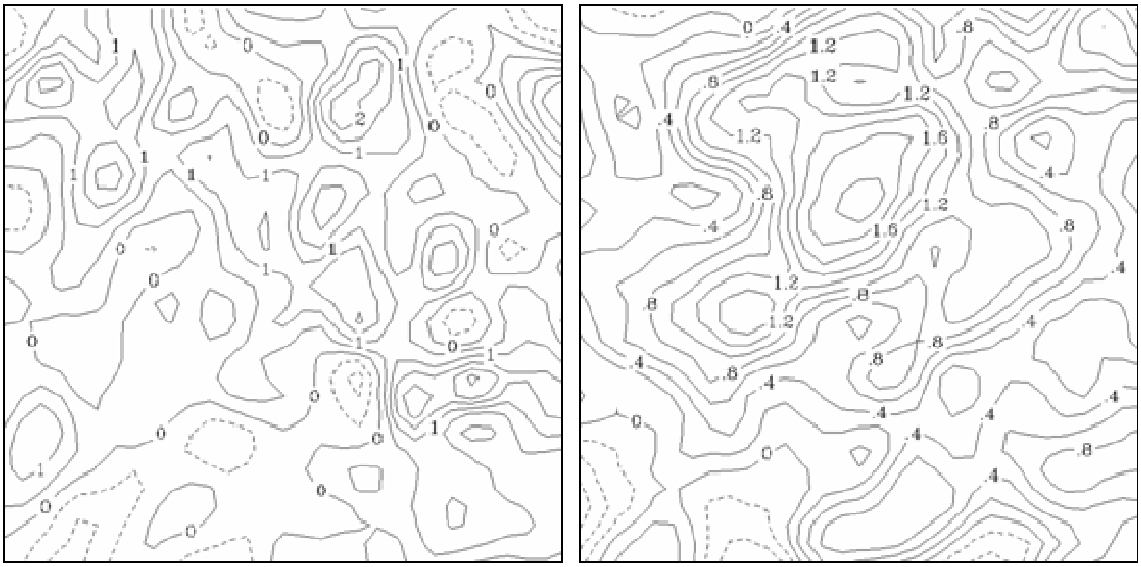

7.5.a) 7.5.b)

Figure 7.5. 12 hour divergence composites from MM5 and ETA-212 data, June-September 2004. 7.5.a) is the MM5 composite (0.5 contour interval), and 7.5.b) is the ETA-212 (0.2 contour interval).

The scatter plots of maximum divergence values from these 43 storms are shown in Figure 7.6. The MM5 plot, 7.6.a), has an average of 14.7 x 10^{-5} s^{-1} with a standard deviation of 16.5 x 10^{-5} s^{-1}. 7.6.b), the ETA plot, shows an average of 7.2 x 10^{-5} s^{-1} and a standard deviation of 4.1 x 10^{-5} s^{-1}.

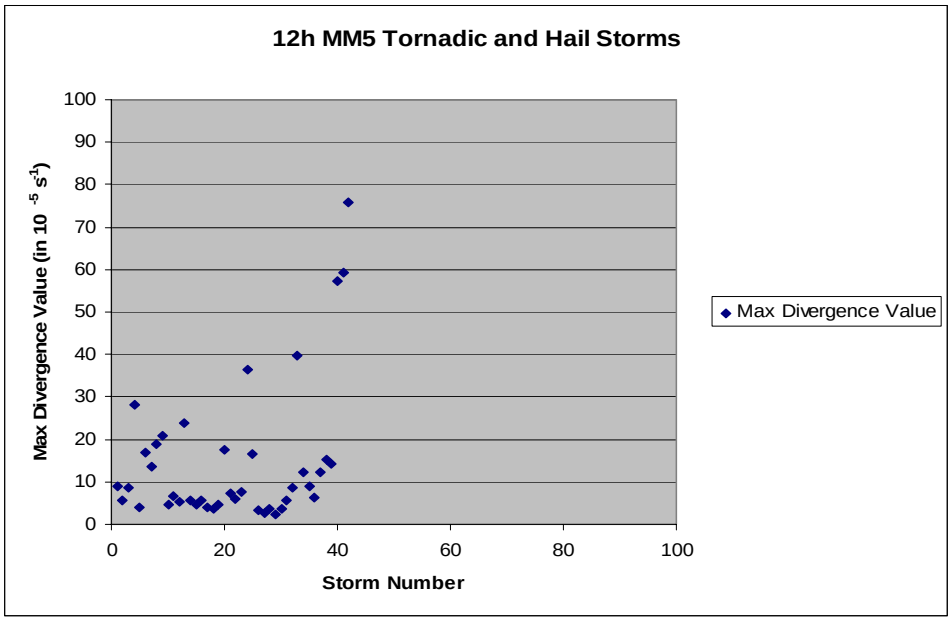

7.6.a)

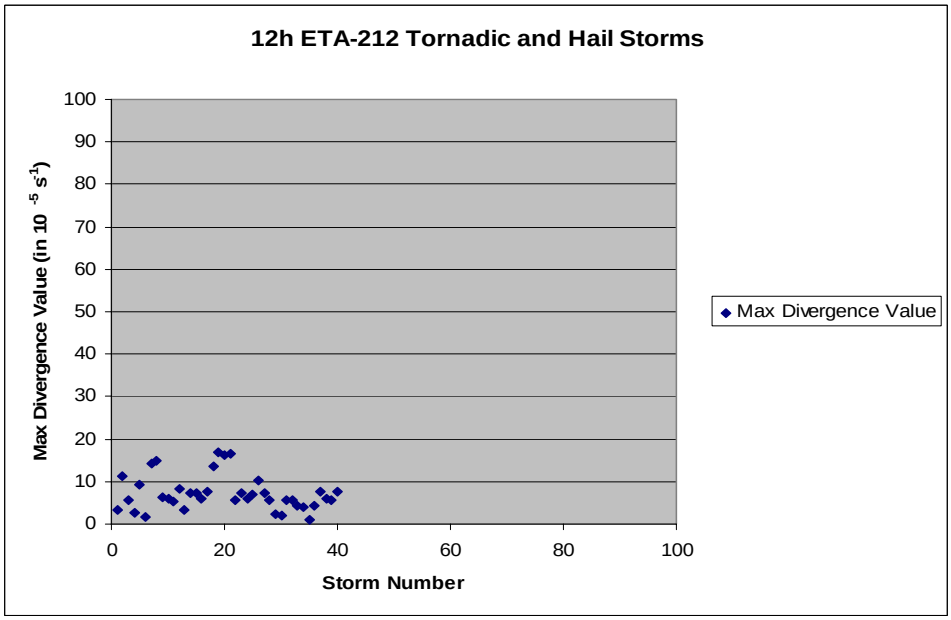

7.6.b)

Figure 7.6. Maximum divergence values from the 12 hour forecasts of MM5 and ETA-212 data, June-September 2004. The maxima were taken from a 52.5 km radius around the center point of the model grid. 7.6.a) is the MM5 plot, and 7.6.b) is the ETA-212 plot.

E. DATA COMPARISON – ALL STORMS, 15 HOUR FORECAST

The 15 hour forecast composites are shown in Figure 7.7, with a sample size of 78 storms. The two images show a general agreement in the divergence pattern, with negative values along the left hand side and an area of positive values through the center and right sides. The MM5 image (7.7.a)) has a maximum divergence value of 3.25 x 10^{-5} s^{-1} near the center of the chart, while the ETA-212 image (7.7.b)) has a much lower maximum of 1.1 x 10^{-5} s^{-1} at the right center of the domain.

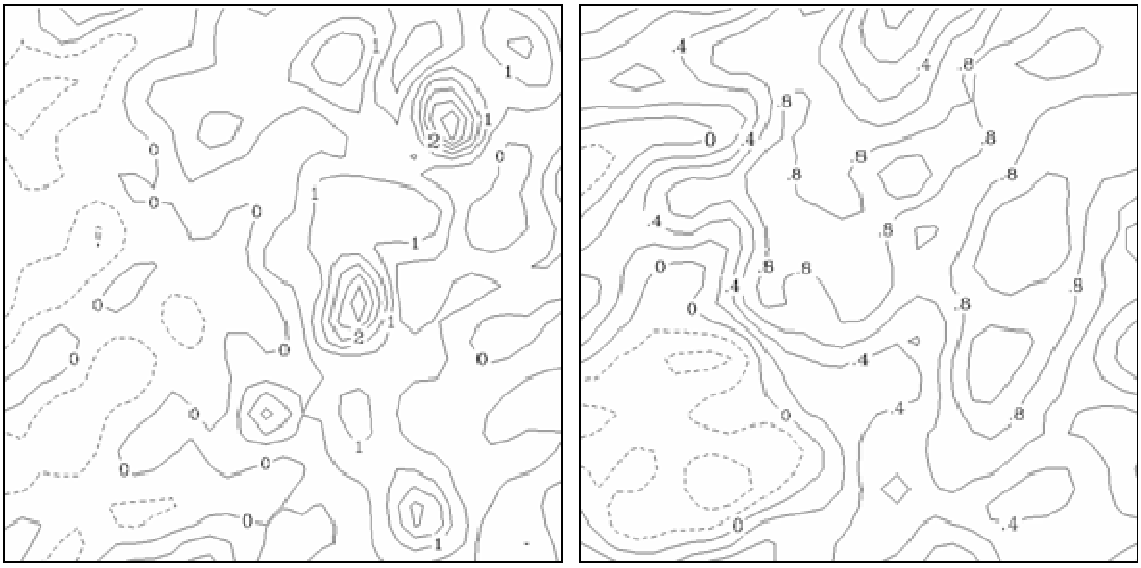

7.7.a) 7.7.b)

Figure 7.7. 15 hour divergence composites from MM5 and ETA-212 data, June-September 2004. 7.7.a) is the MM5 composite (0.5 contour interval), and 7.7.b) is the ETA-212 (0.2 contour interval). Each image consists of a 375 km X 375 km area.

Figure 7.8 shows the scatter plot of maximum divergence values for the 78 storms. The MM5 plot, 7.8.a), has an average of 12.5 x 10^{-5} s^{-1} with a standard deviation of 16.3 x 10^{-5} s^{-1}. 7.8.b), the ETA plot, shows an average of 6.3 x 10^{-5} s^{-1} and a standard deviation of 3.7 x 10^{-5} s^{-1}.

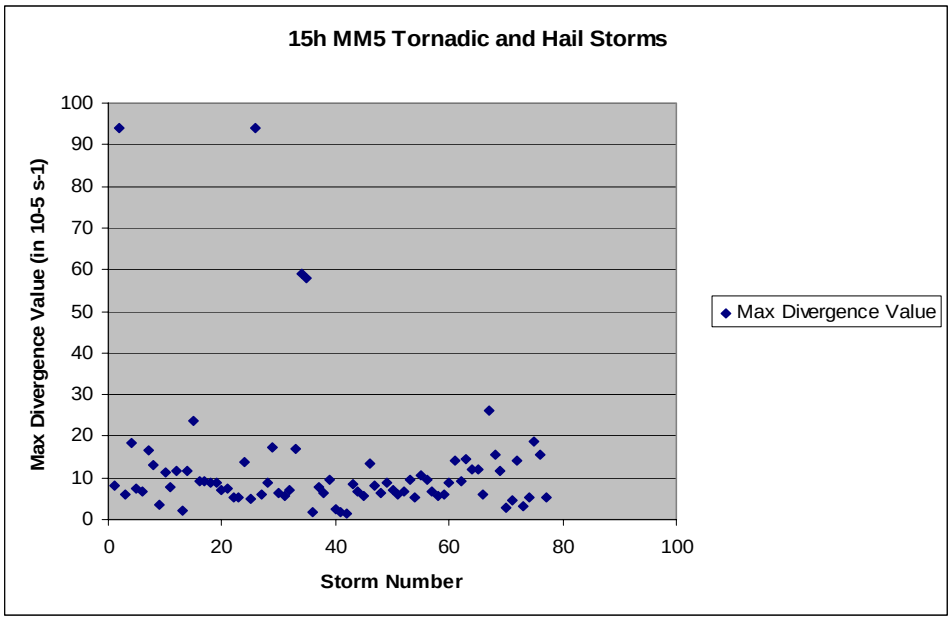

7.8.a)

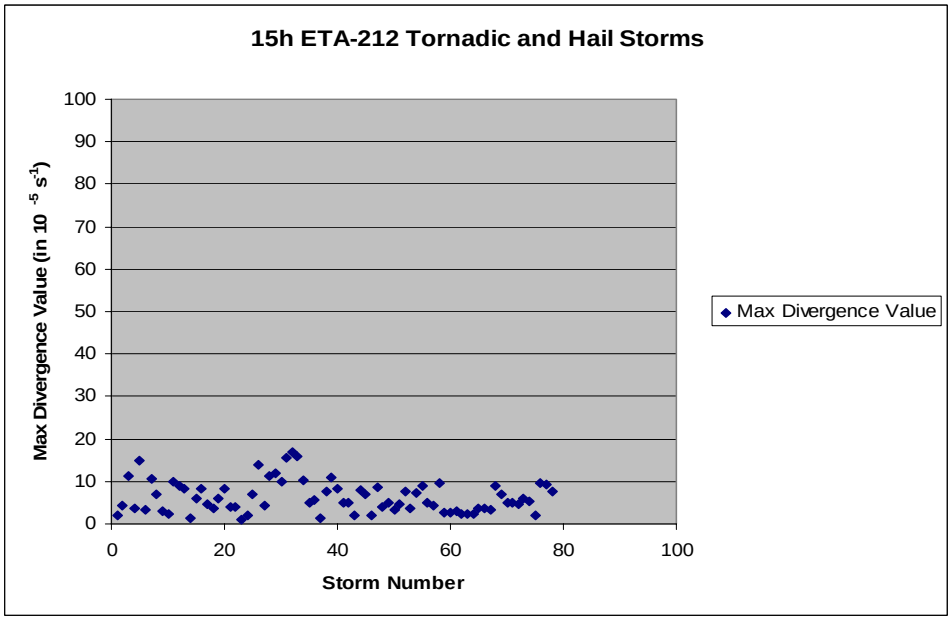

7.8.b)

Figure 7.8. Maximum divergence values from the 15 hour forecasts of MM5 and ETA-212 data, June-September 2004. The maxima were taken from a 52.5 km radius around the center point of the model grid. 7.8.a) is the MM5 plot, and 7.8.b) is the ETA-212 plot.

F. DATA COMPARISON – ALL STORMS, 18 HOUR FORECAST

The divergence composites from the 18 hour forecasts (and a sample size of 89 storms) are shown below, in Figure 7.9. Both composites have an elongated divergence pattern extending from the lower left to the upper right of the image, but the ETA-212 composite is much more organized than the MM5 chart. The MM5 composite (7.9.a)) has a maximum divergence value of 1.75 x 10^{-5} s^{-1} at the upper left corner, while the ETA-212 image (7.9.b)) has a max of 2.0 x 10^{-5} s^{-1} in upper right center.

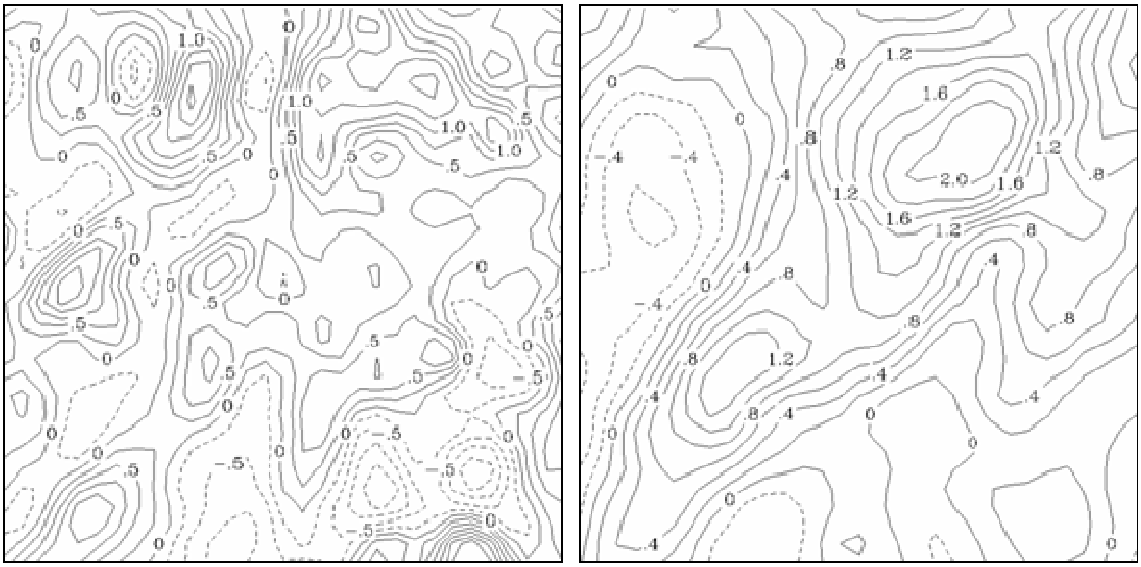

7.9.a) 7.9.b)

Figure 7.9. 18 hour divergence composites from MM5 and ETA-212 data, June-September 2004. 7.9.a) is the MM5 composite (0.25 contour interval), and 7.9.b) is the ETA-212 (0.2 contour interval).

Figure 7.10 shows the scatter plot of maximum divergence values for these 89 storms. The MM5 plot, 7.10.a), has an average of 11.5 x 10^{-5} s^{-1} with a standard deviation of 8.8 x 10^{-5} s^{-1}. 7.10.b), the ETA plot, shows an average of 6.4 x 10^{-5} s^{-1} and a standard deviation of 4.4 x 10^{-5} s^{-1}.

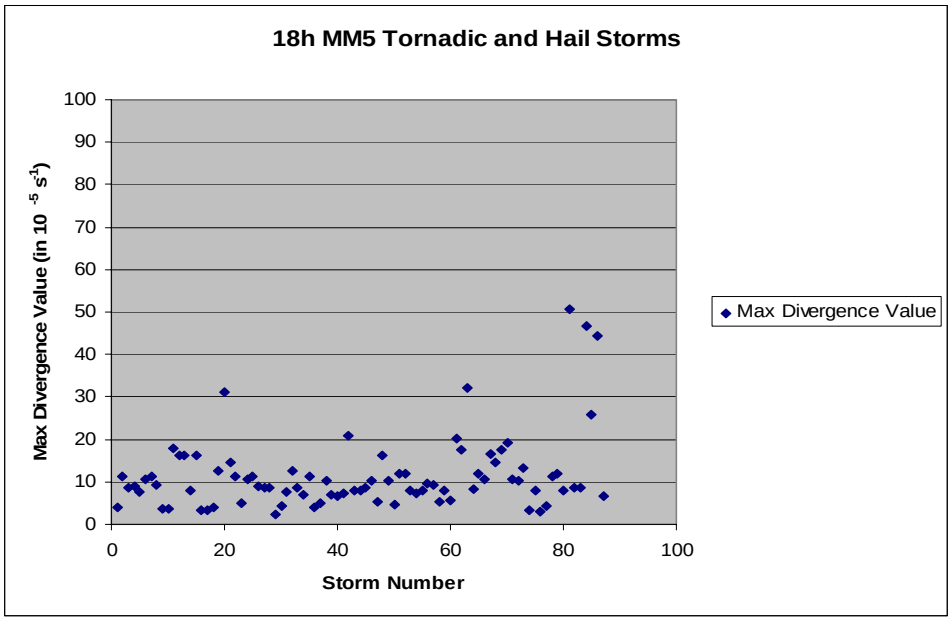

7.10.a)

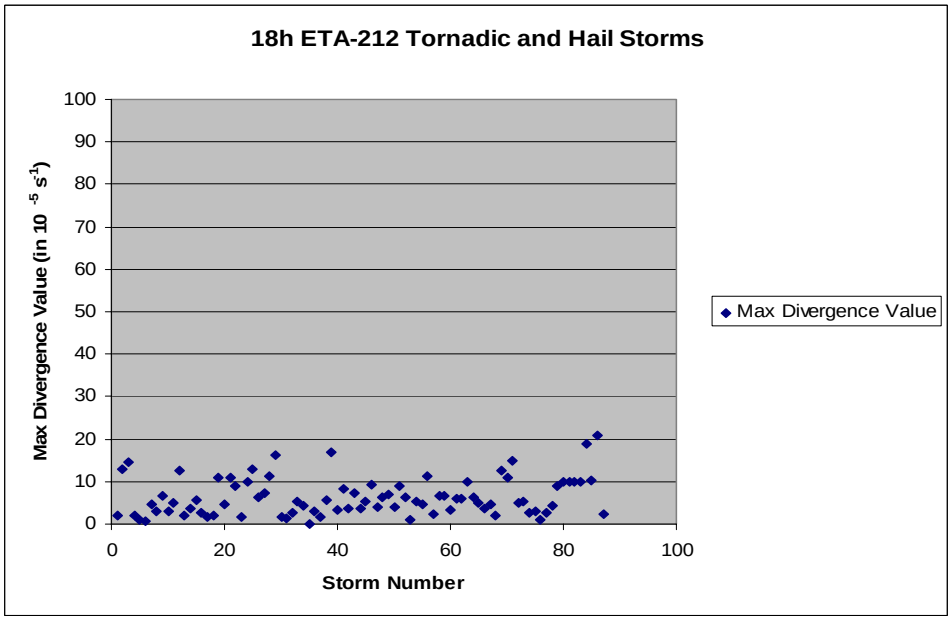

7.10.b)

Figure 7.10. Maximum divergence values from the 18 hour forecasts of MM5 and ETA-212 data, June-September 2004. The maxima were taken from a 52.5 km radius around the center point of the model grid. 7.10.a) is the MM5 plot, and 7.10.b) is the ETA-212 plot.

G. DATA COMPARISON – ALL STORMS, 21 HOUR FORECAST

The divergence composites from the 21 hour forecasts are displayed in Figure 7.11. Each image represents a sample size of 53 storms. As was the case with the 18 hour composites, these images have striking similarity. Both composites have their divergence maxima in the upper right center of the domain, and have a similar general structure of positive divergence values extending through the middle of the images. Once again, however, the ETA-212 chart is more organized. The MM5 composite (7.11.a)) has a maximum divergence value of 4.5 x 10^{-5} s^{-1} at the upper right corner, while the ETA-212 image (7.11.b)) has a max of 3.0 x 10^{-5} s^{-1} in the same area.

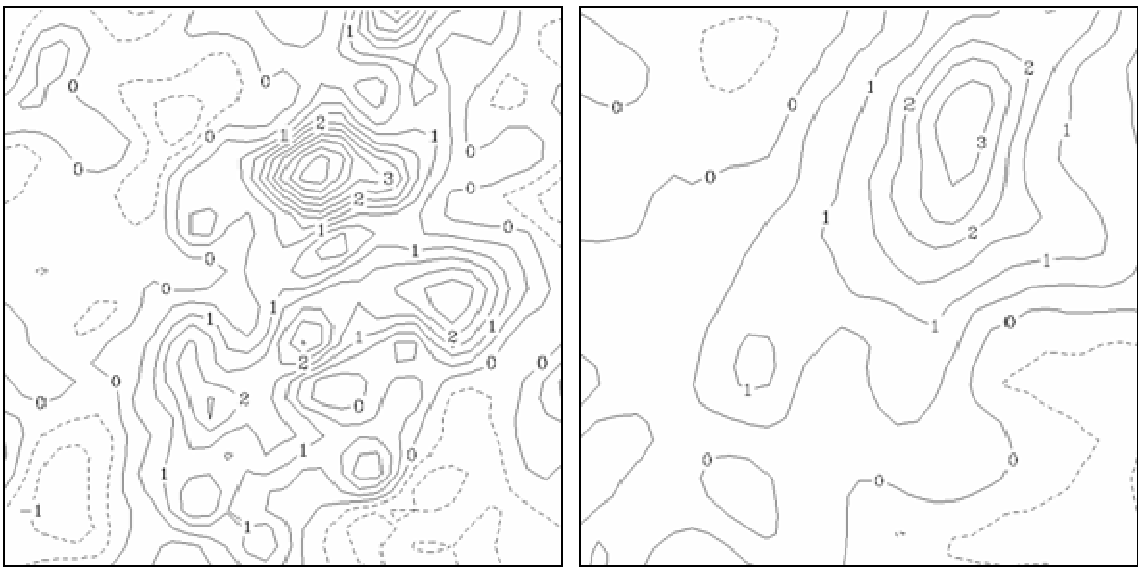

7.11.a) 7.11.b)

Figure 7.11. 21 hour divergence composites from MM5 and ETA-212 data, June-September 2004. 7.11.a) is the MM5 composite, and 7.11.b) is the ETA-212. Each image consists of a 375 km X 375 km area with a 0.5 contour interval.

Figure 7.12 shows the scatter plot of maximum divergence values for these 53 storms. The MM5 plot, 7.12.a), has an average of 18.8 x 10^{-5} s^{-1} with a standard deviation of 20.6 x 10^{-5} s^{-1}. 7.12.b), the ETA plot, shows an average of 8.0 x 10^{-5} s^{-1} and a standard deviation of 5.6 x 10^{-5} s^{-1}.

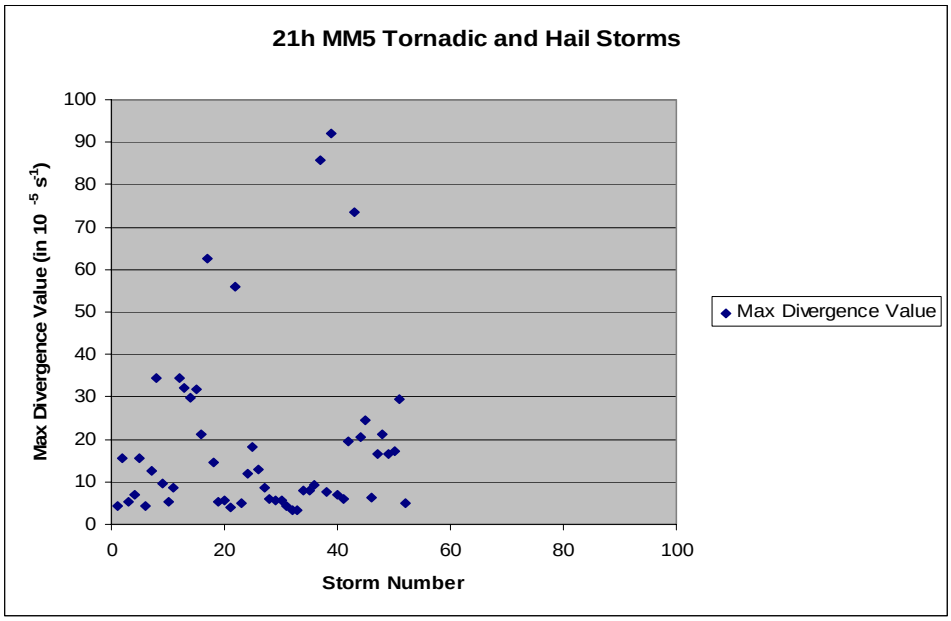

7.12.a)

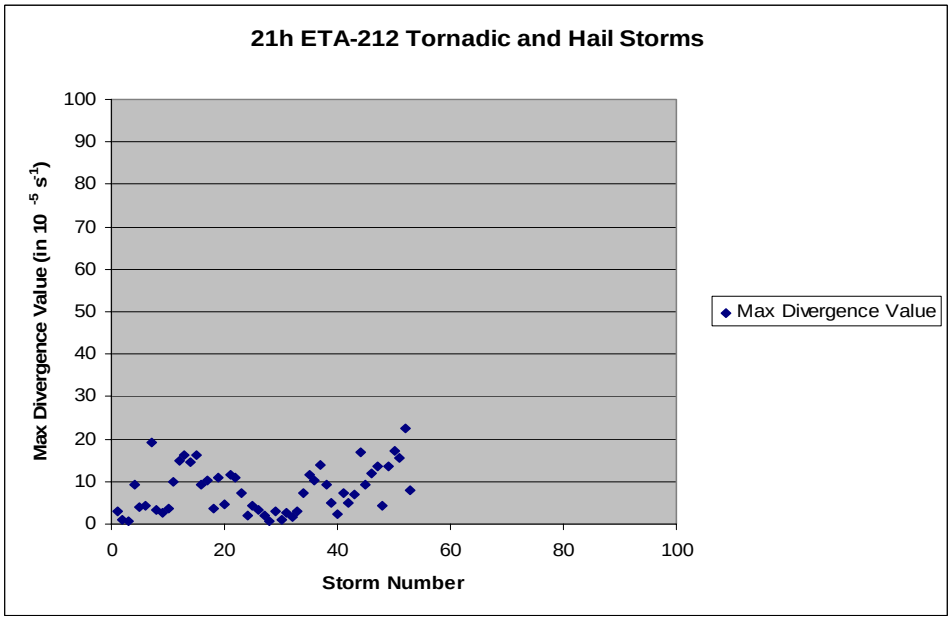

7.12.b)

Figure 7.12. Maximum divergence values from the 21 hour forecasts of MM5 and ETA-212 data, June-September 2004. The maxima were taken from a 52.5 km radius around the center point of the model grid. 7.12.a) is the MM5 plot, and 7.12.b) is the ETA-212 plot.

H. DISCUSSION OF DATA COMPARISON RESULTS

Table 7.2 presents the results of the previous sections grouped by forecast model. It shows the maximum divergence values from both the contour diagrams and the scatter plots, with the scatter plot standard deviation listed as well.

Time	Model	Sample Size	Contoured Max. Divergence	Scatter Plot Max. Divergence	Scatter Plot Standard Deviation
06h	MM5	89 Storms	$1.6 \times 10^{-5}\ s^{-1}$	$7.6 \times 10^{-5}\ s^{-1}$	$8.6 \times 10^{-5}\ s^{-1}$
09h	MM5	48 Storms	$5.0 \times 10^{-5}\ s^{-1}$	$22.5 \times 10^{-5}\ s^{-1}$	$28.0 \times 10^{-5}\ s^{-1}$
12h	MM5	43 Storms	$2.0 \times 10^{-5}\ s^{-1}$	$14.7 \times 10^{-5}\ s^{-1}$	$16.5 \times 10^{-5}\ s^{-1}$
15h	MM5	78 Storms	$3.25 \times 10^{-5}\ s^{-1}$	$12.5 \times 10^{-5}\ s^{-1}$	$16.3 \times 10^{-5}\ s^{-1}$
18h	MM5	89 Storms	$1.75 \times 10^{-5}\ s^{-1}$	$11.5 \times 10^{-5}\ s^{-1}$	$8.8 \times 10^{-5}\ s^{-1}$
21h	MM5	53 Storms	$4.5 \times 10^{-5}\ s^{-1}$	$18.8 \times 10^{-5}\ s^{-1}$	$20.6 \times 10^{-5}\ s^{-1}$

7.2.a)

06h	ETA-212	89 Storms	$2.0 \times 10^{-5}\ s^{-1}$	$7.3 \times 10^{-5}\ s^{-1}$	$5.4 \times 10^{-5}\ s^{-1}$
09h	ETA-212	48 Storms	$2.2 \times 10^{-5}\ s^{-1}$	$8.5 \times 10^{-5}\ s^{-1}$	$5.1 \times 10^{-5}\ s^{-1}$
12h	ETA-212	43 Storms	$2.0 \times 10^{-5}\ s^{-1}$	$7.2 \times 10^{-5}\ s^{-1}$	$4.1 \times 10^{-5}\ s^{-1}$
15h	ETA-212	78 Storms	$1.1 \times 10^{-5}\ s^{-1}$	$6.3 \times 10^{-5}\ s^{-1}$	$3.7 \times 10^{-5}\ s^{-1}$
18h	ETA-212	89 Storms	$2.0 \times 10^{-5}\ s^{-1}$	$6.4 \times 10^{-5}\ s^{-1}$	$4.4 \times 10^{-5}\ s^{-1}$
21h	ETA-212	53 Storms	$3.0 \times 10^{-5}\ s^{-1}$	$8.0 \times 10^{-5}\ s^{-1}$	$5.6 \times 10^{-5}\ s^{-1}$

7.2.b)

Table 7.2. Average maximum divergence values and standard deviations for the 6 hour through 21 hour forecasts of the MM5 and ETA-212 data examined in Chapter VII.

Comparison of the MM5 and ETA-212 data in the table above highlights the differences between a hydrostatic model (the ETA-212) and a non-hydrostatic one (the MM5). Since the ETA-212 is governed by the hydrostatic approximation, the model allows for generally weaker upward vertical motions, and the divergence pattern is smoother and less locally concentrated. In the MM5, the model does not use the hydrostatic approximation, so the model-generated upward vertical motions can be much stronger, resulting in higher, extremely localized divergence maxima. In addition, the convective parameterization used in the MM5 favors stronger convection.

Examining the contour diagram maximum divergence values, the MM5 displays a wider distribution of maximum values by forecast hour, while the ETA-212 shows less variation. While it is difficult to strictly compare one forecast hour to another due to the widely varying sample sizes, the MM5 contour plots are much less centered and organized than the ETA-212 plots. Both models start out looking markedly similar in the 6 hour charts, but quickly diverge in subsequent time steps. The MM5 contour averaged values are generally higher, but their location accuracy is lower as evidenced by the widely varying contour plots. The ETA-212 contour charts are much more organized, with easily identifiable maxima near the center of the diagrams.

The difference between the two models is also evident when comparing the scatter plot data. As with the contour plots, the models have similar 6 hour values but rapidly separate. The MM5 displays significantly higher average maxima and standard deviation values than the ETA-212 at all times after 6 hours. This is consistent with the previously identified differences between a non-hydrostatic and hydrostatic model: since the MM5 is not limited by the hydrostatic approximation, its generated vertical velocities and therefore divergence values are much higher. The standard deviations are higher as well, since there is more variation in the model's derived divergence values without the hydrostatic limitation.

While each forecast hour showed a broad agreement between the two models on the overall divergence pattern, it is difficult to draw a strong correlation between the models for each forecast time step. The 6, 18 and 21 hour divergence contour composites displayed a high degree of similarity, while the 9, 12 and 15 hour contour composites looked less alike. The relatively small sample size of storms considered in this chapter contributes to higher variability in the forecasts; the sample sizes from this section are 4 to 8 times smaller than the storms considered in previous chapters. Additionally, the scatter plot comparisons demonstrated the difficulty in directly comparing divergence values from a hydrostatic model to a non-hydrostatic one. Although the 6 hour data from each model was quite similar, the data for the remainder of the forecast periods showed no strong correlation.

THIS PAGE INTENTIONALLY LEFT BLANK

VIII. CONCLUSIONS AND RECOMMENDATIONS

A. CONCLUSIONS

The ETA-212 model data analyzed in chapters V and VI provides an excellent data set to generate probable divergence threshold values for severe weather occurrence. By combining the magnitude and area averaged contour plots with the magnitude averaged scatter plots, general guidelines for divergence threshold values can be obtained.

As a reminder, the contour plots and scatter plots describe different types of averaging. The maximum divergence values derived from the contour plots have been averaged over both magnitude and distance from the center of the grid; they represent a composite of all cases centered directly on the latitude and longitude of the occurring storm. These plots give a good depiction of the average divergence value at the exact location of the severe weather. Therefore, the maximum divergence values taken from the contour plots will provide a reasonable minimum value for severe storm development.

The divergence values taken from the scatter plots need to be interpreted in a different manner. Here, the average values represent the maximum divergence found anywhere in a 105 km radius of the severe storm location. This approach provides a more accurate depiction of the model's intensity forecast, at the expense of a slight error in the forecast location. The averages from the scatter plots will give a higher threshold value, but with a larger potential spatial error. The standard deviation values derived from the scatter plots can be utilized as well; by subtracting one standard deviation from the average, a much more reliable lower divergence value will be established.

A combination of these two data sets will provide the best method for defining threshold divergence values for severe events. The location-averaged values derived from the contour plots can determine an outer boundary value, while the higher values derived from the scatter plots, minus one standard deviation, could determine regions within the boundary value where severe storms are more likely to occur.

Since the goal is to determine a low-end threshold value, above which severe weather is likely to occur, it will be beneficial to disregard the combined tornadic and hail producing cases, and consider each set of storms separately. Figures 8.1 and 8.2 revisit earlier graphs, with only the tornadic and hail producing storms displayed. Figure 8.3 shows the standard deviation values from the scatter plots presented earlier.

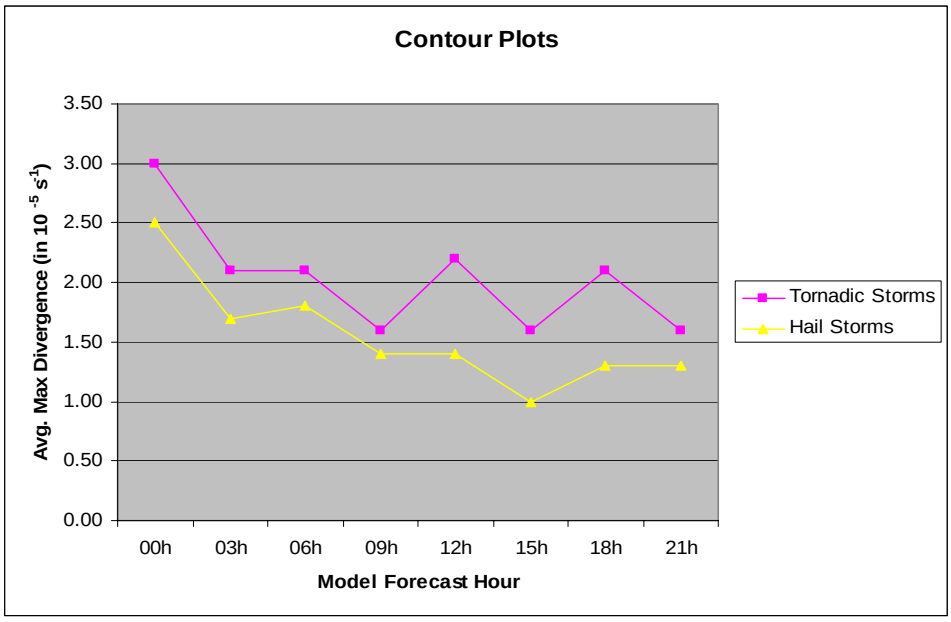

Figure 8.1. Average maximum divergence vs. ETA-212 forecast hour for tornado and hail events from the 2004 storm season, taken from the contour plot averages.

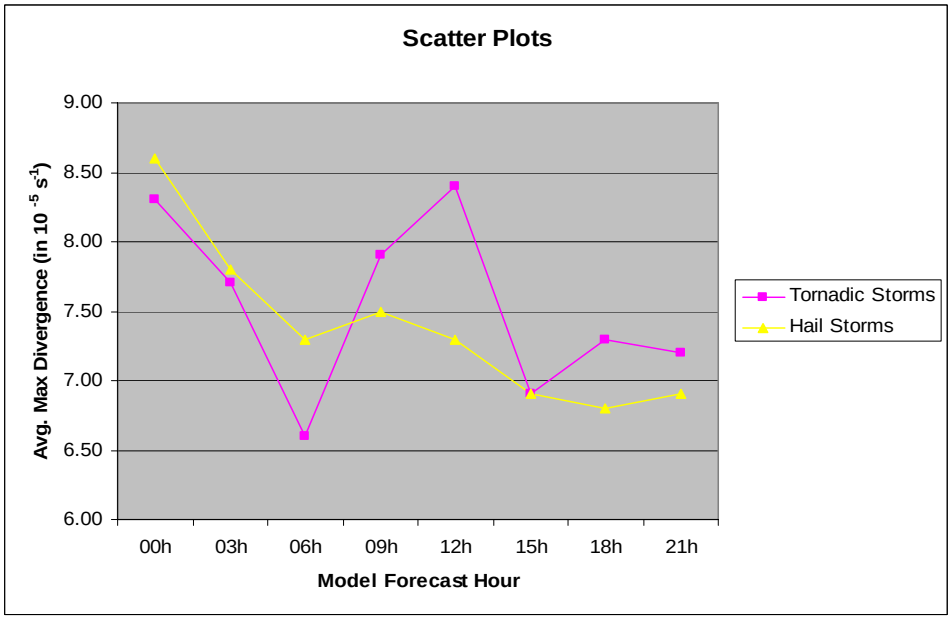

Figure 8.2. Average maximum divergence vs. ETA-212 forecast hour for tornado and hail events from the 2004 storm season, taken from the scatter plot averages.

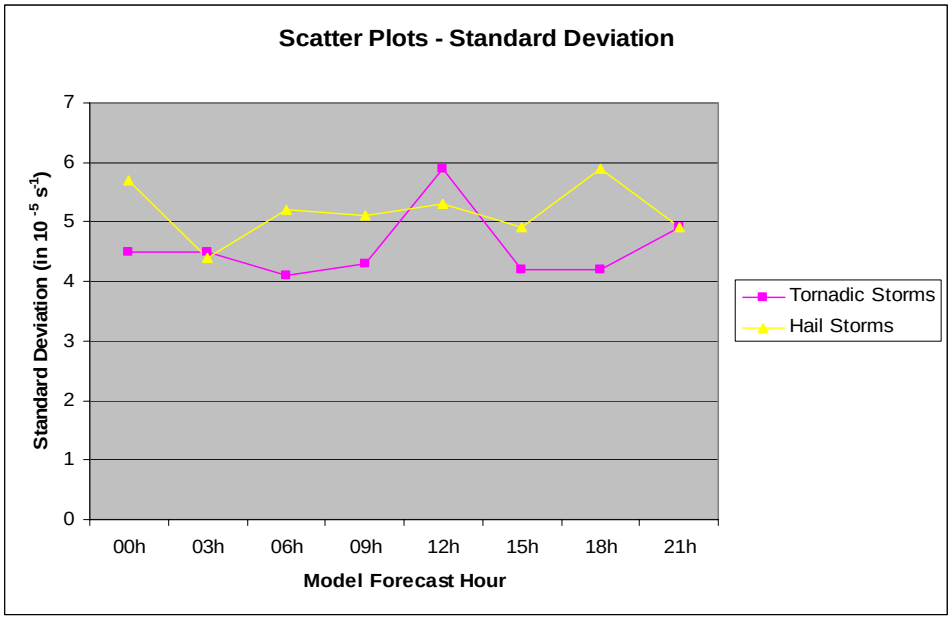

Figure 8.3. Standard deviation values vs. ETA-212 forecast hour for tornado and hail events from the 2004 storm season, taken from the scatter plot averages.

In Figures 8.1 and 8.2, the tornadic storms show a consistent drop-off in maximum divergence values until the 6 hour point, at which time the data becomes less consistent. The hail storms, however, show a general decreasing trend throughout the forecast period, with only slight anomalies at the 3 and 15 hour points in the contour graph and at the 6 and 18 hour points on the scatter graph. Figure 8.3 shows a fairly consistent standard deviation trend with time for the tornadic storms out to 6 hours, and the standard deviation values for hail storms also remain fairly consistent, around 5.0 x 10^{-5} s^{-1}.

Based on Figures 8.1 – 8.3, The recommended divergence threshold values indicative of severe weather are listed in Table 8.1. The "outer divergence threshold" values are derived from Figure 8.1, and the "inner divergence threshold" values are generated by taking the average maximum divergence values from 8.2 and subtracting one standard deviation, from 8.3. The outer divergence thresholds are chosen to represent a minimum divergence value above which severe weather is more likely to occur. On a divergence forecast chart, the outer thresholds will draw the forecaster's attention to regions with an increased risk for severe weather. The inner divergence thresholds are chosen to represent more specific storm thresholds above which severe

weather may occur. On a divergence chart, the inner thresholds will show the specific areas within the outer divergence boundary where severe weather is most likely to occur.

Time	Severe Storm Type	Recommended Outer Divergence Threshold	Recommended Inner Divergence Threshold
00h	Any severe weather	2.5×10^{-5} s^{-1}	3.0×10^{-5} s^{-1}
03h	Any severe weather	1.8×10^{-5} s^{-1}	3.0×10^{-5} s^{-1}
06h	Any severe weather	1.8×10^{-5} s^{-1}	2.4×10^{-5} s^{-1}
09h	Any severe weather	1.4×10^{-5} s^{-1}	2.4×10^{-5} s^{-1}
12h	Any severe weather	1.4×10^{-5} s^{-1}	2.0×10^{-5} s^{-1}
15h	Any severe weather	1.3×10^{-5} s^{-1}	2.0×10^{-5} s^{-1}
18h	Any severe weather	1.3×10^{-5} s^{-1}	2.0×10^{-5} s^{-1}
21h	Any severe weather	1.3×10^{-5} s^{-1}	2.0×10^{-5} s^{-1}

8.1.a)

00h	Tornadic	3.0×10^{-5} s^{-1}	3.8×10^{-5} s^{-1}
03h	Tornadic	2.0×10^{-5} s^{-1}	3.2×10^{-5} s^{-1}
06h	Tornadic	2.0×10^{-5} s^{-1}	2.5×10^{-5} s^{-1}

8.1.b)

Table 8.1. Recommended divergence threshold values for severe weather occurrence (00-21 hour forecasts) and tornadic storm occurrence (00-06 hour forecasts).

The outer divergence threshold values have been conservatively estimated at the 3 hour and 15 hour time steps in 8.1.a) to account for the slight anomalies in the graph at those points, and the inner divergence threshold values have been adjusted at 3, 6, and 18 hours to account for variations in the scatter plot – standard deviation differences. The data for tornadic storms out to 6 hours has not bee adjusted; the values out to this time step showed reasonable correlation with time. No attempt was made to determine divergence thresholds for tornadic storms after the 6 hour point, due to the erratic averaged data at longer time periods.

It is important to keep in mind that these recommended threshold values should not be considered absolute rules for severe weather development; they should rather be used as a guideline or a flag to alert the forecaster for the potential of severe weather

based on the model forecast. Furthermore, the divergence forecasts should not be considered independently; these threshold values should be used in conjunction with other severe weather forecasting parameters such as stability indices, wind shear and SKEW-T diagrams. Also, these derived threshold values are heavily biased towards the Midwestern states; they will work well for any severe weather developing over the central United States, but may not work as well for storms along the East Coast or in New England. These threshold values will also be biased towards afternoon storms, since the majority of the storm cases came from the 21Z – 03Z time period.

Several conclusions were drawn from the MM5 and ETA-212 model comparisons. The initial 6 hour forecast times looked markedly similar, but the magnitudes and locations of the divergence maxima differed to a significant degree at later time steps. The smaller sample size of the model comparisons may have contributed to the variation, but the main reasons for the large disparities in the MM5 and ETA-212 data are the differences in model resolution and the comparison of a hydrostatic and a non-hydrostatic model. Even though the ETA-212 has a higher base resolution of 12 km, the interpolation to the coarser 40 km grid smoothed the divergence values and provided more consistent divergence values than the higher resolution 15 km MM5 data. The scatter plots and standard deviation values highlight the differences in maximum divergence values from the non-hydrostatic MM5 and the hydrostatic ETA-212. The MM5 is not constrained by the hydrostatic approximation, and the model generates stronger vertical velocities and stronger divergence values, with much wider variations in the storm-to-storm intensity. The ETA-212 generates weaker vertical motions due to the hydrostatic constraints, and as a result produces more consistent storm-to-storm divergence values. The extremely large maximum divergence values obtained from the MM5 data made a threshold value much more difficult to obtain due to the widely varying values and high standard deviation. Based on these comparisons, the MM5 does not appear to be the best model to derive divergence threshold values.

B. RECOMMENDATIONS

As a result of this study, the following recommendations for further research are suggested:

- Investigate the correlation of divergence with other severe weather parameters such as wind shear or stability indices.
- Consider the "false alarm" cases of model forecasts. This study only focused on severe events that actually happened; it does not take any incorrect model forecasts into account. More research is needed on cases where the model forecast strong divergence but no severe weather occurred.
- A more in-depth study of MM5 divergence forecasts is needed. The comparison of MM5 and ETA-212 data in this study should only be considered as a preliminary overview; a larger number of storm cases and more detailed analysis of divergence data is needed before any definitive results for MM5 divergence forecasts can be identified. From the small sample sizes utilized in this study, the MM5 does not appear favorable for determining divergence threshold values, but more research is needed.
- Obtain multiple years' worth of data to examine the month to month variation of divergence intensity. A monthly comparison was planned for this study, but there were not enough storm cases to generate consistent monthly divergence data.
- Several years' worth of data may also allow an examination of storms by region. With more storm cases from the East Coast or New England states, separate divergence studies could be conducted on these areas to determine more appropriate regional threshold values.

APPENDIX A - SAMPLE SPC STORM REPORT

SPC Storm Reports

1200 UTC May 08, 2004 - 1159 UTC May 09, 2004

20040508's Storm Reports

Note: All data are considered preliminary

Tornado Reports (in CSV format)

Time	F-Scale	Location	County	State	Lat	Lon	Comments
2317	UNK	3 W YALE	GUTHRIE	IA	4178	9442	(DMX)
0000	UNK	6 S CLARKSON	COLFAX	NE	4164	9712	(OAX)
0009	UNK	4 W REDFIELD	GUTHRIE	IA	4159	9428	(DMX)
0017	UNK	3 N STUART	GUTHRIE	IA	4155	9432	(DMX)
0040	UNK	1 SW SCHUYLER	COLFAX	NE	4144	9707	DESTROYED ONE CENTER PIVOT SYSTEM (OAX)
0155	UNK	9 SSE HARLAN	SHELBY	IA	4165	9533	F0 TORNADO STARTED SOUTH SOUTHEAST OF HARLAN AND PRODUCED DAMAGE TO MAINLY TREES IN SHELBY COUNTY CONTINUED INTO POTTAWATTAMIE COUNTY. (OAX)
0206	UNK	4 SSE WALNUT	POTTAWATTAMIE	IA	4148	9522	TORNADO STARTED IN SHELBY COUNTY AT 855 PM AND CONTINUED TO MOVE SOUTH SOUTHEAST ACROSS POTTAWAT INCREASING TO F1 STRENGTH NEAR AND SOUT DISIPATING AT 906 PM. THERE WAS (OAX)

Hail Reports (in CSV format)

Time	Size	Location	County	State	Lat	Lon	Comments
1224	75	WEBSTER CITY	HAMILTON	IA	4246	9382	(DMX)
1359	88	5 W PAW PAW	VAN BUREN	MI	4222	8599	(GRR)
2035	88	CLYDE	HAYWOOD	NC	3553	8291	FOLLOWED BY PENNY HAIL 10 MINUTES LATER (GSP)
2111	100	AMES	STORY	IA	4202	9363	(DMX)
2120	175	TUCKASEGEE	JACKSON	NC	3527	8312	PUBLIC REPORTED THROUGH 911 (GSP)
2137	100	CANTON	HAYWOOD	NC	3555	8284	PUBLIC REPORT VIA CELL PHONE OF LOTS OF PENNY TO QUARTER SIZE HAIL BEATING UP CARS. ALSO LOCAL F AND TERRIBLE LIGHTNING. (GSP)
2140	75	1 S BANNER HILL	UNICOI	TN	3611	8241	DIME SIZE HAIL NEAR BANNER HILL. REPORTED BY SHERIFFS OFFICE. (MRX)
2153	100	3 SE READLYN	BREMER	IA	4267	9219	(DMX)

2203	88	FLORENCE	FLORENCE	SC	3420	7976	DIME TO NICHEL SIZE HAIL REPORTED AT HOFFMIRE ROAD AND I-95 (ILM)
2204	75	5 ENE CHURDAN	GREENE	IA	4218	9440	ESTIMATED WINDS OF 40-50 MPH. (DMX)
2213	175	READLYN	BREMER	IA	4270	9222	(DMX)
2215	175	4 N ELLSWORTH	HAMILTON	IA	4237	9358	(DMX)
2216	100	IOWA FALLS	HARDIN	IA	4252	9327	(DMX)
2218	75	FAIRBANK	FAYETTE	IA	4264	9205	(ARX)
2247	100	5 NE ELLSWORTH	HAMILTON	IA	4236	9351	(DMX)
2249	175	8 S SCRANTON	GREENE	IA	4190	9455	(DMX)
2249	88	2 SSW RADCLIFFE	HARDIN	IA	4229	9344	(DMX)
2305	150	4 SW LINDSAY	PLATTE	NE	4166	9775	(OAX)
2308	100	8 S STANTON	STANTON	NE	4183	9722	(OAX)
2308	88	2 SSW RADCLIFFE	HARDIN	IA	4229	9344	(DMX)
2311	88	BAGLEY	GUTHRIE	IA	4185	9443	(DMX)
2311	175	8 S SCRANTON	GREENE	IA	4190	9455	(DMX)
2320	100	OVERTON	DAWSON	NE	4074	9954	MAINLY PEA HAIL...BUT SOME QUARTER SIZE (GID)
2320	75	7 S MASON CITY	CUSTER	NE	4112	9930	(LBF)
2330	88	5 S LEIGH	COLFAX	NE	4163	9724	(OAX)
2331	175	YALE	GUTHRIE	IA	4178	9436	FROM KCCI TV. (DMX)
2335	75	4 SSW ENNING	MEADE	SD	4452	10260	(UNR)
2340	100	6 SW BEEMER	CUMING	NE	4187	9689	(OAX)
2355	75	STANTON	STANTON	NE	4195	9722	(OAX)
0005	175	SHEFFIELD	FRANKLIN	IA	4289	9321	(DMX)
0008	75	MADRID	BOONE	IA	4188	9382	FROM KCCI TV (DMX)
0008	150	2 S NEW ALBIN	ALLAMAKEE	IA	4347	9129	HAIL NEW ALBIN 43.50N 91.29W 0.88 INCH ALLAMAKEE IA (ARX)
0013	100	2 NW GOSHEN	ELKHART	IN	4160	8586	(IWX)
0015	175	4 S ROCKWELL	CERRO GORDO	IA	4292	9319	(DMX)
0018	175	3 W ADEL	DALLAS	IA	4161	9409	(DMX)
0020	200	4 NE GUTHRIE CENTER	GUTHRIE	IA	4172	9444	(DMX)
0024	88	N DOWS	WRIGHT	IA	4266	9350	(DMX)
0027	100	NEWAYGO	NEWAYGO	MI	4342	8580	(GRR)
0028	75	BEAVER CITY	FURNAS	NE	4014	9983	(GID)
0028	75	HAMPTON	FRANKLIN	IA	4274	9320	REPORTED BY TRAINED SPOTTER. (DMX)
0035	100	MARBLE ROCK	FLOYD	IA	4296	9287	(ARX)
0038	88	BOVINA	PARMER	TX	3452	10289	(LBB)
0038	100	2 N SCHUYLER	COLFAX	NE	4148	9706	(OAX)
0038	100	4 S ONAWA	MONONA	IA	4197	9609	(OAX)

0045	300	CHARLES CITY	FLOYD	IA	4307	9268	REPORTED VIA KWWL TELEVISION FROM THE EASTERN SIDE OF THE CITY. (ARX)
0049	200	ADEL	DALLAS	IA	4161	9403	FROM KCCI TV. (DMX)
0052	75	7 S LAGRANGE	LAGRANGE	IN	4154	8542	(IWX)
0055	175	1 W EARLHAM	MADISON	IA	4149	9414	(DMX)
0058	100	6 SW GRAY	AUDUBON	IA	4178	9507	(DMX)
0105	125	SCHUYLER	COLFAX	NE	4145	9706	(OAX)
0110	175	NORTH WASHINGTON	CHICKASAW	IA	4312	9242	(ARX)
0110	75	5 W GRINDSTONE	PENNINGTON	SD	4413	10206	(UNR)
0111	175	EARLHAM	MADISON	IA	4149	9412	(DMX)
0120	88	2 E FERRYVILLE	CRAWFORD	WI	4334	9104	(ARX)
0121	88	DE SOTO	DALLAS	IA	4153	9401	REPORTED BY TRAINED SPOTTER. (DMX)
0130	175	NEW HAMPTON	CHICKASAW	IA	4306	9231	REPORTED VIA KIMT TELEVISION. (ARX)
0132	75	LINWOOD	BUTLER	NE	4141	9693	(OAX)
0135	75	15 W MIDLAND	HAAKON	SD	4407	10145	(UNR)
0136	175	MENLO	GUTHRIE	IA	4152	9440	(DMX)
0138	75	RIDGEWAY	WINNESHIEK	IA	4330	9199	(ARX)
0140	100	7 S STUART	ADAIR	IA	4140	9432	(DMX)
0140	75	10 E NEWAYGO	NEWAYGO	MI	4342	8560	(GRR)
0145	88	IRWIN	SHELBY	IA	4179	9521	(OAX)
0145	100	SENECA	CRAWFORD	WI	4327	9097	(ARX)
0148	75	2 SW NORTON	NORTON	KS	3981	9992	(GLD)
0150	75	HARLAN	SHELBY	IA	4165	9533	(OAX)
0154	125	WINTERSET MADISON COUNT	MADISON	IA	4136	9402	(DMX)
0155	88	FREMONT	NEWAYGO	MI	4346	8595	(GRR)
0200	100	AVOCA	POTTAWATTAMIE	IA	4148	9534	(OAX)
0211	88	WINTERSET	MADISON	IA	4134	9402	(DMX)
0215	75	MILLERS CREEK	WILKES	NC	3619	8124	HAIL RANGED FROM DIME TO PENNY SIZE. LASTED FROM 1015 PM UNTIL 1035 PM (RNK)
0220	100	5 N NORTON	NORTON	KS	3991	9989	(GLD)
0224	100	2 E OLTON	LAMB	TX	3418	10210	(LBB)
0236	88	3 SE WINTERSET	MADISON	IA	4131	9398	(DMX)
0239	75	5 NW ROCK SPRINGS	SAUK	WI	4353	8999	(MKX)
0249	100	7 N FONTANELLE	ADAIR	IA	4139	9456	(DMX)

0255	100	5 NW ANITA	CASS	IA	4149	9483	ALONG INTERSTATE 80 NEAR MILE MARKER 64. WINDS ESTIMATED AT 50 MPH AS WELL. (DMX)
0300	75	2 S LAWRENCE PARK	ERIE	PA	4212	8002	(CLE)
0300	75	4 S WAUKESHA	WAUKESHA	WI	4295	8824	(MKX)
0301	75	3 W LEWIS	CASS	IA	4131	9514	(DMX)
0340	100	2 E BEAVER CITY	FURNAS	NE	4014	9979	(GID)
0405	100	SPRUCE PINE	MITCHELL	NC	3592	8207	TWO DEPUTIES REPORTED PENNY TO QUARTER SIZE HAIL FROM AROUND 1155 PM TO 1205 AM IN THE SPRUCE (GSP)
0405	88	3 E PENDER	THURSTON	NE	4211	9665	(OAX)
0409	100	5 NW CROFTON	KNOX	NE	4278	9757	(OAX)
0435	88	YANKTON	YANKTON	SD	4289	9739	(FSD)
0439	100	MANSON	CALHOUN	IA	4253	9454	(DMX)
0450	88	GLENWOOD	MILLS	IA	4105	9574	(OAX)
0500	88	5 E WEBBER	JEWELL	KS	3993	9794	(GID)
0505	75	6 W ORISKA	BARNES	ND	4694	9791	(FGF)
0930	88	OSBORNE	OSBORNE	KS	3944	9870	(GID)

Wind Reports (in CSV format)

Time	Speed	Location	County	State	Lat	Lon	Comments
1945	65	3 SW GREAT FALLS	CASCADE	MT	4750	11129	VISIBILITY REDUCED TO 1 3/4 MILES IN BLOWING DUST DURING THE GUSTY WINDS. (TFX)
1951	71	34 SSW GLASGOW	VALLEY	MT	4774	10692	(GGW)
2040	60	2 E WAYNESVILLE	HAYWOOD	NC	3548	8296	EDGE OF WAYNESVILLE TOWARD HOSPITAL (GSP)
2150	60	1 S HOOVER	BUTTE	SD	4511	10327	TSTM WND GST 6 NW NEWELL 44.78N 103.50W 60 MPH BUTTE SD (UNR)
2221	64	1 N STURGIS	MEADE	SD	4443	10351	(UNR)
2305	70	1 ENE HAYDRAW	MEADE	SD	4445	10271	(UNR)
2310	UNK	UNION CENTER	MEADE	SD	4456	10267	ROOF BLOWN OFF BUILDING, TREE BRANCHES DOWN AND POWER OUT. (UNR)
2329	60	4 SSW ENNING	MEADE	SD	4452	10260	(UNR)
2330	UNK	CORRY	ERIE	PA	4193	7964	TWO LARGE LIMBS DOWN. (CLE)
0015	60	3 NNE CREIGHTON	PENNINGTON	SD	4429	10218	(UNR)
0025	UNK	ERIE	ERIE	PA	4213	8009	NEAR THE AIRPORT TWO LARGE LIMBS DOWN. (CLE)
0045	60	3 NW GRINDSTONE	HAAKON	SD	4417	10201	(UNR)

0050	60	2 N FREMONT	DODGE	NE	4147	9649	(OAX)
0105	80	SCHUYLER	COLFAX	NE	4145	9706	TREES DOWN AND CENTER PIVOTS OVERTURNED (OAX)
0110	60	5 W GRINDSTONE	PENNINGTON	SD	4413	10206	HAIL 5 W GRINDSTONE 44.12N 103.28W 0.75 INCH HAAKON SD (UNR)
0130	60	FORT CALHOUN	WASHINGTON	NE	4146	9603	THUNDERSTORM WINDS DAMAGED TREES AND A POWER POLE IN TOWN. A FEW WINDOWS WERE ALSO BROKEN DU (OAX)
0200	70	1 N WALNUT	POTTAWATTAMIE	IA	4149	9522	TRUCK BLOWN OVER ON I80. WIND SPEED ESTIMATED. (OAX)
0203	70	HARLAN	SHELBY	IA	4165	9533	(OAX)
0225	UNK	2 W LEWIS	CASS	IA	4131	9512	A 7 MILE PATH OF WIND DAMAGE...LARGE TREES DOWN. FROM 2W LEWIS SOUTHEAST TO HIGHWAY 71. (DMX)
0245	UNK	MULBERRY	WILKES	NC	3623	8117	TREES DOWN. (RNK)
0250	UNK	MOBRIDGE	WALWORTH	SD	4554	10044	WINDOW BROKEN AND TREE BLOWN OVER IN NORTH MOBRIDGE. (ABR)
0252	UNK	6 SE ATLANTIC	CASS	IA	4134	9493	LARGE CORN CRIB BLOWN OVER BLOCKING COUNTY HIGHWAY G43. 1 MILE EAST OF ROUTE 71. (DMX)
0326	UNK	4 N WIOTA	CASS	IA	4146	9489	LARGE TREE BLOCKING ROAD. HALF MILE SOUTH OF LEWIS... SEVERAL TREES BLOCKING COLD SPRING PARK (DMX)
0337	70	5 S AFTON	UNION	IA	4096	9420	VISIBILITY ZERO IN DRIVING RAIN. UNION COUNTY SHERIFF. (DMX)
0355	76	LUBBOCK	LUBBOCK	TX	3365	10181	MEASURED AT WFO IN SOUTH LUBBOCK (LBB)
0425	62	2 NE SLATON	LUBBOCK	TX	3346	10162	MEASURED BY TEXAS TECH WEST TEXAS MESONET STATION (LBB)

***Full report* in comma-separated values (CSV) format**

Fields marked UNK are unknown

All Times UTC

Wind Gusts in MPH

Hail Sizes in 1/100 of an Inch (75 = 0.75")

Top

THIS PAGE INTENTIONALLY LEFT BLANK

APPENDIX B – LIST OF MAY STORMS

TORNADO PRODUCING STORMS							
#	**Date**	**Time (Z)**	**Location**	**Lat / Lon**	**Type (A / B)**	**ETA-212 Data**	**MM5 Data**
1	9-May	0000	NE	41.6 / 97.1	A	x	
2	9-May	0009	IA	41.6 / 94.3	A	x	
3	9-May	2129	MD	45.3 / 94.4	B	x	
4	13-May	2359	IL	41.5 / 87.6	A	x	
5	16-May	2353	NE	42.4 / 98.5	A	x	
6	17-May	0005	NE	41.2 / 98.6	A	x	
7	20-May	0007	ND / MN	48.9 / 97.1	A	x	
8	21-May	2058	IA	42.0 / 92.0	B	x	
9	22-May	0030	IA	42.8 / 93.8	A	x	
10	22-May	0313	NE	42.0 / 98.9	B	x	
11	22-May	2035	MI	42.9 / 84.3	B	x	
12	22-May	2110	MI	43.6 / 82.7	B	x	
13	22-May	2334	NE	41.2 / 99.8	A	x	
14	22-May	2352	NE	40.2 / 97.6	A	x	
15	23-May	0005	NE	40.3 / 98.5	A	x	
16	23-May	0008	IA	41.5 / 94.4	A	x	
17	23-May	0010	NE	41.4 / 97.1	A	x	
18	23-May	0012	NE	41.2 / 99.4	A	x	
19	23-May	0025	NE	40.3 / 97.4	A	x	
20	23-May	0230	IA	42.1 / 92.7	B	x	
21	23-May	0247	NE	40.7 / 95.9	B	x	
22	23-May	0300	NE	40.9 / 95.9	B	x	
23	23-May	0324	NE	40.3 / 97.0	B	x	
24	23-May	0330	IA	41.3 / 95.1	B	x	
25	23-May	1147	WI	44.2 / 87.9	A	x	
26	23-May	2129	MI	42.7 / 84.3	B	x	
27	24-May	0001	WI	43.3 / 89.4	A	x	
28	24-May	0027	IL	39.6 / 89.8	A	x	
29	24-May	0030	MI	43.1 / 82.7	A	x	
30	24-May	2102	NE	40.2 / 97.6	B	x	
31	24-May	2130	IA	40.8 / 95.8	B	x	

#	Date	Time (Z)	Location	Lat / Lon	Type (A / B)	ETA-212 Data	MM5 Data
32	24-May	2130	NY	42.1 / 75.5	B	x	
33	25-May	0020	IA	40.7 / 94.2	A	x	
34	25-May	2123	PA	41.5 / 80.2	B	x	
35	28-May	0002	IN	38.5 / 86.0	A	x	
36	29-May	0004	SD	43.2 / 97.3	A	x	
37	29-May	0238	IA	42.3 / 96.0	B	x	
38	29-May	2123	NE	41.0 / 100.3	B	x	
39	29-May	2330	NE	41.3 / 98.1	A	x	
40	29-May	2330	SD	45.5 / 98.6	A	x	
41	29-May	2346	SD	45.4 / 99.0	A	x	
42	30-May	1437	IL	40.4 / 89.6	B	x	
43	30-May	1805	IN	39.2 / 86.9	A	x	
44	30-May	2035	MN	45.5 / 94.0	B	x	
45	30-May	2050	IA	42.2 / 91.9	B	x	
46	30-May	2055	IA	42.2 / 91.2	B	x	
47	30-May	2107	IL	40.6 / 90.5	B	x	
48	30-May	2110	IA	41.7 / 91.5	B	x	
49	30-May	2111	IL	38.8 / 90.0	B	x	
50	30-May	2332	IL	37.7 / 89/3	A	x	
51	30-May	2335	IL	38.3 / 89.2	A	x	
52	30-May	2340	IL	40.9 / 88.3	A	x	
53	31-May	0000	IN	39.7 / 86.2	A	x	
54	31-May	0007	IA	42.4 / 92.0	A	x	
55	31-May	0025	IL	37.6 / 88.8	A	x	
56	31-May	0026	IN	40.3 / 86.8	A	x	
57	31-May	0028	MN	44.3 / 92.6	A	x	
58	31-May	0028	MN	45.6 / 93.0	A	x	
59	31-May	0300	IN	38.0 / 86.2	B	x	
	A Storms: 34			B Storms: 25			

HAIL PRODUCING STORMS							
#	**Date**	**Time (Z)**	**Location**	**Lat / Lon**	**Type (A / B)**	**ETA-212 Data**	**MM5 Data**
1	1-May	2120	OH	40.5 / 83.2	B	x	
2	2-May	1520	IA / IL	40.6 / 90.4	B	x	
3	2-May	1749	IA / IL	42.0 / 91.4	A	x	
4	6-May	1500	MI	43.6 / 86.1	B	x	
5	7-May	0259	IN	41.2 / 85.9	B	x	
6	7-May	0301	MI	41.9 / 83.8	B	x	
7	7-May	0320	NY	42.1 / 79.2	B	x	
8	7-May	0845	MI	42.3 / 85.7	B	x	
9	7-May	0902	IA	41.6 / 91.0	B	x	
10	7-May	1132	IL	41.0 / 88.9	A	x	
11	7-May	1145	OH	41.1 / 82.1	A	x	
12	7-May	1159	IA	41.6 / 91.5	A	x	
13	7-May	1220	IN	41.2 / 85.5	A	x	
14	7-May	1443	OH	40.5 / 82.6	B	x	
15	7-May	1445	PA	40.6 / 79.2	B	x	
16	7-May	1505	OH	40.7 / 83.8	B	x	
17	7-May	2100	WV	38.9 / 79.9	B	x	
18	8-May	0544	WI	43.9 / 90.8	A	x	
19	8-May	0559	MN	43.8 / 92.4	A	x	
20	8-May	0605	IA	43.1 / 95.8	A	x	
21	8-May	0605	IA	43.1 / 95.8	A	x	
22	8-May	0850	MN / IA	43.0 / 93.2	B	x	
23	8-May	1224	IA	42.5 / 93.8	A	x	
24	8-May	2111	IA	42.0 / 93.6	B	x	
25	8-May	2335	SD	44.5 / 102.6	A	x	
26	9-May	0005	IA	42.9 / 93.2	A	x	
27	9-May	0008	IA	43.5 / 91.3	A	x	
28	9-May	0013	IN	41.6 / 85.9	A	x	
29	9-May	0027	MI	43.4 / 85.8	A	x	
30	9-May	0028	NE	40.1 / 99.8	A	x	
31	9-May	0239	WI	43.5 / 90.0	B	x	
32	9-May	0255	IA	41.5 / 94.8	B	x	
33	9-May	0300	PA	42.1 / 80.0	B	x	
34	9-May	0300	WI	43.0 / 88.2	B	x	

#	Date	Time (Z)	Location	Lat / Lon	Type (A / B)	ETA-212 Data	MM5 Data
35	9-May	1451	SD	44.6 / 97.3	B	x	
36	9-May	2105	MI	42.8 / 85.3	B	x	
37	9-May	2344	IL	41.5 / 87.6	A	x	
38	9-May	2350	MN	44.8 / 93.2	A	x	
39	10-May	0000	WI	44.6 / 92.4	A	x	
40	10-May	0010	SD	42.8 / 96.9	A	x	
41	10-May	0020	NE	42.5 / 98.7	A	x	
42	10-May	0245	MN	44.4 / 92.7	B	x	
43	10-May	0254	SD	42.9 / 96.9	B	x	
44	10-May	0255	WI	44.6 / 89.3	B	x	
45	10-May	0326	MD	39.7 / 76.4	B	x	
46	10-May	0603	NE	40.7 / 97.1	A	x	
47	10-May	1209	OH	41.1 / 81.6	A	x	
48	10-May	2110	MI	42.3 / 85.6	B	x	
49	10-May	2111	PA	42.0 / 80.0	B	x	
50	10-May	2356	MI	42.3 / 85.2	A	x	
51	12-May	2103	IL	41.9 / 88.2	B	x	
52	12-May	2107	MI	46.7 / 89.2	B	x	
53	12-May	2130	WI	45.0 / 90.1	B	x	
54	13-May	0300	NE	40.3 / 96.8	B	x	
55	13-May	0305	MI	44.0 / 85.0	B	x	
56	13-May	0915	IA	40.6 / 93.5	B	x	
57	16-May	2102	NE	40.6 / 99.8	B	x	
58	16-May	2125	NE	41.9 / 99.6	B	x	
59	16-May	2348	NE	42.1 / 99.3	A	x	
60	16-May	2355	NE	41.1 / 99.6	A	x	
61	17-May	0008	NE	41.2 / 98.6	A	x	
62	17-May	0015	SD	43.1 / 98.3	A	x	
63	17-May	1815	MI	42.4 / 84.5	A	x	
64	17-May	1830	OH	41.6 / 84.7	A	x	
65	17-May	2105	OH	40.8 / 82.5	B	x	
66	17-May	2110	MI	43.8 / 83.3	B	x	
67	17-May	2120	IA	40.9 / 95.8	B	x	
68	17-May	2126	NE	40.5 / 96.6	B	x	
69	17-May	2344	IA	42.6 / 91.0	A	x	

#	Date	Time (Z)	Location	Lat / Lon	Type (A / B)	ETA-212 Data	MM5 Data
70	17-May	2346	IA	41.4 / 94.2	A	x	
71	17-May	2350	OH	39.1 / 84.1	A	x	
72	17-May	2350	OH	39.6 / 82.5	A	x	
73	18-May	0001	IA	41.0 / 94.7	A	x	
74	18-May	0001	IA	41.4 / 94.2	A	x	
75	18-May	0015	OH	39.2 / 83.8	A	x	
76	18-May	0019	OH	40.7 / 81.5	A	x	
77	18-May	0025	IA	41.4 / 94.0	A	x	
78	18-May	0027	WI	43.2 / 90.1	A	x	
79	18-May	0245	IL	41.4 / 90.9	B	x	
80	18-May	0310	IL	42.4 / 88.8	B	x	
81	18-May	1830	PA	41.9 / 79.0	A	x	
82	18-May	2055	IL	39.1 / 90.1	B	x	
83	18-May	2100	VT	43.6 / 73.2	B	x	
84	18-May	2115	WV / OH	40.8 / 80.6	B	x	
85	18-May	2125	PA	40.8 / 80.3	B	x	
86	18-May	2127	OH	40.6 / 82.8	B	x	
87	18-May	2130	IL	39.2 / 89.5	B	x	
88	19-May	0012	PA	40.4 / 75.2	A	x	
89	19-May	2056	IA	43.0 / 95.8	B	x	
90	19-May	2102	ND	48.6 / 100.3	B	x	
91	19-May	2340	SD	44.4 / 98.9	A	x	
92	19-May	2350	ND	48.4 / 97.8	A	x	
93	20-May	0005	IA	43.4 / 94.1	A	x	
94	20-May	0019	SD	45.2 / 97.9	A	x	
95	20-May	0235	MN	48.0 / 96.5	B	x	
96	20-May	1210	MI	42.8 / 85.9	A	x	
97	20-May	2332	IL	42.4 / 89.4	A	x	
98	20-May	2355	IA	41.5 / 91.8	A	x	
99	21-May	0230	IL	41.1 / 89.9	B	x	
100	21-May	0245	IL	42.1 / 87.9	B	x	
101	21-May	0322	NE	40.9 / 98.4	B	x	
102	21-May	0325	MI	42.7 / 84.4	B	x	
103	21-May	0600	NE	41.9 / 98.9	A	x	
104	21-May	0610	MN	43.5 / 96.0	A	x	

#	Date	Time (Z)	Location	Lat / Lon	Type (A / B)	ETA-212 Data	MM5 Data
105	21-May	0921	WV / OH	40.3 / 80.6	B	x	
106	21-May	1130	IA	42.8 / 91.5	A	x	
107	21-May	1134	WV	38.9 / 80.8	A	x	
108	21-May	1505	IL	42.0 / 87.9	B	x	
109	21-May	1526	IN	40.3 / 86.5	B	x	
110	21-May	1735	IN	41.3 / 85.9	A	x	
111	21-May	1735	IA	42.9 / 92.9	A	x	
112	21-May	1740	IN	41.6 / 85.2	A	x	
113	21-May	1758	WI / IA	43.5 / 91.1	A	x	
114	21-May	1801	MI	42.2 / 83.8	A	x	
115	21-May	2042	IA	42.4 / 92.8	B	x	
116	21-May	2043	IA	42.0 / 92.2	B	x	
117	21-May	2050	OH	40.0 / 82.6	B	x	
118	21-May	2050	IA	42.2 / 95.9	B	x	
119	21-May	2052	OH	40.5 / 83.7	B	x	
120	21-May	2056	OH	40.7 / 81.3	B	x	
121	21-May	2100	OH	41.5 / 80.9	B	x	
122	21-May	2104	IA	42.5 / 92.4	B	x	
123	21-May	2115	IN	40.4 / 85.0	B	x	
124	21-May	2116	OH	40.1 / 82.4	B	x	
125	21-May	2120	SD	44.2 / 103.0	B	x	
126	21-May	2130	NE	42.7 / 102.5	B	x	
127	21-May	2334	WV	38.9 / 80.8	A	x	
128	21-May	2355	IA	42.8 / 94.0	A	x	
129	21-May	2355	SD	44.1 / 101.7	A	x	
130	21-May	2355	MN	43.6 / 94.5	A	x	
131	21-May	2356	IA	42.9 / 92.7	A	x	
132	21-May	2359	IL	42.0 / 90.1	A	x	
133	22-May	0230	MI	42.2 / 83.8	B	x	
134	22-May	0239	IL	41.8 / 88.2	B	x	
135	22-May	0240	NE	42.2 / 97.0	B	x	
136	22-May	0250	MN	43.7 / 93.6	B	x	
137	22-May	0251	MI	42.3 / 83.7	B	x	
138	22-May	0259	NE	41.3 / 102.6	B	x	
139	22-May	0300	SD	42.8 / 96.9	B	x	

#	Date	Time (Z)	Location	Lat / Lon	Type (A / B)	ETA-212 Data	MM5 Data
140	22-May	0305	IA	42.9 / 95.4	B	x	
141	22-May	0306	NE	42.0 / 99.0	B	x	
142	22-May	0327	NE	42.1 / 96.7	B	x	
143	22-May	0535	OH	41.2 / 81.5	A	x	
144	22-May	0558	IA	43.1 / 92.9	A	x	
145	22-May	0620	NE	41.4 / 98.0	A	x	
146	22-May	0845	NE	41.6 / 96.2	B	x	
147	22-May	0856	IA	42.3 / 90.4	B	x	
148	22-May	2050	SD	44.0 / 103.5	B	x	
149	22-May	2055	NE	41.7 / 101.5	B	x	
150	22-May	2105	NE	40.4 / 101.1	B	x	
151	22-May	2116	NE	41.0 / 103.1	B	x	
152	22-May	2117	NE	41.5 / 101.6	B	x	
153	22-May	2335	NY	42.9 / 78.4	A	x	
154	22-May	2347	NE	42.0 / 99.9	A	x	
155	22-May	2351	IA	42.1 / 94.8	A	x	
156	22-May	2358	IA	41.9 / 93.8	A	x	
157	23-May	0000	NY	42.4 / 77.1	A	x	
158	23-May	0001	NE	41.6 / 96.5	A	x	
159	23-May	0310	NE	40.0 / 97.8	B	x	
160	23-May	0315	IA	41.8 / 93.6	B	x	
161	23-May	0631	WI	42.9 / 89.5	A	x	
162	23-May	1824	IN	39.7 / 87.4	A	x	
163	23-May	2047	NY	41.4 / 73.6	B	x	
164	23-May	2108	IN	40.8 / 84.8	B	x	
165	23-May	2112	CT	41.9 / 72.3	B	x	
166	23-May	2351	NY	41.7 / 74.6	A	x	
167	23-May	2357	MA	42.2 / 72.9	A	x	
168	24-May	0000	CT	41.9 / 72.5	A	x	
169	24-May	0017	CT	41.8 / 73.1	A	x	
170	24-May	0020	WI	43.0 / 88.8	A	x	
171	24-May	0030	IL	41.6 / 88.5	A	x	
172	24-May	0030	NY	42.1 / 74.3	A	x	
173	24-May	0230	NE	42.9 / 101.7	B	x	
174	24-May	0230	NY	43.2 / 75.1	B	x	

#	Date	Time (Z)	Location	Lat / Lon	Type (A / B)	ETA-212 Data	MM5 Data
175	24-May	0302	IN	41.6 / 87.1	B	x	
176	24-May	0307	IN	39.5 / 86.8	B	x	
177	24-May	0530	MI	44.5 / 85.4	A	x	
178	24-May	1745	NE	42.4 / 96.8	A	x	
179	24-May	1750	SD	43.0 / 97.1	A	x	
180	24-May	1811	IA	42.2 / 96.2	A	x	
181	24-May	1812	NE	42.4 / 96.5	A	x	
182	24-May	2030	PA	41.3 / 75.3	B	x	
183	24-May	2030	NY	41.6 / 74.3	B	x	
184	24-May	2055	NE	41.2 / 96.0	B	x	
185	24-May	2059	NE	41.2 / 96.7	B	x	
186	24-May	2104	IA	42.6 / 94.5	B	x	
187	24-May	2110	IA	41.6 / 95.6	B	x	
188	24-May	2115	NE	40.8 / 97.2	B	x	
189	24-May	2118	NE	40.6 / 96.4	B	x	
190	24-May	2345	IN	38.1 / 86.6	A	x	
191	24-May	2345	NY	40.7 / 73.6	A	x	
192	24-May	2352	IA	41.4 / 93.8	A	x	
193	25-May	0000	NJ	40.5 / 74.5	A	x	
194	25-May	0000	MA	42.2 / 73.4	A	x	
195	25-May	0018	NH	43.0 / 71.4	A	x	
196	25-May	0253	IL	40.0 / 91.2	B	x	
197	25-May	0617	IL	39.9 / 88.9	A	x	
198	25-May	2030	WV	39.4 / 79.9	B	x	
199	25-May	2035	WV	37.6 / 81.4	B	x	
200	25-May	2035	WV	38.1 / 81.1	B	x	
201	25-May	2057	PA	40.4 / 79.3	B	x	
202	25-May	2100	IL	38.6 / 89.8	B	x	
203	25-May	2120	WV	37.5 / 81.1	B	x	
204	26-May	0005	PA	41.4 / 79.6	A	x	
205	26-May	0010	MD	39.6 / 75.9	A	x	
206	26-May	0230	WV	37.6 / 81.5	B	x	
207	26-May	1506	IL	38.2 / 88.7	B	x	
208	26-May	1519	IL	37.7 / 89.2	B	x	
209	26-May	1810	WV	38.7 / 81.7	A	x	

#	Date	Time (Z)	Location	Lat / Lon	Type (A / B)	ETA-212 Data	MM5 Data
210	26-May	1815	OH	39.0 / 83.9	A	x	
211	26-May	2050	PA	41.0 / 77.3	B	x	
212	26-May	2056	IL	37.2 / 88.7	B	x	
213	26-May	2110	WV	37.3 / 81.3	B	x	
214	26-May	2355	MN	44.5 / 95.8	A	x	
215	26-May	2357	SD	43.5 / 96.7	A	x	
216	27-May	0000	MN	43.7 / 95.6	A	x	
217	27-May	0013	IL	38.6 / 89.8	A	x	
218	27-May	0014	SD	44.1 / 96.5	A	x	
219	27-May	0018	IN	38.4 / 86.9	A	x	
220	27-May	0019	NY	42.3 / 75.9	A	x	
221	27-May	0304	IL / IN	38.1 / 90.0	B	x	
222	27-May	0910	IN	39.0 / 86.9	B	x	
223	27-May	1745	IA	40.7 / 93.6	A	x	
224	27-May	1806	IA	40.6 / 94.9	A	x	
225	27-May	2052	IL	39.3 / 90.8	B	x	
226	27-May	2055	IN	40.1 / 86.0	B	x	
227	27-May	2100	IN	40.2 / 86.5	B	x	
228	27-May	2100	OH / IN	40.1 / 84.4	B	x	
229	27-May	2345	SD	43.2 / 100.8	A	x	
230	27-May	2358	OH	39.2 / 84.5	A	x	
231	27-May	2358	OH	39.3 / 83.4	A	x	
232	27-May	2359	IN	40.3 / 85.6	A	x	
233	28-May	0000	WV	38.9 / 81.4	A	x	
234	28-May	0000	OH	38.9 / 83.6	A	x	
235	28-May	0000	WV	39.3 / 80.8	A	x	
236	28-May	0002	OH	38.9 / 82.8	A	x	
237	28-May	0004	IN	38.9 / 84.9	A	x	
238	28-May	0245	IL	38.0 / 88.3	B	x	
239	28-May	0305	IN	38.3 / 87.0	B	x	
240	28-May	2357	SD	42.8 / 97.1	A	x	
241	29-May	0238	IA	43.3 / 95.0	B	x	
242	29-May	0250	IA	42.9 / 96.3	B	x	
243	29-May	0256	SD	43.3 / 96.8	B	x	
244	29-May	0555	MN	43.9 / 95.1	A	x	

#	Date	Time (Z)	Location	Lat / Lon	Type (A / B)	ETA-212 Data	MM5 Data
245	29-May	2055	SD	42.9 / 98.3	B	x	
246	29-May	2105	SD	45.9 / 98.2	B	x	
247	29-May	2122	NE	40.1 / 97.9	B	x	
248	29-May	2359	SD	43.8 / 96.7	A	x	
249	30-May	0004	SD	44.9 / 97.2	A	x	
250	30-May	0004	SD	45.7 / 100.8	A	x	
251	30-May	0005	NE	41.2 / 99.2	A	x	
252	30-May	0005	SD	43.4 / 101.5	A	x	
253	30-May	0028	NE	42.8 / 97.9	A	x	
254	30-May	0235	MN	44.0 / 95.8	B	x	
255	30-May	0310	NE	41.0 / 98.2	B	x	
256	30-May	0537	IA	41.2 / 95.9	A	x	
257	30-May	0540	IA	40.7 / 93.6	A	x	
258	30-May	2124	WI	42.9 / 88.8	B	x	
259	30-May	2330	IL / IN	39.6 / 87.5	A	x	
260	30-May	2330	IN	41.7 / 86.3	A	x	
261	30-May	2335	IL	40.2 / 88.4	A	x	
262	30-May	2358	IL	41.2 / 88.2	A	x	
263	31-May	0005	IL	42.1 / 88.3	A	x	
264	31-May	0010	IN	40.6 / 87.3	A	x	
265	31-May	0307	OH	40.2 / 84.8	B	x	
266	31-May	0630	OH	38.4 / 82.5	A	x	
267	31-May	1800	MI	42.3 / 85.6	A	x	
268	31-May	2045	IA	41.4 / 91.0	B	x	
269	31-May	2109	IL	41.8 / 89.7	B	x	
270	1-Jun	0020	IL	39.1 / 90.3	A	x	
	A Storms: 135			B Storms: 135			

APPENDIX C – LIST OF JUNE STORMS

TORNADO PRODUCING STORMS							
#	**Date**	**Time (Z)**	**Location**	**Lat / Lon**	**Type (A / B)**	**ETA-212 Data**	**MM5 Data**
1	1-Jun	2130	NJ	40.9 / 74.0	B	x	
2	7-Jun	0017	ND	47.8 / 101.7	A	x	
3	7-Jun	0238	ND	48.8 / 101.5	B	x	
4	7-Jun	0250	ND	47.8 / 99.9	B	x	
5	7-Jun	0530	ND	48.5 / 99.2	A	x	
6	9-Jun	2045	NY	44.4 / 75.4	B	x	
7	10-Jun	2102	NE	41.0 / 102.2	B	x	
8	10-Jun	2330	IL	41.4 / 89.6	A	x	
9	11-Jun	0258	NE	40.1 / 98.6	B	x	
10	11-Jun	2102	IA	43.3 / 94.5	B	x	
11	11-Jun	2332	MN	43.7 / 92.5	A	x	
12	12-Jun	0020	IA	42.4 / 94.4	A	x	
13	13-Jun	1805	MI	43.3 / 85.1	A	x	
14	14-Jun	2355	MD	39.6 / 76.3	A	x	
15	16-Jun	2055	IA	43.2 / 92.9	B	x	
16	17-Jun	1740	PA	41.7 / 79.1	A	x	x
17	17-Jun	2050	PA	41.1 / 76.5	B	x	x
18	24-Jun	0004	WI	44.3 / 90.6	A	x	x
	A Storms: 9			B Storms: 9			

HAIL PRODUCING STORMS							
#	**Date**	**Time (Z)**	**Location**	**Lat / Lon**	**Type (A / B)**	**ETA-212 Data**	**MM5 Data**
1	1-Jun	1732	PA	40.5 / 78.7	A	x	
2	1-Jun	2120	NY	43.2 / 75.9	B	x	
3	2-Jun	1818	NY	42.4 / 73.7	A	x	
4	2-Jun	2335	CT	41.9 / 72.6	A	x	
5	4-Jun	2055	ND	47.0 / 102.2	B	x	
6	4-Jun	2345	SD	43.6 / 101.8	A	x	
7	5-Jun	0235	SD	44.2 / 102.5	B	x	
8	5-Jun	0255	ND	46.1 / 97.2	B	x	

#	Date	Time (Z)	Location	Lat / Lon	Type (A / B)	ETA-212 Data	MM5 Data
9	5-Jun	2050	MN	44.9 / 95.9	B	x	
10	5-Jun	2357	SD	43.9 / 97.8	A	x	
11	6-Jun	2345	ND	48.3 / 102.2	A	x	
12	6-Jun	2355	ND	48.6 / 102.1	A	x	
13	7-Jun	0010	ND	48.0 / 102.7	A	x	
14	7-Jun	0018	ND	49.0 / 101.6	A	x	
15	7-Jun	0255	ND	48.5 / 101.2	B	x	
16	7-Jun	0309	ND	47.8 / 99.9	B	x	
17	7-Jun	0628	MN	47.8 / 96.7	A	x	
18	7-Jun	2357	NE	42.0 / 99.9	A	x	
19	8-Jun	0255	NE	41.5 / 100.2	B	x	
20	8-Jun	0310	SD	44.8 / 98.1	B	x	
21	8-Jun	0320	SD	45.1 / 97.0	B	x	
22	8-Jun	0608	MN	45.0 / 94.5	A	x	
23	8-Jun	0630	SD	45.0 / 97.4	A	x	
24	8-Jun	2057	MI	46.4 / 86.0	B	x	
25	8-Jun	2123	IA	42.5 / 96.4	B	x	
26	8-Jun	2345	NE	40.3 / 101.5	A	x	
27	8-Jun	2345	IA	42.8 / 95.1	A	x	
28	8-Jun	2345	SD	43.1 / 99.5	A	x	
29	9-Jun	0010	SD	43.3 / 100.6	A	x	
30	9-Jun	0245	SD	43.4 / 99.9	B	x	
31	9-Jun	0313	NE	40.0 / 101.9	B	x	
32	9-Jun	1750	MI	42.4 / 84.4	A	x	
33	9-Jun	1820	MI	43.2 / 82.9	A	x	
34	9-Jun	2030	OH	41.6 / 80.8	B	x	
35	9-Jun	2040	MI	43.2 / 84.0	B	x	
36	9-Jun	2100	OH	41.5 / 81.3	B	x	
37	9-Jun	2100	VT	43.6 / 72.5	B	x	
38	9-Jun	2115	NY	43.3 / 78.3	B	x	
39	9-Jun	2338	MA	42.6 / 72.6	A	x	
40	10-Jun	2112	ME	41.5 / 103.3	B	x	
41	10-Jun	2114	IL	40.6 / 89.7	B	x	
42	10-Jun	2114	NE	42.7 / 103.0	B	x	
43	10-Jun	2122	SD	44.3 / 101.7	B	x	

#	Date	Time (Z)	Location	Lat / Lon	Type (A / B)	ETA-212 Data	MM5 Data
44	10-Jun	2130	NE	42.8 / 103.0	B	x	
45	10-Jun	2330	SD	43.6 / 101.7	A	x	
46	10-Jun	2346	NE	41.8 / 99.5	A	x	
47	11-Jun	0000	NE	40.7 / 100.6	A	x	
48	11-Jun	0002	IN	39.6 / 86.5	A	x	
49	11-Jun	0005	NE	41.8 / 101.0	A	x	
50	11-Jun	0010	NE	42.9 / 100.6	A	x	
51	11-Jun	0020	NE	40.1 / 100.1	A	x	
52	11-Jun	1814	IA	42.8 / 95.6	A	x	
53	11-Jun	2330	ND	48.2 / 99.8	A	x	
54	11-Jun	2345	MN	45.0 / 92.9	A	x	
55	11-Jun	2346	IA	40.6 / 94.9	A	x	
56	11-Jun	2350	ND	47.6 / 98.8	A	x	
57	12-Jun	0000	ND	47.2 / 98.1	A	x	
58	12-Jun	0230	IL	42.4 / 89.0	B	x	
59	12-Jun	0255	IA	42.1 / 93.5	B	x	
60	12-Jun	0330	IL	41.5 / 88.0	B	x	
61	12-Jun	1502	IN	38.9 / 86.5	B	x	
62	12-Jun	1515	NE	40.5 / 97.9	B	x	
63	12-Jun	1810	NE	40.6 / 96.5	A	x	
64	12-Jun	2030	NE	40.1 / 99.0	B	x	
65	12-Jun	2104	NE	40.6 / 98.4	B	x	
66	12-Jun	2105	NE	41.3 / 96.0	B	x	
67	12-Jun	2105	NE	42.1 / 98.0	B	x	
68	12-Jun	2330	NE	40.0 / 98.1	A	x	
69	12-Jun	2343	MN	44.1 / 93.5	A	x	
70	13-Jun	0005	MN	46.6 / 96.2	A	x	
71	13-Jun	0006	SD	45.3 / 98.5	A	x	
72	13-Jun	0230	MN	45.2 / 96.2	B	x	
73	13-Jun	0557	SD	44.1 / 98.2	A	x	
74	13-Jun	1219	WI	45.0 / 89.8	A	x	
75	13-Jun	1455	WI	45.4 / 88.9	B	x	
76	13-Jun	2053	NE	41.3 / 97.1	B	x	
77	13-Jun	2054	OH	41.2 / 84.7	B	x	
78	13-Jun	2101	IN	40.9 / 85.5	B	x	

#	Date	Time (Z)	Location	Lat / Lon	Type (A / B)	ETA-212 Data	MM5 Data
79	13-Jun	2115	MI	43.9 / 83.1	B	x	
80	14-Jun	0013	OH	40.5 / 83.8	A	x	
81	14-Jun	0235	SD	44.3 / 99.5	B	x	
82	14-Jun	0900	NE / IA	41.8 / 96.2	B	x	
83	14-Jun	1135	IA	41.0 / 92.0	A	x	
84	14-Jun	1737	MI	42.6 / 85.3	A	x	
85	14-Jun	1742	MI	43.1 / 84.6	A	x	
86	14-Jun	1742	IN	40.7 / 86.1	A	x	
87	14-Jun	2112	OH	38.4 / 82.6	B	x	
88	15-Jun	0015	OH	40.0 / 81.8	A	x	
89	15-Jun	1751	SD	45.1 / 97.2	A	x	
90	15-Jun	1808	IN	39.8 / 87.4	A	x	
91	15-Jun	2110	SD	44.5 / 98.0	B	x	
92	16-Jun	0015	NE	41.6 / 99.9	A	x	
93	16-Jun	0017	NE	41.1 / 100.5	A	x	
94	16-Jun	0025	NE	40.8 / 101.6	A	x	
95	16-Jun	0258	NE	41.1 / 100.8	B	x	
96	16-Jun	0309	NE	41.7 / 103.1	B	x	
97	16-Jun	0318	NE	40.4 / 101.0	B	x	
98	16-Jun	0325	NE	40.9 / 101.4	B	x	
99	16-Jun	0330	MN	44.9 / 95.0	B	x	
100	16-Jun	1756	IA	42.3 / 95.0	A	x	
101	16-Jun	1820	IA	41.6 / 93.8	A	x	
102	16-Jun	2347	WI	43.7 / 89.5	A	x	
103	17-Jun	0302	IL	38.4 / 89.9	B	x	
104	17-Jun	2350	NJ	40.4 / 74.7	A	x	x
105	19-Jun	0005	IL	37.4 / 89.0	A	x	x
106	23-Jun	1457	ND	48.1 / 97.9	B	x	x
107	23-Jun	1750	MN	47.1 / 96.0	A	x	x
108	23-Jun	2120	MN	45.1 / 93.1	B	x	x
109	23-Jun	2127	WI	42.9 / 88.1	B	x	x
110	23-Jun	2330	MI	43.3 / 86.2	A	x	x
111	23-Jun	2345	WI	44.0 / 90.5	A	x	x
112	23-Jun	2349	WI	44.6 / 90.6	A	x	x
113	23-Jun	2358	WI	43.4 / 90.8	A	x	x

#	Date	Time (Z)	Location	Lat / Lon	Type (A / B)	ETA-212 Data	MM5 Data
114	24-Jun	0235	MI	43.1 / 83.4	B	x	x
115	24-Jun	2354	OH	41.0 / 81.7	A	x	x
	A Storms: 62			B Storms: 53			

THIS PAGE INTENTIONALLY LEFT BLANK

APPENDIX D – LIST OF JULY STORMS

TORNADO PRODUCING STORMS							
#	**Date**	**Time (Z)**	**Location**	**Lat / Lon**	**Type (A / B)**	**ETA-212 Data**	**MM5 Data**
1	2-Jul	1805	NE	41.3 / 99.1	A	x	
2	3-Jul	1522	IN	41.7 / 86.2	B	x	x
3	4-Jul	0238	OH	39.9 / 84.4	B	x	x
4	5-Jul	2050	IA	42.4 / 94.6	B	x	
5	5-Jul	2107	IL	41.6 / 90.0	B	x	
6	5-Jul	2335	IA	42.8 / 91.7	A	x	
7	6-Jul	0256	IL	38.5 / 89.0	B	x	
8	10-Jul	2045	SD	43.9 / 101.2	B	x	x
9	10-Jul	2105	MN	49.0 / 95.0	B	x	x
10	10-Jul	2335	ND	47.0 / 100.1	A	x	x
11	11-Jul	0550	SD	44.5 / 99.0	A	x	x
12	11-Jul	2038	WI	45.6 / 89.8	B	x	x
13	13-Jul	0010	NE	42.2 / 98.8	A	x	x
14	13-Jul	1743	IL	41.5 / 89.3	A	x	x
15	13-Jul	2046	WI	44.1 / 87.9	B	x	x
16	16-Jul	0000	NE	42.3 / 98.5	A	x	x
17	19-Jul	0000	ND	47.9 / 97.3	A	x	x
18	19-Jul	0245	ND	46.9 / 97.7	B	x	x
19	27-Jul	2100	NJ	39.9 / 74.6	B	x	x
20	1-Aug	0021	MN	43.6 / 96.0	A	x	x
	A Storms: 9			B Storms: 11			

HAIL PRODUCING STORMS							
#	**Date**	**Time (Z)**	**Location**	**Lat / Lon**	**Type (A / B)**	**ETA-212 Data**	**MM5 Data**
1	1-Jul	1825	NY	44.7 / 73.5	A	x	x
2	1-Jul	1830	NY	43.9 / 73.4	A	x	x
3	1-Jul	2030	NY	43.6 / 75.1	B	x	x
4	1-Jul	2050	MD	39.3 / 76.5	B	x	x
5	1-Jul	2105	VT	44.5 / 72.9	B	x	x
6	1-Jul	2120	NY	44.2 / 74.5	B	x	x

#	Date	Time (Z)	Location	Lat / Lon	Type (A / B)	ETA-212 Data	MM5 Data
7	1-Jul	2125	NY	45.0 / 73.4	B	x	x
8	2-Jul	0012	NY	43.2 / 75.1	A	x	x
9	2-Jul	0625	CT	41.9 / 72.8	A	x	x
10	2-Jul	0625	MA	42.2 / 72.3	A	x	x
11	2-Jul	1740	MA	42.1 / 72.2	A	x	
12	2-Jul	1756	MA	42.6 / 70.8	A	x	
13	2-Jul	1800	CT	42.0 / 73.1	A	x	
14	2-Jul	1815	RI	41.8 / 71.4	A	x	
15	2-Jul	2100	ND	46.8 / 98.3	B	x	
16	2-Jul	2130	NE	42.7 / 103.9	B	x	
17	3-Jul	2030	ND	48.4 / 97.7	B	x	x
18	3-Jul	2050	ND	47.6 / 98.6	B	x	x
19	3-Jul	2100	SD	43.9 / 102.8	B	x	x
20	4-Jul	0000	NE	40.7 / 101.2	A	x	x
21	4-Jul	0005	SD	43.9 / 97.8	A	x	x
22	4-Jul	0240	SD	43.8 / 96.9	B	x	x
23	4-Jul	0251	SD	43.0 / 97.5	B	x	x
24	4-Jul	1815	IL	38.1 / 90.0	A	x	x
25	4-Jul	2059	NE	42.8 / 102.8	B	x	x
26	5-Jul	0030	NE	42.3 / 100.6	A	x	x
27	5-Jul	0241	IA	41.8 / 93.2	B	x	x
28	5-Jul	1500	IL	38.4 / 89.4	B	x	x
29	5-Jul	1754	IL	40.1 / 88.0	A	x	
30	5-Jul	2054	MD	39.7 / 77.6	B	x	
31	5-Jul	2105	NE	41.2 / 104.0	B	x	
32	5-Jul	2336	NE	41.4 / 100.2	A	x	
33	5-Jul	2339	NE	41.7 / 101.2	A	x	
34	6-Jul	0000	NE	40.8 / 99.8	A	x	
35	6-Jul	0240	IL	39.3 / 90.1	B	x	
36	6-Jul	0312	NE	40.4 / 98.4	B	x	
37	6-Jul	0326	IL	40.5 / 90.0	B	x	
38	6-Jul	0544	IN	38.4 / 86.7	A	x	x
39	6-Jul	1755	IL	38.1 / 89.9	A	x	x
40	6-Jul	2104	IL	38.4 / 87.8	B	x	x
41	6-Jul	2111	IL	38.1 / 88.2	B	x	x

#	Date	Time (Z)	Location	Lat / Lon	Type (A / B)	ETA-212 Data	MM5 Data
42	6-Jul	2358	MI	42.3 / 84.8	A	x	x
43	7-Jul	2030	NE	40.0 / 98.4	B	x	x
44	7-Jul	2050	NE	40.8 / 97.1	B	x	x
45	8-Jul	2055	NE	42.9 / 103.8	B	x	x
46	8-Jul	2110	VT	44.7 / 73.3	B	x	x
47	9-Jul	0020	NE	41.2 / 103.3	A	x	x
48	9-Jul	0248	NE	41.3 / 100.2	B	x	x
49	9-Jul	0257	NE	42.6 / 99.6	B	x	x
50	9-Jul	0304	NE	40.7 / 101.7	B	x	x
51	9-Jul	0329	NE	40.9 / 100.0	B	x	x
52	9-Jul	0550	NE	41.7 / 98.0	A	x	x
53	10-Jul	2045	SD	43.9 / 101.2	B	x	x
54	10-Jul	2105	MN	49.0 / 95.0	B	x	x
55	10-Jul	2335	ND	47.0 / 100.1	A	x	x
56	11-Jul	0550	SD	44.5 / 99.0	A	x	x
57	12-Jul	0000	SD	44.2 / 101.9	A	x	x
58	12-Jul	0010	SD	44.3 / 103.1	A	x	x
59	12-Jul	0235	ND	46.9 / 103.7	B	x	x
60	12-Jul	0330	SD	45.8 / 103.1	B	x	x
61	12-Jul	1825	SD	43.9 / 99.3	A	x	x
62	12-Jul	2105	SD	43.1 / 98.7	B	x	x
63	12-Jul	2350	SD	43.8 / 96.6	A	x	x
64	13-Jul	0254	SD / MN	44.6 / 96.4	B	x	x
65	13-Jul	0259	SD	44.2 / 96.7	B	x	x
66	13-Jul	0300	ND	47.0 / 96.9	B	x	x
67	13-Jul	0316	NE	41.0 / 98.9	B	x	x
68	13-Jul	0530	IA	43.4 / 94.5	A	x	x
69	13-Jul	0534	MN	43.5 / 96.0	A	x	x
70	13-Jul	0535	MN	46.5 / 95.1	A	x	x
71	13-Jul	0616	IA	43.1 / 95.6	A	x	x
72	13-Jul	1803	MI	45.6 / 87.3	A	x	x
73	13-Jul	2056	MI	44.5 / 84.6	B	x	x
74	13-Jul	2057	WI	45.0 / 88.1	B	x	x
75	13-Jul	2059	IL	40.4 / 88.5	B	x	x
76	13-Jul	2100	WI	44.0 / 88.2	B	x	x

#	Date	Time (Z)	Location	Lat / Lon	Type (A / B)	ETA-212 Data	MM5 Data
77	13-Jul	2100	MI	45.1 / 83.7	B	x	x
78	14-Jul	0023	MI	42.9 / 86.2	A	x	x
79	14-Jul	0025	IN	38.0 / 87.4	A	x	x
80	14-Jul	0245	SD	43.1 / 103.7	B	x	x
81	14-Jul	0315	IN	41.2 / 85.9	B	x	x
82	14-Jul	0545	IN	38.7 / 85.6	A	x	x
83	14-Jul	0600	IN	39.2 / 85.9	A	x	x
84	14-Jul	0607	IN	38.6 / 86.5	A	x	x
85	14-Jul	0855	PA	41.8 / 80.2	B	x	x
86	14-Jul	0916	OH	41.6 / 81.5	B	x	x
87	14-Jul	2045	SD	43.9 / 103.5	B	x	x
88	14-Jul	2105	MD	38.3 / 76.4	B	x	x
89	14-Jul	2108	MD	39.6 / 75.8	B	x	x
90	15-Jul	0300	ND	46.0 / 103.4	B	x	x
91	15-Jul	0530	ND	48.4 / 101.9	A	x	x
92	15-Jul	0532	ND	47.4 / 102.3	A	x	x
93	15-Jul	1445	SD	43.4 / 97.7	B	x	x
94	16-Jul	0005	NE	40.7 / 100.4	A	x	x
95	16-Jul	0230	NE	40.0 / 101.0	B	x	x
96	16-Jul	1739	WI	44.8 / 89.2	A	x	x
97	16-Jul	2040	WI	43.1 / 89.4	B	x	x
98	19-Jul	0020	MN	48.1 / 96.9	A	x	x
99	19-Jul	1225	WI	45.2 / 92.0	A	x	x
100	19-Jul	1430	WI	44.9 / 91.7	B	x	x
101	19-Jul	1750	WI	44.1 / 91.2	A	x	x
102	19-Jul	2105	IA	43.2 / 91.9	B	x	x
103	19-Jul	2117	MI	46.1 / 87.6	B	x	x
104	21-Jul	2054	ND	46.1 / 96.7	B	x	
105	21-Jul	2100	IL	41.7 / 88.3	B	x	
106	21-Jul	2105	SD	45.4 / 98.1	B	x	
107	21-Jul	2109	SD	43.8 / 98.5	B	x	
108	21-Jul	2110	MI	43.1 / 85.8	B	x	
109	21-Jul	2126	MN	46.1 / 96.4	B	x	
110	21-Jul	2331	SD	43.0 / 97.6	A	x	
111	21-Jul	2340	IL	40.0 / 87.6	A	x	

#	Date	Time (Z)	Location	Lat / Lon	Type (A / B)	ETA-212 Data	MM5 Data
112	21-Jul	2342	IN	40.8 / 87.2	A	x	
113	21-Jul	2354	NE	41.2 / 101.8	A	x	
114	22-Jul	0000	IN	40.2 / 87.5	A	x	
115	22-Jul	1750	IL	40.0 / 89.5	A	x	
116	22-Jul	2130	IL	38.5 / 89.6	B	x	
117	23-Jul	0007	IL	38.5 / 90.0	A	x	
118	23-Jul	0019	OH	40.7 / 84.7	A	x	
119	23-Jul	0029	IL	37.4 / 88.6	A	x	
120	28-Jul	0000	ND	46.8 / 100.7	A	x	x
121	28-Jul	0015	SD	44.0 / 99.4	A	x	x
122	29-Jul	2040	SD	43.3 / 103.3	B	x	
123	30-Jul	0000	NE	42.0 / 102.6	A	x	x
124	30-Jul	0025	NE	41.5 / 102.6	A	x	x
125	30-Jul	0328	NE	41.2 / 102.6	B	x	x
126	30-Jul	0328	NE	41.8 / 103.3	B	x	x
127	31-Jul	2345	ND	48.8 / 98.4	A	x	x
128	1-Aug	0005	SD	43.7 / 97.1	A	x	x
129	1-Aug	0259	IA	43.0 / 96.5	B	x	x
130	1-Aug	0259	IA	43.2 / 95.7	B	x	x
131	1-Aug	0300	IA	43.4 / 95.9	B	x	x
132	1-Aug	0303	MN	44.9 / 94.2	B	x	x
133	1-Aug	0313	MN	44.4 / 95.9	B	x	x
134	1-Aug	0315	SD	43.5 / 99.8	B	x	x
135	1-Aug	0535	NE	42.8 / 99.7	A	x	
136	1-Aug	0914	MN	44.2 / 94.0	B	x	
137	1-Aug	1142	NE	41.7 / 97.4	A	x	x
	A Storms: 62			B Storms: 75			

THIS PAGE INTENTIONALLY LEFT BLANK

APPENDIX E – LIST OF AUGUST STORMS

TORNADO PRODUCING STORMS							
#	**Date**	**Time (Z)**	**Location**	**Lat / Lon**	**Type (A / B)**	**ETA-212 Data**	**MM5 Data**
1	2-Aug	0905	MN	46.4 / 95.9	B	x	x
2	3-Aug	0303	NE	43.0 / 102.0	B	x	x
3	4-Aug	1516	IN	39.2 / 86.6	B	x	x
4	8-Aug	2102	MN	48.3 / 96.2	B	x	x
5	8-Aug	2118	ND	49.0 / 97.6	B	x	x
6	9-Aug	0003	MN	48.6 / 96.6	A	x	x
7	24-Aug	0005	SD	44.6 / 96.6	A	x	x
8	26-Aug	2345	IA	40.7 / 95.0	A	x	x
9	30-Aug	0000	MN	46.1 / 94.8	A	x	x
	A Storms: 4			B Storms: 5			

HAIL PRODUCING STORMS							
#	**Date**	**Time (Z)**	**Location**	**Lat / Lon**	**Type (A / B)**	**ETA-212 Data**	**MM5 Data**
1	1-Aug	2045	IA	40.7 / 94.2	B	x	x
2	2-Aug	0010	SD	45.6 / 101.6	A	x	x
3	2-Aug	0305	SD	44.6 / 100.0	B	x	x
4	2-Aug	0845	ND	47.2 / 97.6	B	x	x
5	2-Aug	1152	MN	46.1 / 95.7	A	x	x
6	2-Aug	1501	WI	43.5 / 89.7	B	x	x
7	2-Aug	1504	WI	44.1 / 91.7	B	x	x
8	2-Aug	1750	MI	45.4 / 84.2	A	x	x
9	2-Aug	1755	MI	46.2 / 86.4	A	x	x
10	2-Aug	1826	MI	45.0 / 83.7	A	x	x
11	2-Aug	2040	IL	41.6 / 87.9	B	x	x
12	2-Aug	2048	SD	44.2 / 97.3	B	x	x
13	2-Aug	2109	MI	42.7 / 84.9	B	x	x
14	2-Aug	2111	MI	44.4 / 83.3	B	x	x
15	2-Aug	2330	NE	42.8 / 99.7	A	x	x
16	2-Aug	2330	MI	43.2 / 82.9	A	x	x
17	2-Aug	2340	SD	43.7 / 103.2	A	x	x

#	Date	Time (Z)	Location	Lat / Lon	Type (A / B)	ETA-212 Data	MM5 Data
18	3-Aug	0247	SD	43.5 / 98.6	B	x	x
19	3-Aug	0330	SD	43.5 / 103.2	B	x	x
20	3-Aug	0915	SD	44.8 / 102.0	B	x	
21	3-Aug	1130	SD	44.7 / 100.8	A	x	x
22	3-Aug	1500	SD	43.7 / 98.0	B	x	x
23	3-Aug	1737	IA	43.4 / 95.9	A	x	x
24	3-Aug	1811	MA	42.1 / 72.4	A	x	x
25	3-Aug	2050	MN	43.8 / 91.8	B	x	x
26	3-Aug	2100	WI	43.6 / 90.1	B	x	x
27	3-Aug	2110	IA	42.2 / 94.5	B	x	x
28	4-Aug	0003	IA	41.7 / 94.9	A	x	x
29	4-Aug	0006	NE	41.3 / 96.2	A	x	x
30	4-Aug	0010	NE	42.7 / 103.1	A	x	x
31	4-Aug	0250	NE	41.9 / 101.9	B	x	x
32	4-Aug	0610	IL	41.1 / 88.8	A	x	x
33	4-Aug	1813	OH	40.1 / 80.8	A	x	x
34	8-Aug	2049	NE	40.4 / 97.0	B	x	x
35	8-Aug	2105	ND	47.6 / 98.6	B	x	x
36	8-Aug	2110	MN	47.1 / 96.2	B	x	x
37	8-Aug	2120	NE	40.6 / 96.2	B	x	x
38	8-Aug	2125	IA	42.2 / 95.0	B	x	x
39	8-Aug	2335	MN	45.5 / 93.0	A	x	x
40	8-Aug	2335	MN	47.9 / 96.2	A	x	x
41	8-Aug	2340	MN	47.7 / 94.6	A	x	x
42	8-Aug	2345	WI	45.5 / 92.0	A	x	x
43	9-Aug	0005	WI	44.5 / 89.3	A	x	x
44	9-Aug	0030	MN	46.1 / 93.4	A	x	x
45	9-Aug	2330	MI	44.9 / 86.1	A	x	x
46	10-Aug	0000	IL	40.2 / 89.2	A	x	x
47	10-Aug	0029	IN	41.7 / 86.3	A	x	x
48	10-Aug	0303	NE	40.4 / 101.5	B	x	x
49	10-Aug	1747	NE	41.1 / 100.8	A	x	x
50	10-Aug	2110	NY	42.3 / 77.3	B	x	x
51	10-Aug	2120	PA	40.6 / 79.6	B	x	x
52	11-Aug	0015	PA	40.4 / 76.9	A	x	x

#	Date	Time (Z)	Location	Lat / Lon	Type (A / B)	ETA-212 Data	MM5 Data
53	19-Aug	1815	PA	40.6 / 79.6	A	x	x
54	19-Aug	2040	PA	40.3 / 79.5	B	x	x
55	19-Aug	2100	PA / OH	40.5 / 80.5	B	x	x
56	19-Aug	2102	PA	40.0 / 76.7	B	x	x
57	20-Aug	1810	PA	40.8 / 78.1	A	x	x
58	20-Aug	1825	MA	42.6 / 71.9	A	x	x
59	20-Aug	2045	MA	42.6 / 71.2	B	x	x
60	20-Aug	2047	CT	41.6 / 73.4	B	x	x
61	20-Aug	2049	NY	42.4 / 75.6	B	x	x
62	20-Aug	2105	PA	40.9 / 78.2	B	x	x
63	20-Aug	2129	PA	40.9 / 79.9	B	x	x
64	20-Aug	2355	PA	39.8 / 77.7	A	x	x
65	21-Aug	1756	CT	41.9 / 72.5	A	x	x
66	23-Aug	2104	IA / SD	42.5 / 96.4	B	x	x
67	23-Aug	2349	SD	43.5 / 97.6	A	x	x
68	24-Aug	0000	SD	43.3 / 99.9	A	x	x
69	24-Aug	0000	MN	44.4 / 95.4	A	x	x
70	24-Aug	0000	ND	46.8 / 101.8	A	x	x
71	24-Aug	0012	NE	41.7 / 99.9	A	x	x
72	24-Aug	0250	SD	44.5 / 96.5	B	x	x
73	24-Aug	0255	ND	46.3 / 100.2	B	x	x
74	24-Aug	0530	ND	47.6 / 98.0	A	x	x
75	24-Aug	0625	ND	47.0 / 97.2	A	x	x
76	25-Aug	1430	NE	40.0 / 97.0	B	x	x
77	25-Aug	1730	IA	41.1 / 94.5	A	x	x
78	25-Aug	2100	MN	45.4 / 96.4	B	x	x
79	25-Aug	2334	MN	44.6 / 92.8	A	x	x
80	25-Aug	2334	MN	45.1 / 94.0	A	x	x
81	25-Aug	2340	ND	47.2 / 100.8	A	x	x
82	25-Aug	2350	ND	48.2 / 102.4	A	x	x
83	26-Aug	0008	ND	46.2 / 97.7	A	x	x
84	26-Aug	0245	ND	47.2 / 98.4	B	x	x
85	26-Aug	2102	MN	48.4 / 93.0	B	x	x
86	26-Aug	2107	IA	42.9 / 93.8	B	x	x
87	26-Aug	2117	IA	42.7 / 94.5	B	x	x

#	Date	Time (Z)	Location	Lat / Lon	Type (A / B)	ETA-212 Data	MM5 Data
88	26-Aug	2343	MN	43.9 / 91.9	A	x	x
89	26-Aug	2345	MN	43.7 / 92.3	A	x	x
90	26-Aug	2357	IA	42.2 / 95.3	A	x	x
91	27-Aug	0005	SD	45.9 / 96.9	A	x	x
92	27-Aug	0010	ND	46.2 / 97.4	A	x	x
93	27-Aug	0245	IA	41.0 / 94.0	B	x	x
94	27-Aug	0255	IA	43.4 / 91.7	B	x	x
95	27-Aug	0255	MI	46.5 / 87.3	B	x	x
96	27-Aug	0308	WI	43.4 / 90.5	B	x	x
97	27-Aug	0330	WI	44.0 / 90.1	B	x	x
98	27-Aug	2035	OH	41.8 / 81.0	B	x	x
99	27-Aug	2345	IA	41.1 / 93.8	A	x	x
100	29-Aug	1820	NY	43.4 / 75.6	A	x	x
101	29-Aug	2125	NY	42.3 / 78.5	B	x	x
102	29-Aug	2129	ND	47.8 / 97.1	B	x	x
103	29-Aug	2340	MN	48.3 / 96.3	A	x	x
104	29-Aug	2350	MN	47.2 / 96.2	A	x	x
105	29-Aug	2353	IA	42.7 / 96.3	A	x	x
106	30-Aug	0010	MN	46.1 / 96.4	A	x	x
107	30-Aug	0020	MN	46.7 / 96.4	A	x	x
	A Storms: 57			B Storms: 50			

APPENDIX F – LIST OF SEPTEMBER STORMS

TORNADO PRODUCING STORMS							
#	**Date**	**Time (Z)**	**Location**	**Lat / Lon**	**Type (A / B)**	**ETA-212 Data**	**MM5 Data**
1	5-Sep	2340	WI	44.7 / 92.5	A	x	x
2	6-Sep	0015	IA	42.5 / 93.9	A	x	x
3	8-Sep	1830	MD	39.7 / 77.8	A	x	x
4	30-Sep	1150	MD	38.4 / 76.3	A	x	x
	A Storms: 4			B Storms: 0			

HAIL PRODUCING STORMS							
#	**Date**	**Time (Z)**	**Location**	**Lat / Lon**	**Type (A / B)**	**ETA-212 Data**	**MM5 Data**
1	3-Sep	2100	MI	43.4 / 85.8	B	x	x
2	5-Sep	2350	SD	43.6 / 97.9	A	x	x
3	13-Sep	2330	NE	41.9 / 97.9	A	x	x
4	13-Sep	2330	SD	43.1 / 96.9	A	x	x
5	13-Sep	2340	NE	42.3 / 97.7	A	x	x
6	13-Sep	2345	IA	43.5 / 96.5	A	x	x
7	14-Sep	0021	SD	43.5 / 96.7	A	x	x
8	14-Sep	2045	NE	41.6 / 104.0	B	x	x
9	14-Sep	2100	NE	41.7 / 103.1	B	x	x
10	14-Sep	2352	IA	42.2 / 95.3	A	x	x
11	15-Sep	0002	NE	41.2 / 102.8	A	x	x
12	15-Sep	0015	NE	41.5 / 102.3	A	x	x
13	15-Sep	0240	NE	41.3 / 100.8	B	x	x
14	15-Sep	0300	NE	40.3 / 100.2	B	x	x
15	17-Sep	0250	SD	43.8 / 98.1	B	x	x
16	18-Sep	0925	IA	41.1 / 94.6	B	x	x
	A Storms: 9			B Storms: 7			

THIS PAGE INTENTIONALLY LEFT BLANK

LIST OF REFERENCES

15th Operational Weather Squadron, Scott AFB, IL, cited September 2004: 15th OWS Orientation Briefing, 8 Jan 2004.

American Meteorological Society, cited January 2005: Glossary of Meteorology. [Available online at http://amsglossary.allenpress.com/glossary/]

Beebe, R.G. and Bates, F.C., 1955: A Mechanism for Assisting in the Release of Convective Instability. *Monthly Weather Review*, **83**, 1-10.

David, Clarence L. 1976: A Study of Upper Air Parameters at the Time of Tornadoes. *Monthly Weather Review*, **104**, 546-551.

Fowle, Michael A. and Roebber, Paul J. 2003: Short Range (0-48 h) Numerical Prediction of Convective Occurrence, Mode, and Location. *Weather and Forecasting*, **18**, 782-794.

House, D.C., 1958: Air Mass Modification and Upper-Level Divergence. *Bulletin of the American Meteorological Society*, **39**, 137-143.

Maddox, Robert A. and Doswell, Charles A., 1982: An Examination of Jet Stream Configurations, 500mb Vorticity Advection and Low Level Thermal Advection Patterns During Extended Periods of Intense Convection. *Monthly Weather Review*, **110**, 184-197.

McNulty, Richard P., 1978: On Upper Tropospheric Kinematics and Severe Weather Occurrence. *Monthly Weather Review*, **106**, 662-672.

Mills, G.A. and Colquhoun, J.R. 1998: Objective Prediction of Severe Thunderstorm Environments: Preliminary Results Linking a Decision Tree with an Operational Regional NWP Model. *Weather and Forecasting*, **13**, 1078-1092.

Moore, James T. and VanKnowe, Glenn E., 1992: The Effect of Jet-Streak Curvature on Kinematic Fields. *Monthly Weather Review*, **120**, 2429-2441.

Nuss, Wendell A. and Titley, David W., 1994: Use of Multiquadratic Interpolation for Meteorological Objective Analysis. *Monthly Weather Review*, **122**, 1611-1631.

NWS Storm Prediction Center, cited May 2004 – February 2005: Index of Severe Thunderstorm Events. [Available online at http://www.spc.ncep.noaa.gov/exper/archive/events/searchindex.html]

Ohio State University, cited February 2005: Convective Available Potential Energy Help Page. [Available online at http://twister.sbs.ohio-state.edu/helpdocs/cape.html]

Rose, Stanley F., Hobbs, Peter V., Locatelli, John D., and Stoelinga, Mark T., 2004: A 10-Yr Climatology Relating the Locations of Reported Tornadoes to the Quadrants of Upper-Level Jet Streaks. *Weather and Forecasting*, **19**, 301-309.

Stensrud, David J., Cortinas, John V., and Brooks, Harold E. 1997: Discriminating between Tornadic and Nontornadic Thunderstorms Using Mesoscale Model Output. *Weather and Forecasting*, **12**, 613-632.

United States Air Force, cited May 2004: AF Weather OWS AORs – CONUS. [Available online at http://www.e-publishing.af.mil/pubfiles/af/15/afva15-136/afva15-136.pdf]

University Corporation for Atmospheric Research, cited February 2005: Operational Models Matrix: Characteristics of Operational NWP Models. [Available online at http://meted.ucar.edu/nwp/pcu2/index.htm]

University of Wisconsin – Stevens Point, cited December 2004: Stages of Thunderstorm Development. [Available online at http://www.uwsp.edu/geo/faculty/ritter/geog101/textbook/weather_systems/thunderstorms_p_2.htm]

Weisman, Morris L. and Klemp, Joseph B. 1986: Characteristics of Isolated Convective Storms. *Mesoscale Meteorology and Forecasting*, Peter S. Ray Ed., American Meteorological Society, 331-358.

INITIAL DISTRIBUTION LIST

1. Defense Technical Information Center
   Ft. Belvoir, Virginia

2. Dudley Knox Library
   Naval Postgraduate School
   Monterey, California

3. 15th Operational Weather Squadron
   Scott Air Force Base, Illinois

4. Wendell A. Nuss
   Monterey, California

5. Carlyle H. Wash
   Monterey, California

6. Department of Meteorology
   Naval Postgraduate School
   Monterey, California

7. Scott C. Lisko
   Scott Air Force Base, Illinois